College of Engineering

Development of Green Low Surface Energy (Superhydrophobic) Material for Various Surfaces

By Celina Dlofo

Under supervision of Dr Shirin Alexander

Dissertation submitted for MSc by Research in Energy Innovation
30th June 2021

Abstract

Superhydrophobic materials maintain air at the solid-liquid interface, when in contact with water and it can be defined as the tendency of a surface to repel water droplets. These surfaces possess high contact angles of at least 150°, low hysteresis contact angle <10°. Superhydrophobic surfaces have a wide range of application due to their self-cleaning, antifogging, anticorrosion, biomedical characteristics.

A substantial body of research is based around the use of relatively expensive fluorocarbons and environmentally hazardous methods to obtain superhydrophobic surfaces. This study proposes an alternative method of fabricating superhydrophobic surfaces, through a cleaner and more cost-effective process which adopts highly branched hydrocarbon chains.

To meet the objective of this study, superhydrophobic surfaces were fabricated, which make use of environmentally friendly, non-hazardous (i.e., when in contact with skin) as well as cost effective.

We focus on the nanoparticles Al_2O_3 (13 nm) and SiO_2 (10-20 nm), particularly on the impact of the nanoparticle sizes, properties, and shape. As a result of this alternative method, alumina (Al_2O_3) and silica (SiO_2) nanoparticles were easily synthesized with the appropriate carboxylic acid and then spray coated unto different surfaces.

After the fabrication process, a static contact angle of 153° were obtained for the functionalized Al_2O_3 (13 nm) nanoparticles with lanolin (1:5), showing low affinity with water and the droplet of water rolls off easily across the surface.

Keywords: superhydrophobic, nanoparticles, contact angle

Declaration and Statement

This work has not previously been accepted in substance for any degree and is not being concurrently submitted in candidature for any degree.

Signed..... 

Date..... 30/06/2021.....

This thesis is the result of my own investigations, except where otherwise stated. Other sources are acknowledged by footnotes giving explicit references. A bibliography is appended.

Signed..... 

Date..... 30/06/2021.....

I hereby give consent for my thesis, if accepted, to be available for photocopying and for inter-library loan, and for the title and summary to be made available to outside organisations.

Signed..... 

Date..... 30/06/2021.....

The University's ethical procedures have been followed and, where appropriate, that ethical approval has been granted.

Signed..... 

Date..... 30/06/2021.....

Acknowledgement

First and foremost, I would like to thank God for making this moment and all the moments that led to this achievement possible. I would like to take this opportunity to thank everyone who supported me during my MSc research work in Swansea University. Furthermore, this dissertation would not have been possible without the support and encouragement mother, Mariamo Mocopoto and family, for your love, support, understanding, patience, and optimism. Above all, I would like to thank my supervisor Dr Shirin Alexander for her invaluable guidance and support throughout this dissertation, I would also like to show my gratitude for your time, dedication, patient with all my errors and mistakes.

- I would like to thank KESS 2 (Knowledge Economy Skills Scholarship) in collaboration with Salts Healthcare for generously provided the scholarship
- "*This work is part-funded by the European Social Fund (ESF) through the European Union's Convergence programme administered by the Welsh Government*".
- I would like to thank Don and Wafaa for their generous, kind help and suggestion regarding my experiments
- I would like to thank James Russell for SEM characterization and analysis

Table of Contents

Abstract ..... ***ii***

Declaration and Statement ..... ***iii***

Acknowledgement ..... ***iv***

List of Tables ..... ***vii***

List of Figures ..... ***viii***

List of Abbreviations ..... ***x***

Chapter I: Introduction ***1***

Project Information **1**

Objective of the thesis **2**

Project rationale **2**

Organisation of the thesis **3**

Chapter II: Background ***4***

Fundamentals of superhydrophobic surface **4**

Lanolin **6**

Nanoparticles **6**

Size and shape of nanoparticles 8

Superhydrophobicity **9**

The Sphere Theorem 11

Natural superhydrophobic surfaces **12**

Surface Free Energy (SFE) **15**

Roughness measurements 15

The difference between liquid droplets and rigid spheres at an interface 16

Surface wettability **16**

Work of adhesion 17

Work of cohesion 17

Characterisation of a solid surface 18

Measurements of surfaces with superwettability **18**

Contact angle 19

Static contact angle 21

Dynamic contact angle 22

Sliding angle (SA) 23

Contact angle hysteresis (advancing and receding) 24

The effect of roughness on contact angles **25**

Fully wet surfaces: Wenzel's equation 25

Bridging the roughness: Cassie-Baxter's equation 26

Wenzel-Cassie hysteresis 27

Chapter III: Literature review ***29***

Manufacturing of superhydrophobic surfaces **29**

Top-down methods **29**

Photolithography 29

Plasma method ... 31
Chemical method ... 34
Aluminium oxide (alumina) ... 35
Silicon dioxide (silica) ... 35

Bottom-up methods ... 36
Chemical vapor deposition (CVD) ... 36
Electrospinning ... 37
Sol-gel processing ... 40
Layer-by-layer (LBL) deposition ... 42

Applications of superhydrophobic surfaces ... 44
Anti-icing ... 44
Self-cleaning surfaces ... 45
Anti-corrosion resistant coatings ... 46
Water-resistant fabrics ... 47
Biomedical ... 48

Discussion ... 49

Chapter IV: Experimental method ... 51

Methodology used for the development of green low surface ... 52
Synthesis of carboxylate functionalized nanoparticles ... 52
Reflux reaction ... 53
Centrifuge ... 54

Deposition technologies ... 57
Preparation of the slurry ... 57

Chapter V: Analytical and Measuring Instruments ... 60

Attenuated total reflectance – Fourier transform infrared (ATR – FTIR) spectroscopy ... 60

Thermogravimetric Analyser (TGA) ... 62

Scanning Electron Microscopy (SEM) ... 64

Measurement of static contact angle ... 64
Drop shape analyser ... 65

Chapter VI: Results and discussion ... 69

Infrared spectroscopy ... 69

Thermogravimetric analysis ... 77

Surface morphology and surface roughness ... 83

Wettability of the Nanoparticles ... 88

Wettability behaviour of a cardboard coated with the nanoparticles ... 95

Chapter VII: Conclusions ... 99

Conclusions ... 99

Recommendations ... 101

Challenges ... 101

Reference: ... 103

Appendix ... 115

List of Tables

Table 1: Abrasion resistance of different superhydrophobic surfaces [107] 32
Table 2: Select properties of the PAH/SiO_2 multilayer system [128] 43
Table 3: Table: Different ratio of the synthesis (functionalised agents).....52
Table 4: IR characterisation band of as received isosteric acid [181], [182].....70
Table 5: IR characterisation band as received lanolin[182], [186], [187] 71
Table 6: IR characterisation band of functionalized Al_2O_3 (13 nm) nanoparticles with isosteric acid.....73
Table 7: IR characterisation band of functionalized Al_2O_3 (13 nm) nanoparticles with lanolin (1:5).....74
Table 8: IR characterisation band of unfunctionalized SiO_2 (10-20 nm) nanoparticles [187] 75
Table 9: IR characterisation band of functionalized SiO_2 (10-20 nm) nanoparticles with lanolin (1:5).....76
Table 10: Calculated grafting density as a function of the organic mass loss data obtained using TGA for the functionalized Al_2O_3 (13 – 50 nm) and SiO_2 (10-20 nm) nanoparticles [164].....82
Table 11: Contact angle measurements with deionised water obtained on a glass substrate for different functionalised nanoparticles.....92
Table 12: contact angle measurements with deionised water obtained on a fabric substrate for different functionalised nanoparticles.....93
Table 13: Weight of the uncoated and coated cardboard with the functionalised nanoparticles 98

List of Figures

Figure 1: Classification of contact angle coating [33] 9
Figure 2:Lotus Effect; images of water droplets resting onto different substrates and SEM of Dentical, Fractal and Layered cuticle illustrating a water contact angle [57] 13
Figure 3: Different wetting states [58] 14
Figure 4: Contact angle at three-phase interface on a smooth surface [77] 20
Figure 5: Advancing and receding contact angle [33] 25
Figure 6: Cassie state without actuation and Wenzel state with electrowetting actuation [51] 28
Figure 7: Schematic diagram of the experimental microchannel flow cell including the important physical dimensions [106] 30
Figure 8: Schematic diagram outlining the procedure for creating of superhydrophobic surfaces [106] 31
Figure 9: Illustration of O_2 plasma etching of epoxy/silica nanoparticles composite films for surface rough structures [107] 32
Figure 10: Illustration of the abrasion test on a superhydrophobic surface [107] 32
Figure 11: Surface morphology from SEM images a) surface before etching, b) O_2 plasma etched for 1 minutes, c) 5 minutes, d) 10 minutes and e) 15 minutes [107] 33
Figure 12: Scheme showing patterning of copper samples [108] 34
Figure 13: Confocal profiles of etched copper surface a) 40 µm pattern, b) 30 µm pattern, c) 20 µm pattern and d) 5 µm pattern [108] 35
Figure 14: Illustration for the experimental setup of the preparation of the coatings [119] 37
Figure 15: a) Schematic for the preparation of the coatings on both sides of the glass substrates b) to d) SEM images of the sample**s [119]** 37
Figure 16: Electrospinning setup [122] 38
Figure 17: Contact angle and roll off angle results (broad bars represent contact angle and narrow bars roll off angle) [123] 39
Figure 18: Cross-sectional views of the glass surfaces coated with solutions containing different concentrations of PVDF [123] 40
Figure 19: Schematic illustrating the change in particle shape with a reduction in % PVDF in the solution (aspect ratio is indicated in brackets) [123] 40
Figure 20: Schematic illustration of the procedure to prepare silica rough surfaces [126] 41
Figure 21: Effect of spin speed on contact angle and contact angle hysteresis on SiO_2 films [126] 42
Figure 22: Simplified schematic of the multilayer film showing the three main assembly blocks [128] 43
Figure 23: Image of reflux reaction of Al_2O_3 (13nm) with isostearic acid. Source: Author's picture based on the experimental setup 53
Figure 24: Image of refluxed nanoparticles before centrifugation. Source: Author's picture based on the experimental observation 54
Figure 25: Heraeus Megafuge 16 Centrifuge. Source: Author's picture 55
Figure 26: Image of refluxed nanoparticles after centrifugation. Source: Author's picture based on the experimental observation 56
Figure 27: Image of functionalised Al_2O_3 (13nm) nanoparticles dispersed on 2-propanol, ready to be spray coated onto substrates. Source: Author's picture based on the experimental setup 58

Figure 28: Image of functionalised Al_2O_3 (13 nm) nanoparticles with isostearic acid deposited on a glass substrate. Source: Author's picture based on the results obtained from the experimental setup 58
Figure 29: Image of functionalized Al_2O_3 (5 nm) nanoparticle after being dispersed in 2-propanol ready to be sprayed onto substrates. Source: Author's picture based on the experimental setup 59
Figure 30: Image of IR spectroscopy. Source: The author's picture 62
Figure 31: Thermogravimetric analyser (TGA). Source: Author's picture 63
Figure 32: Scanning electron microscopy (SEM) [174] 64
Figure 33: Drop shape analyser (Krüss). Source: Author's picture 66
Figure 34: IR spectrum of as received isosteric acid 70
Figure 35: IR spectrum of as received lanolin 71
Figure 36: IR spectrum of unfunctionalized Al_2O_3 (13 nm) nanoparticles 72
Figure 37: IR spectrum of functionalized Al_2O_3 (13 nm) nanoparticles with isosteric acid 73
Figure 38: IR spectrum of functionalized Al_2O_3 (13 nm) nanoparticles with lanolin (1:5) 74
Figure 39: IR spectrum of unfunctionalized SiO_2 (10-20 nm) nanoparticles 75
Figure 40: IR spectrum of functionalized SiO_2 (10-20 nm) nanoparticles with lanolin (1:5) 76
Figure 41: TGA data of the as received lanolin. 78
Figure 42: TGA data of the alumina (13 nm) with lanolin (1:5), dashed curves correspond to derivatives 81
Figure 43: TGA of a) unfunctionalized Al_2O_3 (13 nm) nanoparticles, b) functionalized Al_2O_3 (13 nm) with isosteric acid, c) unfunctionalized SiO_2 (10-20 nm) nanoparticles, d) functionalized Al_2O_3 (13 nm) with lanolin (1:5) and e) functionalized SiO_2 (10-20 nm) with lanolin (1:5) 83
Figure 44: SEM images of film spray coated onto a microscope slide of unfunctionalized Al_2O_3 (13 nm) nanoparticles 84
Figure 45: SEM images of films spray coated onto a microscope slide of unfunctionalized SiO_2 (10-20 nm) nanoparticles 85
Figure 46: SEM images of film spray coated onto a microscope slide of unfunctionalized Al_2O_3 (50 nm) nanoparticles 85
Figure 47: SEM images of film spray coated onto a microscope slide of a) functionalized Al_2O_3 (13 nm) nanoparticles with isosteric acid; b) functionalized Al_2O_3 (13 nm) nanoparticles with lanolin (1:5) 86
Figure 48: SEM image of film spray coated onto a microscope slide of Al_2O_3 (13 nm) nanoparticles functionalized with lanolin (1:10) 87
Figure 49: SEM image of film spray coated onto a microscope slide of Al_2O_3 (13 nm) nanoparticles functionalized with lanolin (1:15) 87
Figure 50: SEM images of film spray coated onto a microscope slide of SiO_2 (10-20 nm) nanoparticles functionalized with lanolin (1:5) 88
Figure 51: Functionalised Al_2O_3 (13 nm) nanoparticles with isostearic acid deposited onto microscope slide 94
Figure 52: Functionalised Al_2O_3 (13 nm) nanoparticles with lanolin (1:5) deposited onto microscope slide 95
Figure 53: Droplet of water onto fabric substrate a) uncoated b) functionalized Al_2O_3 (50 nm) with lanolin (1:10) 95

List of Abbreviations

PDMS – Polydimethylsiloxance

LSEMs – Low surface energy material

SEM – Scanning electron microscopy

IR – Infrared spectroscopy

TGA – Thermogravimetric analysis

CVD – Chemical vapor deposition

NPs – Nanoparticles

PVDF – Polyvinylidene fluoride

FSM – Fluorinated silane molecules

DMF – Dimethyl formamide

TEOS – Tetraethoxysilane

SPS – Poly (sodium 4-styrenesulfonate)

PAH – Poly (allylamine hydrochloride)

PFOS – Perfluorooctyl trichlorosilane

PTFE – Polytetrafluoroethylene

PFOS – Perfluorooctyl trichlorosilane

PU – Polyurethane elastomer

Si – Silicon

rpm – Rotation per minute

Al_2O_3 – Aluminium oxide (alumina)

SiO_2 – Silicon dioxide (silica)

PEDOT – Poly (3,4 – ethylenedioxythiophene)

HCL – Hydrochloride

LBL – Layer-by-layer

ESRI – Energy Safety Research Institute

Chapter I: Introduction

Project Information

This project studies the use of green low surface energy materials (LSEMs) to obtain alternatives to the current costly and environmentally hazardous waterproof analogues. Currently, most widely used waterproof coatings are made using fluorocarbons which are not environmentally friendly and are very expensive.

In this thesis, we propose an alternative method of manufacturing superhydrophobic surfaces, through a cleaner and more cost-effective process using highly branched hydrocarbon chains.

The manufactured green materials are potentially an asset for SALTs Healthcare products, which is the company sponsoring a part of this research. Their interest in this alternative coating method stems from its applicability to different surfaces, the cost efficiency, its environmental friendliness, and non-hazardous waterproof material (e.g., in contact with the skin) compared to its analogues.

The methodology used in this thesis was inspired from natural plant leaves, such as Lotus leaves, which whenever water is dropped onto their surface, it cleans the surface, and the water bounces off. This type of surface is scientifically called superhydrophobic surface, in recent decades they have caught the attention of researchers due to their varied applications.

The manufacture was generally for the purpose of taking advantage of the superhydrophobic coating in different surfaces and commercialise for industrial and daily water repellence applications among other properties.

Potentially the solution proposed in this thesis can have many benefits for the environment as well as improve general quality of life. Since products coated with these solutions do not lose their recyclability, durability, non-hazardous (when in contact with the skin) and has the potential to enhance consumers satisfactions.

Objective of the thesis

The objective of this thesis is to synthesise, characterise and investigate a superhydrophobic surface using a novel methodology that is more cost effective and environmentally friendly. To this end, we will first outline a fabrication methodology that is easy, inexpensive, and environmentally friendly and we then characterise the output of this methodology, using contact measurements, IR spectroscopy, TGA and SEM.

Project rationale

This project (Development of Green Low Surface Energy superhydrophobic Material for Various Surfaces) was designed to develop alternatives to costly and environmentally hazardous waterproof analogues. Existing waterproof coatings are made of fluorocarbons which are bio-persistent and very expensive. The novel and green materials are valuable materials for SALT's products as solutions can be coated onto a different surface to make them environmentally friendly and non-hazardous (i.e., when in contact with the skin). This is because products coated with these materials can be recycled, have durability, and used for longer. These solutions can be coated in cardboard used in packaging which are usually not recyclable if they get wet. This is very likely in the UK and particularly in Wales. This project will allow the end users and companies to recycle their boxes (e.g., for storages and deliveries). As it is possible to synthesise Al_2O_3 (13 nm) with lanolin, we can create a coating that is cheap, easy to process and useful for SALT's as it is something that they can apply on their production line. We believe this approach is going to be best suited for SALTs with alumina nanoparticle and it will be investigated if instead of using expensive carboxylic acids that are bought form chemical companies. We could react the particles with the carboxylic acids that are in lanolin. The manufacturing of superhydrophobic surfaces remains lacking because most of the methods involve expensive equipment and being developed on small sizes.

Organisation of the thesis

The presented work is organised in seven chapters. On chapter two, the theoretical aspects of the superhydrophobic surfaces and their applications will be briefly introduced and explained. The fundamentals of the superhydrophobic surfaces are introduced, the basic concepts regarding wetting states, contact angle, the relationship between the superhydrophobicity and the surface roughness are described. On chapter three, the manufacturing methods for the superhydrophobic surfaces such as top-down and bottom-up methods are discussed followed by their respectively applications. On chapter four, the methodology used on this project will be presented. On chapter five, the analytical and measuring instruments such as IR spectroscopy, TGA and SEM and contact angles will be presented. On chapter six the results and respective discussion are included. On chapter seven we present the conclusions.

Chapter II: Background

On this chapter, we discuss the fundamental theories, and historical aspects of superhydrophobic surfaces.

Fundamentals of superhydrophobic surface

In the latest decades, the application of nanotechnology has obtained huge attention in the field of biomedicine. Nanotechnology was first introduced by American theoretical physicist Richard P. Feynman on '*There's plenty of room at the bottom'* and he described the concept of nanotechnology as the capability to manipulate matter on an atomic level and molecular scale [1], [2].

Since early 20st century, nanomaterials engaged in developing new possibilities to the area of research such as morphology control and surface functionalization. Meanwhile, the characteristics of superhydrophobic surfaces have captivated interest as a result of their potential applications in the manufacture of self-cleaning surfaces [3]. A generally known example of a naturally occurring surfaces with superhydrophobicity is the Lotus plant leaf [4], [5] in which the interplay of surface microstructure and chemical composition originates a spherical bead whenever water droplets fall on the surface. Consequently, the droplets of water roll off easily, cleans the surface and presents a contact angle of at least 150^{o} and a sliding angle less than 10^{o}. The predominant reason to observe a superhydrophobicity is the exclusive surface structure of the Lotus leaf, in addition, the fact that the surface of the leaf has a low surface energy material. In favour of having a superhydrophobic surface or coating, the surface must be in possession of hierarchical micro and nano roughness and low surface energy simultaneously. The hierarchical micro and nanoscale roughness due to the low wettability and self-cleaning characteristics traps air on the surface and as a result decreases the possibility of connection between the water and the surface [6].

The nature phenomenon of superhydrophobicity has permanently continued to be the motivation for researchers to expand the fundamental understanding about diverse phenomena taking place in it, such as the involvement of different materials, their properties, design, and textures.

The worldwide research on superhydrophobic surfaces has always focused on easier methods of manufacturing these materials focusing more on large-scale production, theories on their

distinctive wettability towards water and applications. Different methods have been effectively used to manufacture superhydrophobic surfaces on diverse substrates, also denoted to as '*top-down approaches'* such as photolithography and etching among others [7]. These methods are mostly dependent substrate and involve the use of expensive equipment. Therefore, coating methods also denoted as *'bottom-up approaches'* are classified as the most effective way to modify the properties on a solid surface and obtain superhydrophobic surface for large-scale practical applications.

It is generally known that appropriate roughness combined with the materials with low surface energy can be used to prepare superhydrophobic surfaces [8]. Moreover, most of the techniques used to manufacture superhydrophobic surfaces involve the use of not so cost-effective equipment and with most approaches limited to a laboratory scale. Most procedures used to obtain superhydrophobicity coating dwell mainly in two steps: first make a hierarchical surface roughness followed by the surface modification by a low surface energy.

The manufacture of superhydrophobic surfaces through this method has several applications, but these surfaces also carry several disadvantages that prevent the application of water repellency in certain materials. For instance, most manufactured superhydrophobic surfaces are characterized by poor mechanical durability which limits their use in commercial or industrial applications [9]. Alternatively, a possible solution for this drawback, which this study proposes to use, is to manufacture superhydrophobic surfaces in the form of nanocomposite coating followed by using a facile and effective spraying coating deposition technique that enables the deposition of the coating into different types of surfaces, which can potentially be used in "large-scale" applications.

The motivation of this project is to attempt to obtain environmentally friendly superhydrophobic surface and improve our understanding in this concept. By studying the fundamental concept of superhydrophobic surfaces, this project aims to manufacture it in simple, least time consumption, large, cost effectiveness and versatility (ability to adapt for different application).

Lanolin

Lanolin is a soft, waxy material originated from the oily coating on raw wool [10] that is broadly utilized in pharmaceuticals, cosmetics and food industries, above all, natural waxes have a lot of additional industrial applications [11]. Moreover, lanolin is generally regarded to be composed of a mixture of naturally formed esters[1] originated out of increased alcohols and increased fatty acids [13]. Crude lanolin also known as wool wax and wool grease incorporates between 5 to 25% of the weight of newly shorn wool. For instance, the wool from a single sheep can generate around 250-300 mL of recoverable wool grease [14]. Lanolin results from an extraction process, which initiates by cleaning the wool in hot water along with wool scouring detergent to eliminate dirt, sweat salts, wool grease (crude lanolin) and everything that could possibly be attached to the wool. The wool wax is then achieved by means of centrifugal separation or solvent extraction [14].

Nanoparticles

The history of nanomaterials is extensive, nevertheless, significant development inside nanoscience have been explored throughout the last two decades.
Nanoparticles have diverse applications such as industrial sector, domestic, medical and among other. On the other hand, nanoparticles can present a negative impact on the environment due to their specific properties such as potential toxicity, high surface reactivity that may cause several diseases for human health [15]. Nanoparticles are defined as a small particle in the range of 1 to 100 nanometres in size [16].

Even though beneficial aspects of nanoparticles are clearly distinguishable, certain number of reports have mentioned the negative impact of nanomaterials can cause on the living cells. The diverse array of surface properties reached resulted to the reduction in particle size that catalyses the surface chemistry of nanoparticles is responsible for their respective toxic potential [17], [18]. For instance, physical parameters such as surface area, surface charge and particle size have high importance [19], [20] on the provision of mechanistic details [21] in the

[1] Ester is a chemical compound obtained from an acid such as organic or inorganic that minimally one hydroxyl group is substitute by an alky group [12].

uptake, persistence, and biological toxicity of nanoparticles inside the cells. Based on previous reviews, it is evident that nanotechnology can modify the properties and applications of industrial and research materials. Both the selectivity and reactivity achieved as a result of the very small size have produced an extensive diversity of applications of nanoparticles [22].

Humankind are exposed to airborne nanosized particles on a daily basis [23]. Nanosized particles can enter the human body through different routes and could remain in the system [24] due of the incapability of the macrophages to phagocytose them [25]. If the persisting nanosized particles reacts with the body, stay inert or interact with the system will control and manage their toxic properties and is mainly dependent on their surface properties. Both the airborne inhalation of nanosized particles and entry through the respiratory tract are the most probably way of exposure to nanoparticles [26]. The absorbed nanoparticles are efficiently deposited by diffusional mechanisms in almost all areas of the lungs [17].

One of the side effects of vast utilisation of nanotechnologies is the release of nanomaterials in the environment. With the intensification of nanotechnology industrial use, the production of waste containing residue nanomaterials have become increasingly required [27].

One of the positive impact of nanoparticles is the fact that we managed to produce superhydrophobic surfaces. On the other hand, negative impact of the nanoparticle is the fact that after they are exposed for too long in water the nanoparticles lose their durability/coating. While the toxicity of silica and alumina nanoparticles is quite low but by washing off or removing the nanoparticle coating and subsequently exposed to the environment there is possibility that they might be toxic. Consequently, nanoparticles can negatively impact the environment due to their specific properties such as potential toxicity.

Size and shape of nanoparticles

During early research in nanoparticles, their size and shape were often an object of interest, because of their role in the fabrication of superhydrophobic surfaces. In addition, with more research it was discovered that the properties of such systems, such as: as clay pastes, paints, polymers and gels, relied to a great extent upon the size and shape distribution of the colloidal components [28].

The expansion of the scientific literature relating to nanostructured materials evolved greatly in last few years. Especially since different synthesis techniques are key elements applied to the field of research as well as engineering for tailoring nanoparticles shape and size, to accommodate specific purposes.

Nanoparticles are a promising material for a broad variety of applications such as chemistry, biology, materials, health science [29], physics, electronics. Researchers and more organizations are giving increased attention to nanotechnology since this field is opening new doors for industries.

It is well known that the size of nanoparticles the size of the nanoparticles can bring different properties such as electronic and crystal band structure change. Additionally, the effect of the nanoparticle size can also present properties such as surface plasmon resonance in some metal particles in particular on the surface, superparamagnetism in magnetic materials and quantum confinement effect within semiconductor particles [30]. Chart 1 illustrates the classification of the nanoparticles, although the group of inorganic nanoparticles are most common used nanomaterials, and this is since they present excellent conductivity, catalytic abilities, and potential applications however the stability of colloidal nanoparticles obtained after functionalization remain serious challenge.

Motivated by these potential applications, number of groups of researchers have dedicated their attention to the fabrication of inorganic nanomaterials because these nanoparticles demonstrate properties that bridge the gap among bulk materials and molecular structures [31].

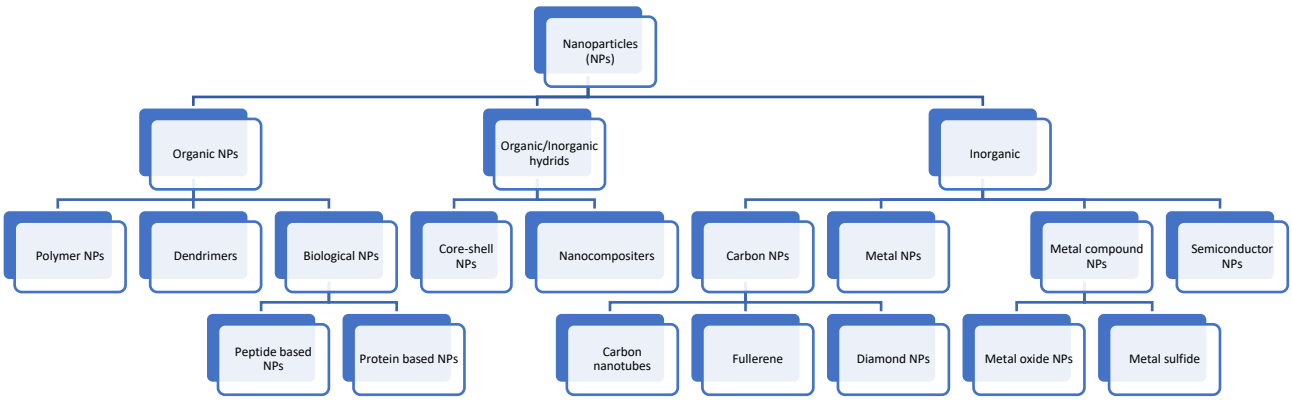

Chart 1: Classification of nanoparticles [30]

Superhydrophobicity

Whether wetting behaviour happens between a liquid and a solid surface is dependent on the surface being either hydrophilic, hydrophobic or superhydrophobic [32]. Figure 1 illustrates how water behaves on a solid surface. For this experiment, we focus on superhydrophobic surfaces.

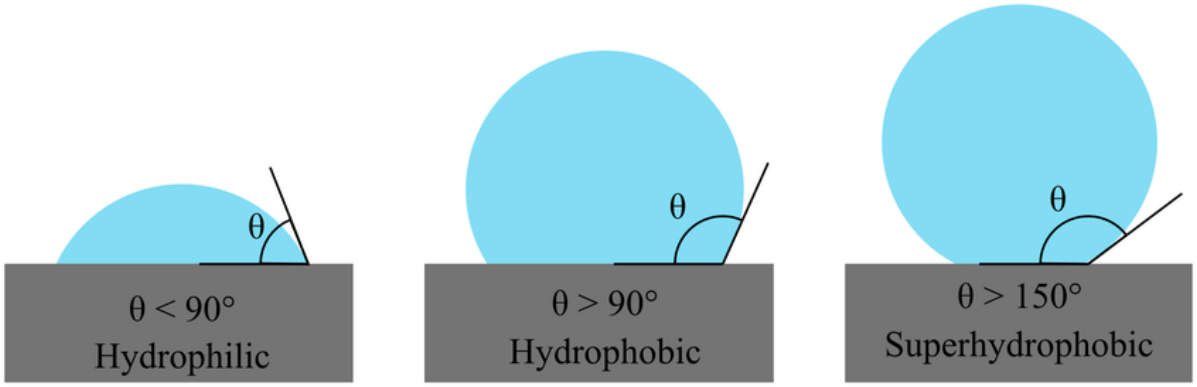

Figure 1: Classification of contact angle coating [33]

A surface can be classified as hydrophilic, if the surface has a high attraction with water [32], hence water spreads out consistently on a solid surface resulting in high surface energy, water is absorbed and the surface is wetted [32]. This type of surface is characterized by a low contact angle, range of 10^{o} to 90^{o} [32], [34].

A hydrophobic surface is capable of repelling water and has low affinity between the surface and water. On contact the water beads into small spherical droplets and the shape of the droplet presents a low surface energy and high contact angle between 90^{o} and 150^{o} [32], [34]. The term superhydrophobic was introduced by Reick, in 1976 [35], superhydrophobic is a special wetting phenomenon which has extreme water-repellency, in which the shape of the droplet of water remains almost spherical and the force of adhesion is negligible [36], [37]. Generally, the superhydrophobic surface has a wetting contact angle of at least 150^{o}, however, contact angle can barely exceed 120^{o} on a smooth surface [38], even on highly low surface energy materials, e.g., silicone resin of 22 mN/m, fluorine resin of 10 mN/m [39].

Barthlott and Neinhuis studied the surface chemicals of beyond 200 water-repellent plant species, the micro morphologies and their self-cleaning abilities [4], [40]. Illustrated by the 'leaf of the Nelumbo nucifera', the wavy surface texture was essential in increasing the repellence of water and self-cleaning of the leaf [41], this illustration was based by pouring water on the surface of leaf designated as rough structure and rolled off easily as a consequence eliminate impurities from the surface although some residues remain [41]. This mechanism was called the 'lotus effect' [4].
In 2002, the superhydrophobic mechanism was clearly interpreted, the 'lotus effect' with high contact angle and low sliding angle, as a consequence of micro and nanoscale hierarchical structures: nanostructure contributed to high apparent contact angle, therefore, the water sliding angle reduces for nano and microstructures effectively [8].

Superhydrophobic materials maintain air at the solid-liquid interface, when in contact with water. These surfaces possess high apparent contact angles, by definition 150° [34], [36] as a result of the composite solid-air surface formed under a water droplet, consequently they are characterized by very low roll off angle, very low contact angle hysteresis [42] and very low adhesion. The droplets of water bounce off the surface and it can be applied as water repellent, self-cleaning [43], micro and nano devices [44], anti-icing [45], anti-corrosion [38], anti-friction, drag reduction [46] and biotechnology [42], [47].
As seen in figure 1, for the superhydrophobic droplet of water, a spherical shape is observed assuming that the droplet of liquid is suspended in a vapour phase and the shape of the droplet of water is determined by the gravity as well as the surface tension acting on the liquid-vapour

interface (γ_{lv}). Moreover, cohesion in all directions attracts every molecule inside the droplet. However, the molecules in every direction of the droplet and the surface molecules are consequently pulled inwards, hence the droplet presents a minimum surface area. Taking in consideration that the sphere is the one presenting the smallest surface area, the surface tension force ($\gamma_{lv}\ x\ d$) causes the droplet to form a spherical shape [34]. Meanwhile, the gravitational force ($\rho g d^3$) attempts to spread the droplet across the surface [34]. In mathematical terms, the droplet size is compared with capillary length, k_c and the equation 1, can be used to determine if the droplet size is smaller or not and is described mathematically as:

Equation 1

$$k_c = \sqrt{\frac{\gamma_{lv}}{\rho g}}$$

Where, γ_{lv} is interfacial tension liquid-vapour, ρ density and g the gravity.

At ambient conditions, the capillary length for water presents a value of around 2.7 mm. If the droplet of water is smaller than the capillary length, ($diameter\ < k_c$), the gravitational force is ignored and the surface tension dominates [48], [49].

Capillary length, also known as capillary constant, is characterized by the ratio of the Laplace pressure – associated to the size of a microscopic droplet – to the hydrostatic pressure [50], [51], notably is the length factor that links surface tension and gravity.

The Sphere Theorem

It is established that a sphere is the least surface area that can surround a given volume. Where the radius r is the distance from the centre to its perimeter; the international system (SI) units for radius and volume v are m and m^3, respectively.

Equation 2

$$V = \frac{4}{3}\pi r^3$$

Spherical shapes is predominate in contact angle problems on the ground that a sphere has the good property which is the intersection between a given plane and the apparent contact angle, moreover, this interaction is conditional to the distance of the plane from the centre of the sphere and not on the orientation of the plane [51].

The gravity in spherical shape as energy minimizers is presumed to be absent, therefore the total energy of the system is characterized as the sum of the free surface area and the contact energy. Mainly, the sphere theorem states that if a spherical droplet appears to reach the surface of a convex region with precisely correct contact angles, consequently the spherical droplet reduces the total energy [51].

Natural superhydrophobic surfaces

Water droplets are highly likely to roll off from superhydrophobic surfaces and this phenomenon is similar to the natural lotus leaves. Superhydrophobic surfaces play an important role in the fundamental research in fields of chemistry, biology, engineering and physics [4] ,[52] , [53].

An additional condition sometimes included in the superhydrophobic definition is a low roll-off angle, which is below 10° [54] so the droplet of water does not stick to the surface and turns out to be spherical. The 'Lotus leaf effect' was discovered by Barthlott and Neinhuis [4], [34], [36] whom concluded that a waxy material and numerous microscopic bumps are the primary cause of superhydrophobicity in leaf surfaces [34] and as a result the surface is observed to have a self-cleaning [55], water repelling properties. The exclusive ability of water repellency on superhydrophobic surfaces makes the surface practical to operate as an excellent barrier to prevent the engineering materials from corrosion, icing, friction [35], [56].
As seen is figure 2, higher contact angle results into more superhydrophobic surface and superhydrophobicity can be observed in Lotus plants, insects, and birds.

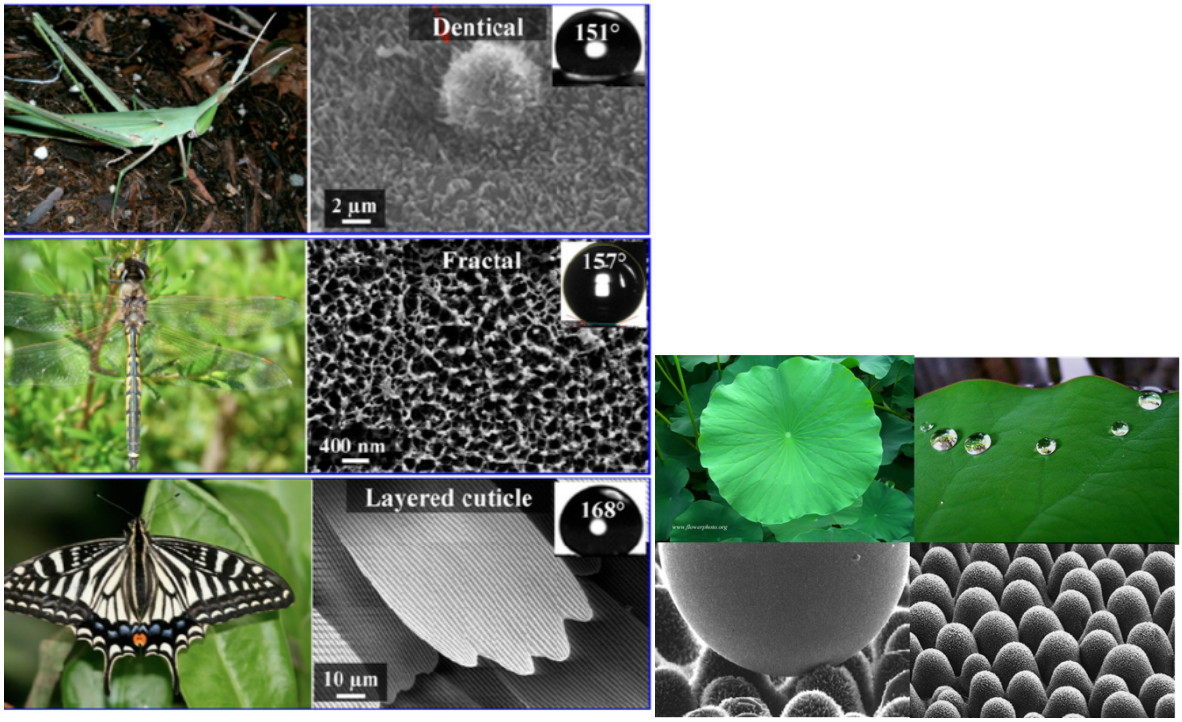

Figure 2:Lotus Effect; images of water droplets resting onto different substrates and SEM of Dentical, Fractal and Layered cuticle illustrating a water contact angle [57]

A liquid droplet can be in two different states when resting on a solid surface which can be described as 'Wenzel state and Cassie-Baxter state' [42]. As seen in Figure 3, once hydrophobic surfaces are roughened or patterned in appropriate length scale and morphology feature of the nanoparticles films, air is trapped between the surface structures and liquid droplet and this phenomenon is called Cassie state [42] for instance the increase in roughness leads to higher hydrophobicity, the water droplet stays at the top of the asperities and can also easily roll off from the solid surface.

In the other hand, if water droplets wet the surface in parts or consistently, they form a liquid film on the surface with no air void retained which is a phenomenon called Wenzel state [42]. Consequently, Cassie-Baxter state might be more desirable compared to Wenzel state to obtain superhydrophobic surfaces.

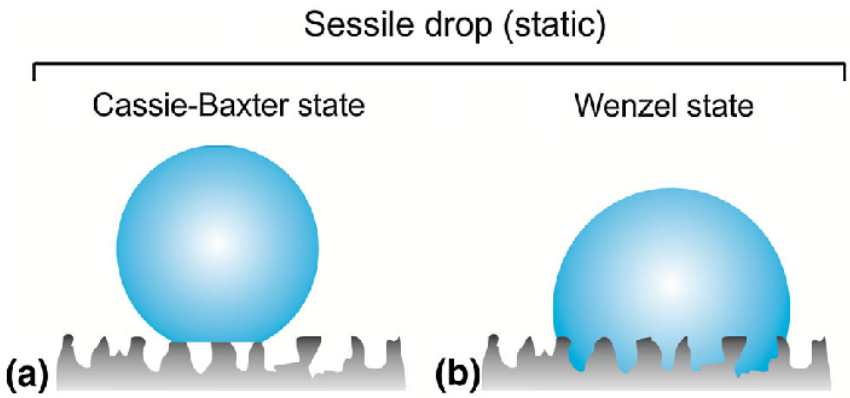

Figure 3: Different wetting states [58]

Wettability is an important property of superhydrophobic surfaces and is determined by the interfacial tension which can be described as the energy per unit area at the surface between phases [59], in other words, wettability is the ability that a liquid has to maintain in contact with a solid surface.

Although a strategy was developed by Wenzel to obtain superhydrophobic surfaces such as increasing roughness, the solid-liquid contact area was similarly increased a "sticky" surface in the Wenzel state was obtained [60]. Consequently, Cassie and Baxter established a different process to describe wetting on porous surface [61] and that was the birth of the name Cassie-Baxter wetting state [62]. An illustration of this liquid droplet is seen in figure 3a), the liquid droplet is suspended on such surface this phenomenon is a result of the contact of the liquid with the solid surface and gas phase.

As is generally known, in a water/air/solid system, superhydrophobic surfaces arise from the establishment of new composite substrates. In accordance with the theory established by Cassie, consistent air molecules are present on the surface of micro/nanostructures, developing a water/air/solid interface. When a surface roughness also known as surface texture acquires in contact with water, air trapping in the roughness area makes a significant contribution on the ability to increase the hydrophobicity of the surface [63].

Surface Free Energy (SFE)

Contact angle is an essential parameter to determine the wetting ability of a solid surfaces. Physical and chemical properties can both be classified as solid surface properties. For instance, physical properties can be described as the properties that are independent of the atomic elements, such as, surface morphology, which just relies on atomic arrangement. In contrast, surface chemical properties rely on the elements, such as, surface energy, that can be defined for presenting higher energy for silicon when compared for wax [64]. Additionally, surface morphology strongly influences the surface phenomena, such as, adhesion, contact angle, friction, light reflection and photon absorption [65].

This focuses on the main principles of contact of angle including the theoretical background and importance of contact angle. Furthermore, important concepts related to contact angle such as: advancing, receding and hysteresis contact angles will be described.

Roughness measurements

Roughness measurements parameters are component of surface texture and the measurements begin from height variation of profiles (one dimension, 1D) or surfaces (two dimensions, 2D) and in the same way, used to demonstrate the level of surface roughness [66]. In general, the measured height data is in discrete format[2] and the distance in the midst of two data points also known as sampling distance is constant. Roughness profiles are much easier to measure, moreover, they can be defined as the result of electronic high-pass filtering of the primary profile with a cut off wavelength and many surfaces of those roughness profiles are developed from parallel profiles [67]. Stylus instruments are commonly used in profile measurements and the primary advantage of it is the fact that the electrical signal available could be addressed to achieve any required roughness parameter, registered for demonstration and analysis [68]. In this project, a scanning electron microscopy (SEM) was used to carry out the micro/nanoscale roughness measurements. The fundamental principle of these instruments can be described as: a probe scans through a profile and its interactions with the surface are registered and analysed to collect profile height data. The interactions it might be contact forces for the majority of stylus instruments and atomic force microscopy [69]. Resolution of profile height measurement

[2] Discrete format data is rearranged in in rows and columns

depends on probe size, for stylus instruments it is commonly in micron-millimetre scale, on the contrary, in nano to microscale for SEM.

The difference between liquid droplets and rigid spheres at an interface

Although the Neumann's force balance is consistently applicable at the triple line, it is important to mention that there is a significant difference among a deformable liquid droplet and a non-deformable body at an interface. In the liquid droplet illustration, the vertical profile of the liquid droplet presents a singularity at the intersection of the triple line, for example, the perpendicular outline is continuous, on the other hand, at the point of intersection with the triple line the vertical profile is not distinguishable. In this instance the Neumann law tends to be used to describe the contact. At the same time, a rigid body – for example a rigid sphere – acts as a solid planar surface and the Young law may be used to characterize the contact at the triple line [51].

In the occasion of a rigid body, the question is: what is the outcome of the non-zero resultant perpendicular to the surface? In the occasion of a spherical rigid body situated at the surface of a liquid with a well-formed or balanced contact line, the answer can be as simple as: the normal resultants though/along the triple line would cancel by symmetry [51].

In the occasion of a particle of nonspherical shape, the particle will keep rotating until an equilibrium position is found for the particle in which the resultants of the normal components of the surface tensions would cancel. An interesting study of the orthorhombic particles at balanced position towards an interface has been carried out by Morris et. al. [70]. They have several times shown that the shape of the particle, particularly its aspect ratio, changes the balanced position of floatation [51].

Surface wettability

The word of wettability is vast, as it plays a very important part in different technological areas [42] and the wetting property is one of the most significant parameters of the solid surface [35], [56]. Wettability can be defined as the ability of water or any other liquid to disperse on a solid surface [71] and there are two different forces behind wettability adhesive [72] and cohesive.

In this section, some important concepts of wettability such as work of adhesion and work of cohesion are introduced and these two concepts are valid for solids or immiscible liquids. When

implemented to a solid and a liquid interface, Young-Dupré equation can be produced based on the concept of work of adhesion joined with Young's law [51].

Work of adhesion

Adhesive work (liquid to surface) are the forces between solid surfaces and water droplets. These forces can be controlled by chemical or physical bonding; thus, water droplets can roll out easily on surface materials with low adhesive force. However, with high adhesive force, they spread across solid surfaces resulting in the separation of the solid from the liquid. Adhesion among a solid and liquid is characterized as the work needed to separate the solid from the liquid. Consequently, the work of adhesion includes the creation of new surfaces such as vapour-liquid and solid-vapour, and the elimination of the liquid-solid surface [73]. The Dupré equation is described mathematically as:

Equation 3

$$W_{ls} = \gamma_{sv} + \gamma_{vl} - \gamma_{ls} = W_a$$

Where W_a is the work of adhesion, W_{ls} is the work needed to separate the solid from the liquid surface and γ_{sv}, γ_{sl} and γ_{lv} are the interfacial tension of solid-vapor, solid-liquid and liquid-vapor respectively.

Work of cohesion

Cohesive work (liquid to liquid) are intermolecular attractions between molecules/atoms of any liquid by primary or secondary bonding, such as hydrogen bonding. In other words, liquid drops produced by interconnected water polar molecules with strong hydrogen bonding can form a spherical shape, especially on low energy surfaces. In contrast, with high energy surfaces, the shape of water droplets is spread even or flatten completely and the cohesive is characterized by the separation of the liquid from itself. In a similar way cohesion can be understood as the formation of two liquid-vapour interfaces and the elimination of a liquid-liquid interface. The cohesive nature of a liquid (or solid) requires the separation of the liquid from the liquid [73]. On the other hand, the work of cohesion, W_c, can be seen to be

Equation 4

$$W_c = 2\gamma_{vl}$$

Therefore, the balance between work of adhesion and cohesion can control surface wettability and, as a result, surface hydrophobicity. Furthermore, using contact angle methods, the surface wettability can be measured experimentally. Alternatively, the surface energy can be stated as half the cohesion.

On the other hand, wetting properties of realistic surfaces are more complicated taking in consideration that such surfaces are normally rough and chemically heterogeneous[3]. Wenzel described the wetting phenomenon as a thermodynamic process from the perspective of specific surface energy [35].

Characterisation of a solid surface

One approach to characterise the solid surface also known as solid-gas or solid-liquid interface, is the use of several liquids with different surface tension, that can be achieved in series that are composed of hydrocarbons with identical functional group and observe the surfaces that get wet and the ones that do not get wet [73]. Generally, we can conclude that that for wetting behaviour, the surface energy of the solid-gas interface is very likely to be greater compared the surface tension of the liquid-gas interface. On term of fluids such as gas and liquid, the order of priority can be arranged, which tends to give a good sign of the solid surface energy from the non-wetting condition. Despite that, we can go beyond than the previous description of fluids using the homologous series of liquids, as drops, on the surface [73].

Measurements of surfaces with superwettability

One of the principal parameters for the study of superhydrophobicity is contact angle. The contact angle measures the angle of wettability created by the liquid on a solid surface. In this section the concepts such as: static and dynamic (advancing and receding) contact angles will be described.

[3] Heterogeneous composed of different interfaces

Contact angle

Whenever a liquid is disposed on a solid surface it can result in two distinguished observations, such as, the liquid spreads on the surface and creates a continuous film or creates discrete droplets [73]. Contact angle (CA), one the main parameters used to study surface wettability, measures the degree of wettability on a solid surface produced by a liquid [42] and this parameter can be defined as the angle formed by the water droplet when it reaches the solid surface [34]. In addition, CA is grounded on the assumption of an ideal smooth surface. CA was initially noted by Thomas Young [74] including the concept of the *interfacial tensions of the liquid, solid and vapor interfaces* [42]. Young associated the CA to the interfacial tensions of the liquid, solid and vapor, based on the fact of the equilibrium at the triple line, i.e., the line in which occurs contact between the solid, liquid and vapor phases [42].

The calculations for the contact angle are based on the membrane surface topography [36] that affects the liquid or solid interface adhesion [75]. Moreover, the surface topography can be classified in two distinct type of surfaces: smooth and rough [76].

Historically, in 1804 and 1805, Thomas Young was the first scientist to describe contact angle [36], [74], and in nineteenth century [34] expressed a mathematical term, which is used to determine the contact angle of a droplet of liquid on a solid surface. The diagram of contact angle can be seen in Figure 4, the diagram also demonstrates the shape of droplet attached by the liquid at the three-phase line in contact aiming to decrease the total energy of the system, the wettability of a solid surface can be measured using Young's equation and contact angle is expressed mathematically as:

Equation 5

$$cos\ \theta_o = \frac{\gamma_{sv} - \gamma_{sl}}{\gamma_{lv}}$$

Where θ_o is the surface contact angle, and γ_{sv}, γ_{sl} and γ_{lv} are the interfacial tension of solid-vapor, solid-liquid, and liquid-vapor, respectively [N/m] [J/m^2].

Even though Young's equation was in the first place implemented for a liquid droplet on a solid surface in air, it has been implemented as well as to a liquid droplet on a solid surface in the existence of a solid liquid.

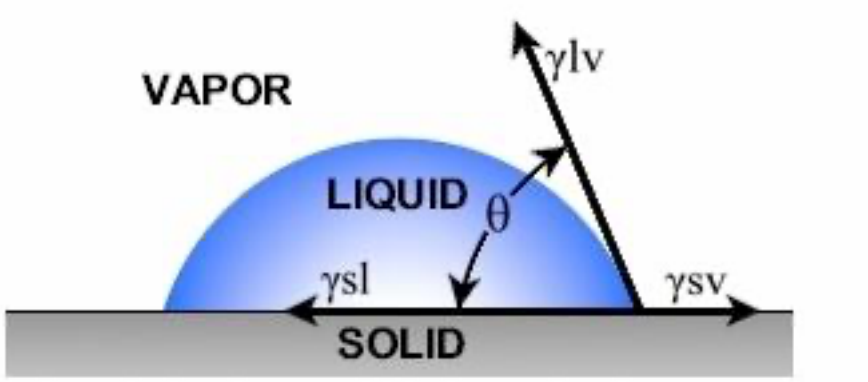

Figure 4: Contact angle at three-phase interface on a smooth surface [77]

Young's equation can also be obtained from the surface and interfacial energies and their changes [78] but will only be interpreted by surface energies and not as a balance of surface tensions[4] [79]. The contact angle is an important parameter used to measure the contact between the three phases such as solid, liquid and vapor. For small droplets on a horizontal surface the droplets tend to form spherical caps, spheres intersecting the surface [80]. Other factors, for example, electric fields, might as well affect the droplet shape, in which the gravity plays a part in deforming larger droplets. At the contact line the angle obtained tends to the Young angle except if the contact line also known as solid surface is not stable such as being in movement [81].

The Young's angle is theoretical the foundation for contact angle measurements which constitute the lowest free energy equilibrium state between the three states of matter regarding a drop of liquid on a surface [82]. The contact angle parameter is an ideal value that has at least one of the five assumptions: surface is smooth, rigid, chemically homogeneous, insoluble, and non-reactive. Taking in consideration that the real-world samples violate at least one of these assumptions, a range of the contact angle is the value presented for the most researchers and scientists in their reviewed papers. Surface heterogeneities, for example roughness or chemical differences, can enable liquid drops to exist in a number of metastable states [83]. An example of this in everyday life is the differences in the shape of droplets of water on a car after it rains. Even though the car is clean, the water droplets would form various angles on the surface because of the potential differences in the finish roughness, tilt, etc. In the same way, static

[4] Surface tension is the tendency of liquids to decrease into minimum surface area possible

droplets of water provide only restricted information regarding the behaviour of a surface because these droplets of water are highly likely to exist in these metastable states against to global lowest-energy state.

Static contact angle

The characterization of the wettability[5] is usually obtained through static contact angle measurement of a surface or material. Generally, volume of liquid between 2 to 5 µL were used to obtain the various values of contact angles. Diverse fitting modes of the static contact angle such as circle fitting, ellipse fitting, tangent searching, and Laplace-Young fitting were used to obtain the appropriate shapes of water droplets on the solid surfaces. It is notably that different fitting modes will result in different values for static contact angle, such value for the superhydrophobic surface can vary from 150º to 180º with similar shape [84]. For instance, water droplet of volume 5 µL, presents a contact angle of about 156º by using ellipse fitting, comparing to Laplace-Young fitting mode which can reach a contact angle of 179º [84]. Consequently, the fitting mode must be clearly well-known with static contact angles to reflect the real situation of solid surface wettability [84]. It is important to use the same volume of liquid droplet whenever measuring the contact angle in case there's needed to compare the superhydrophobicity of different surfaces. Because the contact angle is mainly influenced by the volume of the liquid droplets and the gravity force, volume between 2 or 3 µL may be a convenient value to use while measuring contact angle of water droplet on solid surfaces. However, it is relevant to mention that volume lower than 4 µL is highly difficult to obtain for water droplet when measuring a contact angle, this is due to the fact of the low water adhesion in multiple superhydrophobic surfaces [85]. In the act to decrease the effect of the deformation of the water droplet produced by the gravity force, Zhang et al. [84] suggested a new method to evaluate the contact angles by using a significantly lower volume of water droplet. First, a volume of 5 µL of water droplet is deposited on a superhydrophobic surface and a contact angle of about 154º is obtained. In the case of volume of 0.3 µL water droplet a contact angle of 173º was obtained following a vaporization for around 40 minutes under ambient conditions [86].

[5] Wettability refers to the study of how a liquid interacts with a surface

The standard droplet of water size used in contact angle measurements was in the range between 1 and 10 microliters. Consequently, water droplets larger than 10 microliters are not commonly used. The influence of water droplet size in microliter range has been widely studied. Drelich [87] reviewed these studies and come to the conclusion that the droplet volume has no significant effect on the contact angle with close-to-ideal surfaces, such as clean quartz plates. The close to perfect surface present characteristics such as being smooth, rigid, chemically homogeneous, insoluble, and non-reactive [88]. However, the larger a contact angle hysteresis is, the greater impact droplet volume has on contact angle. The contact angle hysteresis can be quantified by dynamic contact angle measurement, where the advancing contact angle is the largest value and receding contact angle the smallest value.

Dynamic contact angle

The contact angle hysteresis can be employed to consider the different superhydrophobic state, in which for Wenzel state the roughness increases the surface area of the solid while for Cassie state air can remain trapped at the bottom of the water droplet. For example, Cassie state frequently demonstrates a high static contact angle and a low contact angle hysteresis under normal conditions [89]. Consequently, a set of procedures have been established to obtain the contact angle hysteresis measurements, such as advancing angle, receding angle, tilt angle.

Kwoun and co-workers [90] introduced a methyltrimethoxysilane (MTSM) sensor to distinguish superhydrophobic surfaces that presented an identical contact angles yet distinct contact angle hysteresis by employing high-frequency shear acoustic waves produced or created by a piezoelectric quartz resonator thickness-shear mode (TSM) sensor. Through the TSM measurement, frequency between 1-100 MHz, in order of 10-100 nanometres were obtained for the penetration depth. If the superhydrophobic surface presents a low contact angle hysteresis, the water layer shall not wet the top of the surface and remains hard to infiltrate into the roughness structure. Moreover, for the low contact angle hysteresis surface the harmonic frequency shift is significantly lower compared with a high contact angle hysteresis surface.

As the surface is moved forward to be in contact with a water droplet suspended from a needle, the advancing and receding contact angle of a nonplanar surface, such as, gold thread which has a larger radius, can be measured [91]. If the advancing and receding contact angle are practically not observed, the droplet of water just is displaced at one side of the respective gold thread with a small shape deformation. On the other hand, if contact angle hysteresis is

obtained, the droplet of water will stick to the surface and shall not move. The findings show that the interaction among the droplet of water and the gold thread is significantly weaker compared to the droplets of water and needle.

Furthermore, Gao and McCarthy reported a procedure to differentiate the contact angle hysteresis by decreasing the superhydrophobic surface towards a droplet and compressing/releasing several times [92]. It has been showed that the surface which presents low contact angle hysteresis it's unable to adsorb the droplet of water after release; on the other hand, the superhydrophobic surface that presents high hysteresis contact angle possesses a strong affinity concerning the droplet of water.

The drop bouncing off method has also been shown to be adaptable for the characterization of hysteresis contact angle, for instance, once a liquid droplet is released towards to a solid surface without wetting the surface, the droplet will rebound with extraordinary elasticity [93]. Consequently, the bouncing capability of a liquid droplet on superhydrophilic surfaces may as well be reflected on the hysteresis contact angle.

Sliding angle (SA)

Other important parament to characterize superhydrophobic surfaces is the sliding angle also known as tilt angle, that refers to critical angle permitting the droplet of water to move while inclining the solid substrate [94] and this method can be used during experimentally measurements through a simple inclined plane, moreover, for this project a Drop shape analyser (Krüss) was used for this analyses. A superhydrophobic surface with a sliding angle lower than 10^{o} frequently demonstrates that the surface possesses a self-cleaning property [8], [95]. Furthermore, it is important to mention that the sliding angle makes no attempt to be the result of the difference between advancing angle and receding angle.

Moreover, it is possible to use surfactant solution as an alternative way to measure contact angle to reflect the hysteresis contact angle. Furthermore, McCarthy [96] as well as Ferrari et al. [85] demonstrated that adding surfactant molecules to water results in the reduction of contact angles on certain superhydrophobic surfaces that presents high hysteresis contact angles. Nevertheless, for superhydrophobic substrates with low hysteresis contact angle, the contact angles are normally similar and there is no difference either if a pure droplet of water or a droplet of water including surfactant is used as a probe. Therefore, this method can be

developed to differentiate among a self-cleaning surface and a normal superhydrophobic surface [85], [96].

Contact angle hysteresis (advancing and receding)

In majority of systems there is a certain uncertainty in contact angle referred to as contact angle hysteresis [81]. After the approach of contact angle was introduced, it was understood that contact angle alone cannot fully characterize wetting behaviour. Additionally, there is more than single value of the contact angle, however it can have a set of measurements, such as $\theta_{rec} \leq \theta \leq \theta_{adv}$, where θ_{rec} and θ_{adv} are the receding and advancing contact angles, respectively [42]. The advancing and receding angles describe the *dynamic wettability of a solid surface* [36].

Leach et al. (1962), studied the characteristics of advancing and receding contact angles, by locating a drop of oil among two parallel plates, one of the plates was displaced parallel to the stable plate enabling water to advance against the oil droplet and recede opposite of the droplet [71].

As seen in Figure 5, the contact angle can be obtained on a tilted surface, although it is acknowledged that the obtained readings through this process do not always give the most accurate measurements for the advancing and receding angles [97]. The difference between the advancing and receding contact angle is called contact angle hysteresis [42], [98]. Hysteresis angle can also be defined as the water droplet stickiness with a solid surface [34], this angle provides information related to the chemical and topographical heterogeneity [57].

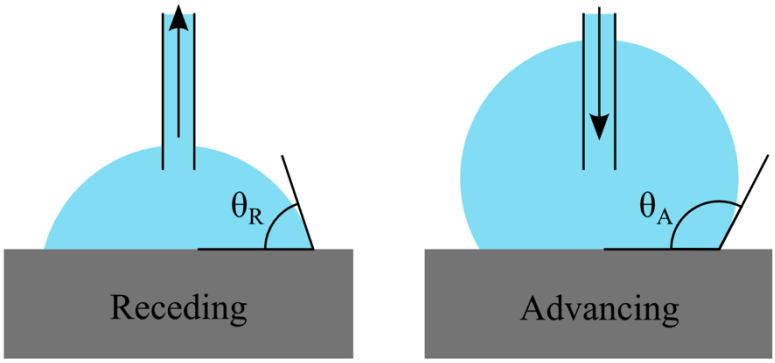

Figure 5: Advancing and receding contact angle [33]

The static contact angle may vary, the contact line initiates a movement at a specific angle such as whenever the liquid front is classified as advanced and at a different angle when it recedes [99]. For this reason, it's easier to obtain the contact angle measurements, frequently the highest and the lowest stable angle are measured can be classified as either the advancing and receding angles. This is normally performed by introducing liquid gradually into a droplet and removing it again. Frequently the advancing and receding angles are of more convenient to make use of when compared to the static contact angle, although the static contact angle value can be used to derive surface energies [81]. For instance, the advancing contact angle is associated to the wettability and surface energy, on the other hand, the receding contact angle is associated to the repellency of the liquid from the surface and surface roughness [100].

The effect of roughness on contact angles

Fully wet surfaces: Wenzel's equation

If the roughness is increased the water at the beginning wets the whole surface, the increasing surface area of the interface indicates that the contact angle higher than 90^{o} increases for the advancing contact angle on a surface with a flat, on the other hand, for contact angle lower than 90^{o} the advancing contact angle decreases. A surface that presents precisely 90^{o} contact angle would demonstrate no effect of roughness [81]. The fully wet surfaces can, for the reasons above, be taken into consideration to be an amplification of the properties of the surface through the roughness. The contact angle of a rough surface of the fully wet surfaces can be calculated on the basis of Wenzel's equation [101], which changes the cosine of the angle by the specific surface area, r, and it's important to mention that the amount of times the surface is greater than a flat surface of the same size [81]

Equation 6

$$cos\theta = r\ cos\theta_Y$$

Where θ is the apparent contact angle and θ_y is the equilibrium contact angle from Young's equation on an ideal solid without roughness.

It has been noticed that roughness of the solid wall changes the contact among the liquid and the solid interfaces. However, the effect of roughness on the contact angle is not intuitive. It might seem a surprise the fact that roughness amplifies the hydrophilic or hydrophobic character of the contact of an interface with a wall [51].
A significant finding is that the scale of the roughness on the solid surface is small in comparison to that of the droplet. In fact, if not, it would be impossible to describe a unique contact angle; for instance, in the event that the characteristic dimension of the asperities[6] of the surface presents a similar order to the droplet size, the droplet position would consequently alter according to the position where the droplet is placed [51].

Bridging the roughness: Cassie-Baxter's equation

Cases where the surface is roughened, can be advantageous for the liquid assuming that it can sit on the top of the roughness and also decrease the area of the interface [81].
In 1944, the most simple expression for the contact angle on a surface in which is roughened was expressed by Cassie and Baxter [61]. It is assumed that the cosine of the angle to be the average of the cosines of both contributing surfaces weighted by their relative areas, represented by f, the fraction of the interface which is solid [81].

Equation 7

$$cos\theta = f\ (1 + cos\theta) - 1$$

This equation acknowledges the solid-liquid and the liquid-gas interfaces to be planar, which only happens if the surfaces is composed of equal height flat-topped pillars. The original Cassie

[6] Asperities are high spots on surfaces that come into contact during wear or friction

and Baxter paper permitted for deviations from this in practical terms the use of Wenzel's equation for the wetted part and permitting changes in the effective roughness with penetration. The principal problem with this approach is that it is frequently hard to determine where the liquid-solid interface reposes [81].

Both Wenzel and Cassie-Baxter equations can be obtained from forces at the contact line same as from interfacial areas. The effectively use of the interfacial areas contemplates a reduction to a minimum of the surface energy of the system. A force-balance argument is equivalent but takes the view that the surface energy from the forces it produces conceptual challenges whenever sharp edges are considered [102]. Due to the interfacial area in the Wenzel case and the reduction in the interfacial area in the Cassie-Baxter case it is noted that the hysteresis increases in the Wenzel state as well as decrease in the Cassie-Baxter state, resulting in an increase to the low water adhesion in the Cassie-Baxter state.

The Cassie-Baxter law describes several unexpected experimental results. From time to time – if sufficient care is not taken during microfabrication – a microfabricated surface might present chemical non-homogeneity and the wetting properties are not the ones that were planned. For instance, if a uniform layer of PTFE is deposited on a substrate, the surface should be transformed into a hydrophobic. On the other hand, in case the deposited film is too thin, the PTFE film might be porous and the coating non-homogeneous; the wetting properties are therefore adjusted in accordance to the Cassie-Baxter law and the gain in hydrophobicity might not be as higher as anticipated [51].
In relation to Wenzel's law, an important observation at this point is the fact that the scale of change of the different chemical materials of the solid surface is lower when compared to that of the droplet. Indeed, if this is not the case, it would be impossible to characterize a unique contact angle [51].

Wenzel-Cassie hysteresis

It is important to mention that the situation we have just characterized does not all the time correspond to reality. It occurs that a droplet is not all the time in its lowest energy level and from time-to-time droplets are in metastable regimes, for example, droplet deposited through a pipette on a pillared surface. Even though it should be in a Wenzel state and droplets are

meant to enter among the pillars, it is more likely to stay on top of the pillars. It requires an impulse, mechanic, electric or acoustic to enter or penetrate the predictable Wenzel state [103], [104]. Cassie droplet can be shifted to a Wenzel droplet through electrowetting actuation [105] as seen in the figure below in a) the droplet initial is in a Cassie state without actuation and on b) the droplet immerses in the substrate due to the electrowetting actuation and the droplet has now transited from Cassie state to Wenzel state [51].

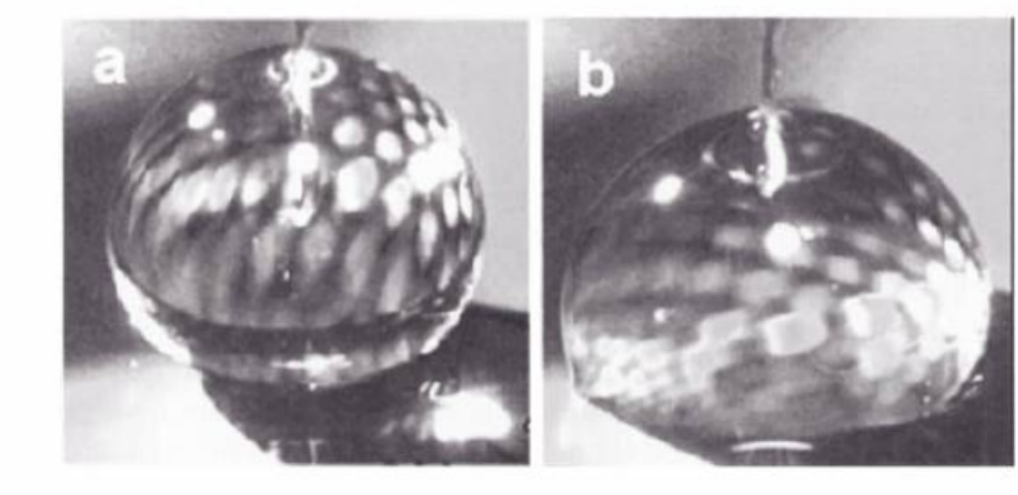

Figure 6: Cassie state without actuation and Wenzel state with electrowetting actuation [51]

Chapter III: Literature review

This chapter presents a summary of previous work that explores different superhydrophobic surfaces manufacture methods.

Manufacturing of superhydrophobic surfaces

Superhydrophobicity is obtained by selecting the appropriate roughness, surface texture and low surface energy materials. In this section, we discuss approaches used to manufacture of artificial superhydrophobic surface including some used by previous researchers which were inspired by nature. Different methods have been used to synthesise nanoparticles of diverse size, shape, and orientation. Generally, these technical methods can be classified as top-down and bottom-up methods. Both methods are very important for the manufacture and improvement of fabricated superhydrophobic surfaces. The main problem with top-down approach (physical methods) is regarding the imperfection of the surface structure that is observed, which would have a considerable impact on both the physical and chemical properties of nanostructures and nanoparticles. The bottom-up methods present more notable advantages as most of these are associated with a relative lower cost and a straightforward fabrication method when compared to top-down methods.

Top-down methods

Generally, the top-down methods, are related to the material removal process. Top-down methods involve the breaking down of the bulk material into nanosized structures or particles and the main challenge during those process is the imperfection of surface structure.

Photolithography

Ou et al., 2004 [106] used photolithography method to fabricate superhydrophobic/ ultrahydrophobic surfaces from silicon wafer. Figure 7 illustrates the experimental flow cell and was used to measure the pressure drop resulting from the laminar flow of water throughout a rectangular microchannel.

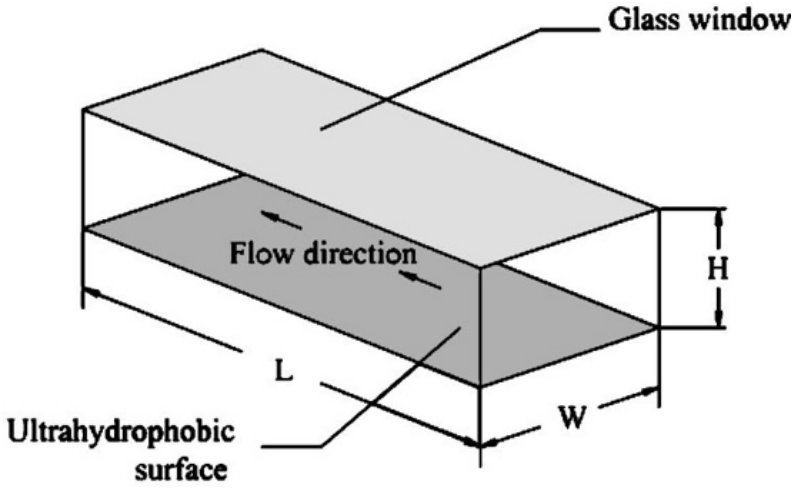

Figure 7: Schematic diagram of the experimental microchannel flow cell including the important physical dimensions [106]

Figure 8 illustrates a schematic diagram that outlines the procedure of the manufacture of superhydrophobic surfaces using photolithography method in which AutoCAD™ was applied to design the spacing, size and alignment of the required micropatterned surface. The transparency served as a mask for contact photolithography using a positive photoresist on a silicon wafer and with a help of a spin coater a silicon wafer was coated on both sides. Buffered oxide solution (BOE) (J. T. Baker Co.) of 10% hydrofluoric acid in water was used to etch the area of silicon dioxide surface not covered by the photoresist. As soon as the desirable roughness is presented on the silicon wafer, a reaction with a silanizing agent was done aiming to make it superhydrophobic and a contact angle between 130º to 174º was obtained.

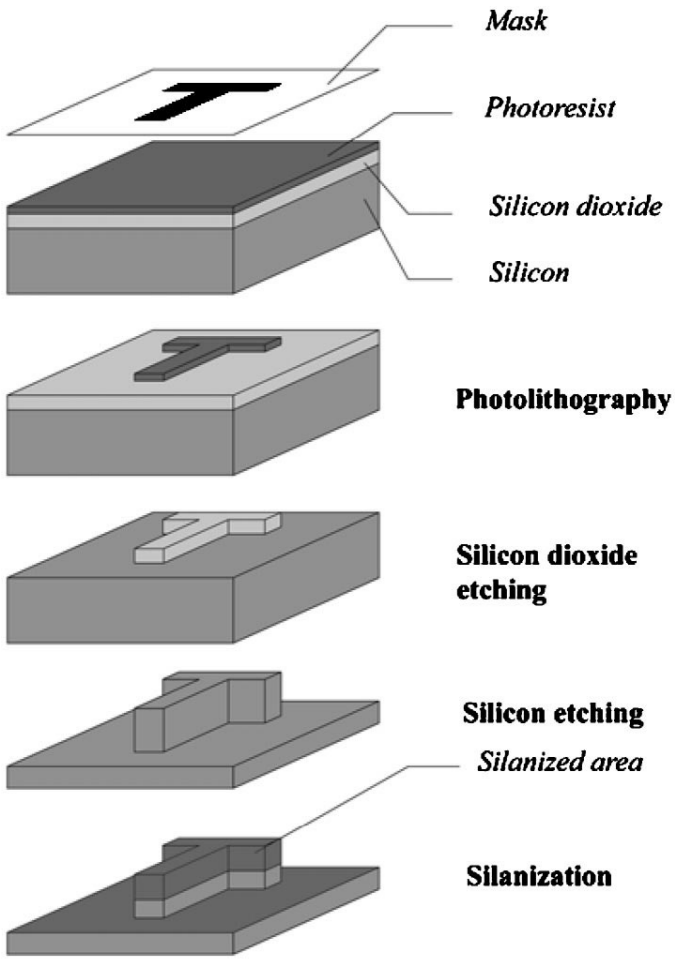

Figure 8: Schematic diagram outlining the procedure for creating of superhydrophobic surfaces [106]

Plasma method

Xiu et al., 2012 [107] explored the use of bis-phenol into a based epoxy resin and silica nanoparticles to obtain superhydrophobicity through plasma etching method followed by plasma etching. Silica nanoparticles ($100\ nm$) were mixed in toluene and sonicated for 5 minutes; followed by the addition of diglycidyl ether (EPON 828), hexahydro-4-methylphthalic anhydride and imidazole then stirred for 30 minutes to obtain the final coating mixture. Glass slides with a thickness of $70\ \mu m$ were cleaned to eliminate possible impurities and using a dip coating or doctor blading the drops of the prepared mixture were covered on the glass. Figure 9 illustrates the plasma etching done under the following conditions: $150\ W$ rf power, $0.5\ torr$ pressure and O_2 flow rate of $75\ sccm$. Surface fluorination was then done by immersing treatment in perfluorooctyl trichlorosilane (PFOS) and in sequence to examine the abrasion resistance of the surface, Figure 10 illustrates the procedure.

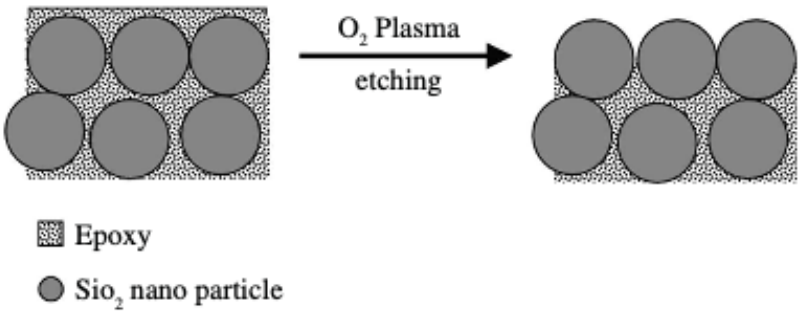

Figure 9: Illustration of O_2 plasma etching of epoxy/silica nanoparticles composite films for surface rough structures [107]

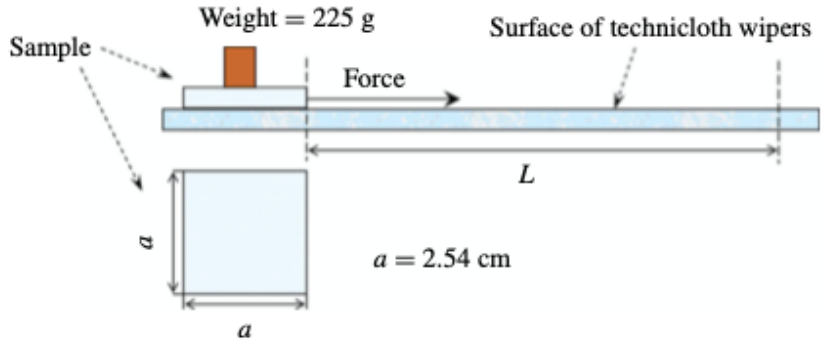

Figure 10: Illustration of the abrasion test on a superhydrophobic surface [107]

Contact angles were obtained with a Ramé-Hart goniometer that had a charge-coupled device camera equipped for image capture and the data obtained are seen in Table 1.

Table 1: Abrasion resistance of different superhydrophobic surfaces [107]

Superhydrophobic surfaces	Initial contact angle	Contact angles after abrasion length of 25 cm
PU	168.1 ± 1.6º	138.7 ± 5.0º
PTFE	161.3 ± 1.0º	130.2 ± 4.0º
Silica	165.4 ± 1.5º	124.3 ± 5.0º
Si nanostructures	166.4 ± 1.5º	133.2 ± 4.5º
Epoxy/silica nanoparticles	169.2 ± 1.1º	168.6 ± 1.7º

SEM images for after coating are seen in Figure 11, and it was found that a surface hydrophobic treatment by PFOS was not enough to reach a superhydrophobic self-cleaning state and as illustrated on Figure 11.a) as a contact angle $< 140^{o}$ was obtained. Therefore, to improve the surface roughness, a O_2 plasma etching was performed for several times and surface morphologies as seen in Figure 11.b) to 11.e) and is notable that the surface roughness increased with etching time.

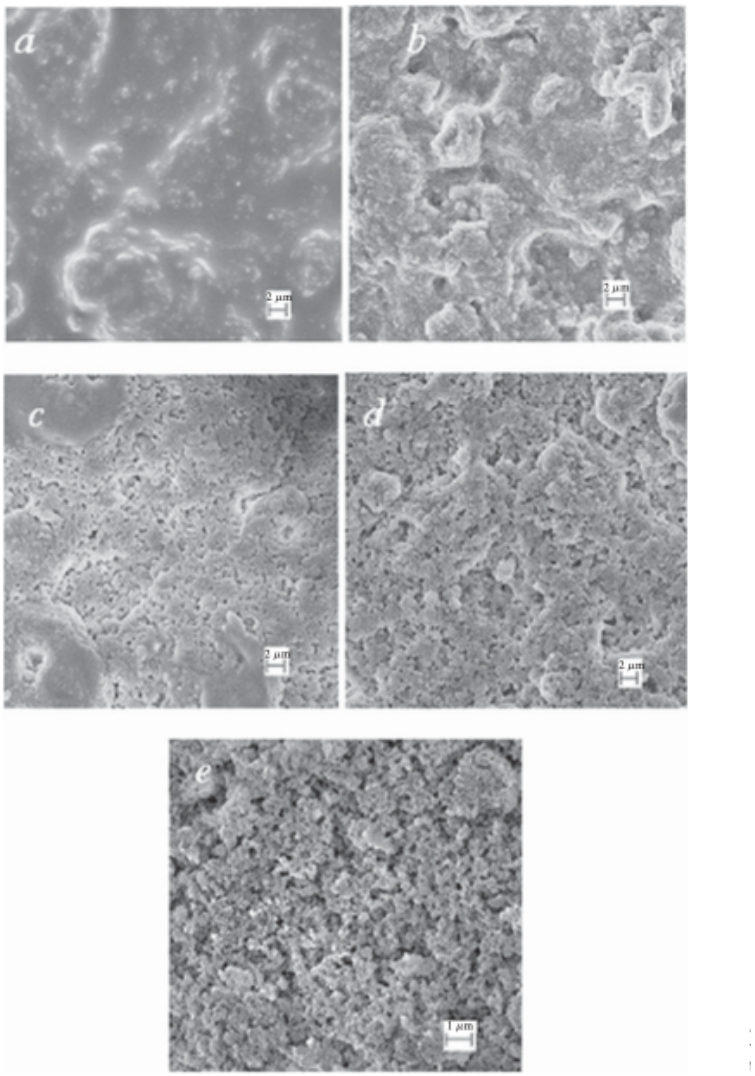

Figure 11: Surface morphology from SEM images a) surface before etching, b) O_2 plasma etched for 1 minutes, c) 5 minutes, d) 10 minutes and e) 15 minutes [107]

Chemical method

Shirtcliffe et al., 2005 [108] used a chemical etching method to produce superhydrophobicity on a copper surfaces and separately using electrodeposition. S18-13 photoresist (Shipley) was spun onto few of the copper sheet ($99 + \%, 0.127\ mm$) on glass slides using a spin coater at $3000\ rpm$, and copper was used as a sample base and counter electrode. Figure 12 illustrates the pattern of the copper samples composed of tessellating squares with a circle on the mask. Etching on the copper samples was carried out in a potassium persulfate solution and then chemically polished for $3\ s$. Afterwards they were dropped into $0.1\ M$ potassium hydrogen carbonate to halt etching and finally rinsed.

Contact angle measurements were obtained using Krüss DSA10, volume of $5\ \mu L$ droplet of distilled deionized water. Consequently, equilibrium contact angle of 152 ± 3^o were obtained on the etched samples and the contact angle hysteresis increased and then decreased as the contact angle increased. And the contact angle increased to 155 ± 3^o when the sample was stripped of photoresist after etching and then the tops of the pattern were roughened by etching for $30\ s$ in the same persulfate solution, therefore longer etch times reduced the area of the tops of the peaks. Figure 13 illustrates the surface texture of etched copper patterns produced using diverse sized masks, the pattern size indicates to the diameter of the circle on the mask and the centre of each circle is separated at twice its diameter from the centre of the next.

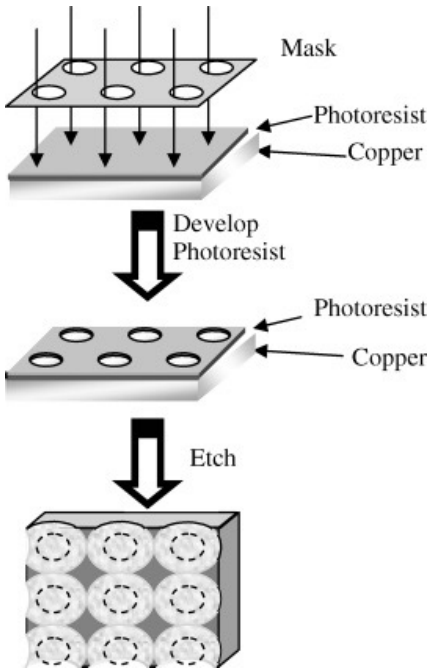

Figure 12: Scheme showing patterning of copper samples [108]

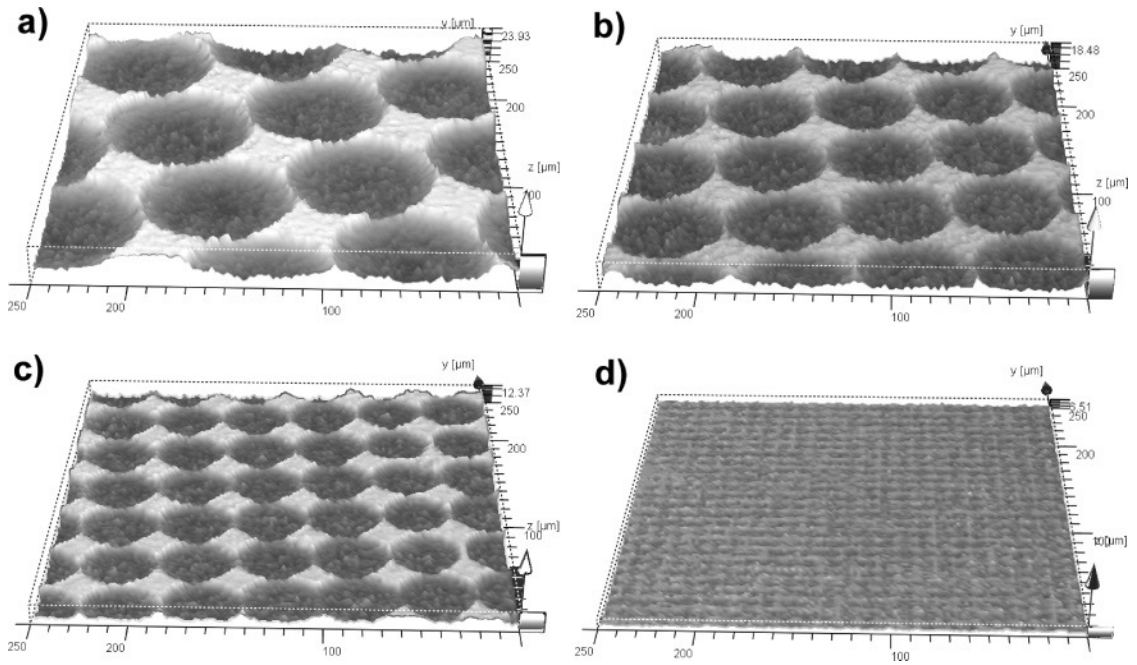

Figure 13: Confocal profiles of etched copper surface a) 40 µm pattern, b) 30 µm pattern, c) 20 µm pattern and d) 5 µm pattern [108]

Aluminium oxide (alumina)

In 1786, Morveau proposed the word "alumine" and this was anglicized to "alumina" in England, while in Germany "tonerde" it is still used, meaning clay earth [109], [110]. The properties of the alumina are determined, first and foremost, by the crystal structure [109]. The main advantage of an alumina coated surface is the absence of chemical interactivity with most metals, a good heat transfer and absence of wettability [111]. Alumina can be characterised as a typical illustrative of the group of structural ceramics [110].

Silicon dioxide (silica)

Silicon dioxide (SiO_2) nanoparticles has attracted remarkable attention due to its versatility, specifically how its properties and composition can accommodate different requirements based on where it's applied. Silica nanoparticles are robust inorganic materials [112], of low toxicity [113] which presents a three-dimensional (3D) structure [114] with extremely open spaces linked to each other, and that makes it easy to introduce functional groups [115]. Silica nanoparticles play a significant role in the manufacture of rough and hierarchical structure

surface [116]. Furthermore, silica presents very important applications when synthesized such as optically transparent, good bio-compatible material , outstanding surface chemistry among others applications [30].

Bottom-up methods

Based on the Wenzel-Baxter equation the superhydrophobicity can be achieved if the air fraction is low and θ_Y is high. The bottom-up methods are suitable to fabricate very low air fraction superhydrophobic surfaces and are more economical when comparing to the top-down method.

Chemical vapor deposition (CVD)

CVD can be applied to produce rough surfaces or to depose a very thin layer of hydrophobic compound on various surfaces and uses a mixture of chemically reactive components, that are coated on the surface [117], [118].

Shen et al. 2014 [119] manufactured a micro-nanostructured superhydrophobic silicone-carbon surface by oxidative chemical vapor deposition. As seen in Figure 14, the experiment was setup on a chamber with a volume of $\sim 1.2\ L$, with electrically heating panel, in which T_1 is the bottom heating panel and creates the decomposition temperature and T_2 is the top heating panel which produce the oxidative deposition temperature. The temperatures were individual monitored by thermocouples. The substrates were treated before placed on the chamber by immersing in a piranha solution at the boiling point for 30 minutes then rinsed and dried at 100ºC for 1h. The bulk silicone (Dom Corning, America) was randomly cut and placed as uniform as possible on T_1. Subsequently, the mixture gas $O_2 - N_2$ with volume ration of $\sim 1:4$ flowed into the reactor and then stopped. The values of T_1 and T_2 was increased in a rate of $\sim 30^o C/min$ and this chemical vapor deposition was done for around 3 h before the superhydrophobic surface was obtained.

As seen in Figure 15, silicone-carbon composite coatings which was prepared with $0.5\ g$ bulk silicone at $T_1 = 320^o C$ but diverse deposition temperatures obtained a contact angle of 175º and 160º using a DropMeter™ A – 100P equipped with a CCD camera.

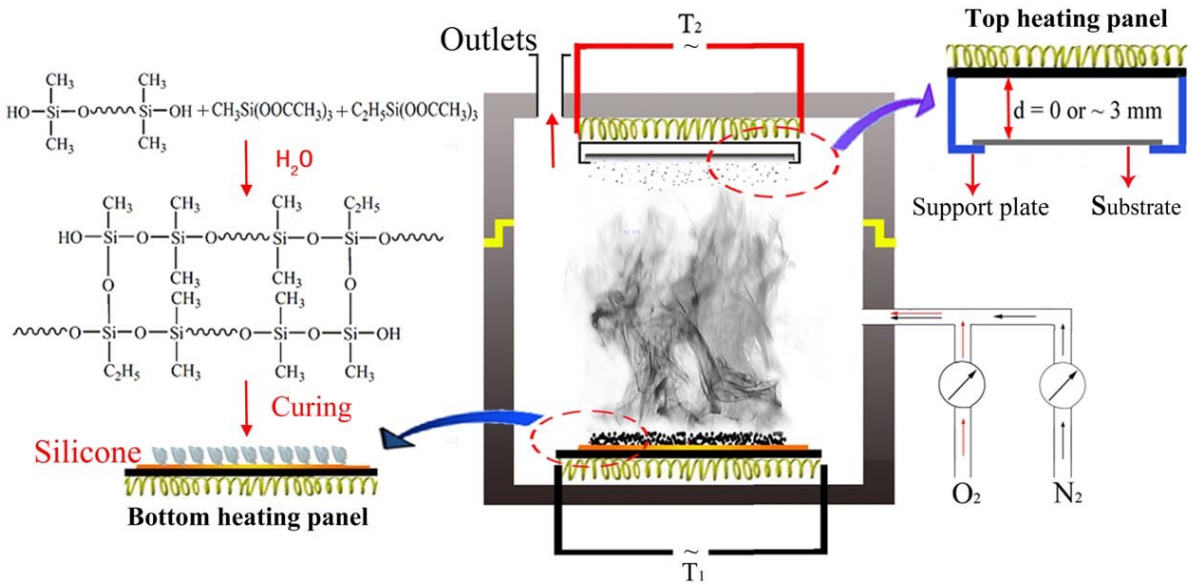

Figure 14: Illustration for the experimental setup of the preparation of the coatings [119]

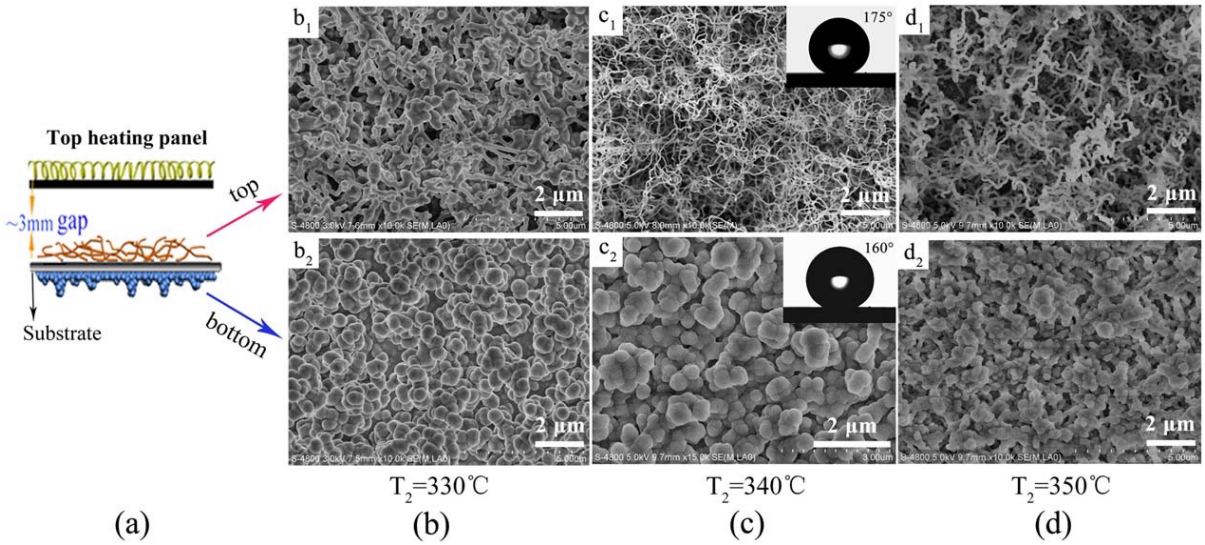

Figure 15: a) Schematic for the preparation of the coatings on both sides of the glass substrates b) to d) SEM images of the samples ***[119]***

Electrospinning

Electric force is used on the electrospinning method to draw charged threads of polymers, nanoparticles, metal and ceramics fibres normally between 100 nm and 1 μm in diameter and adhere them on to the substrate [120], [121], [122]. This method is used to manufacture

superhydrophobic surfaces by monitoring the surface roughness under suitable conditions, a schematic electrospinning setup of polymer nanofibers is illustrated in Figure 16.

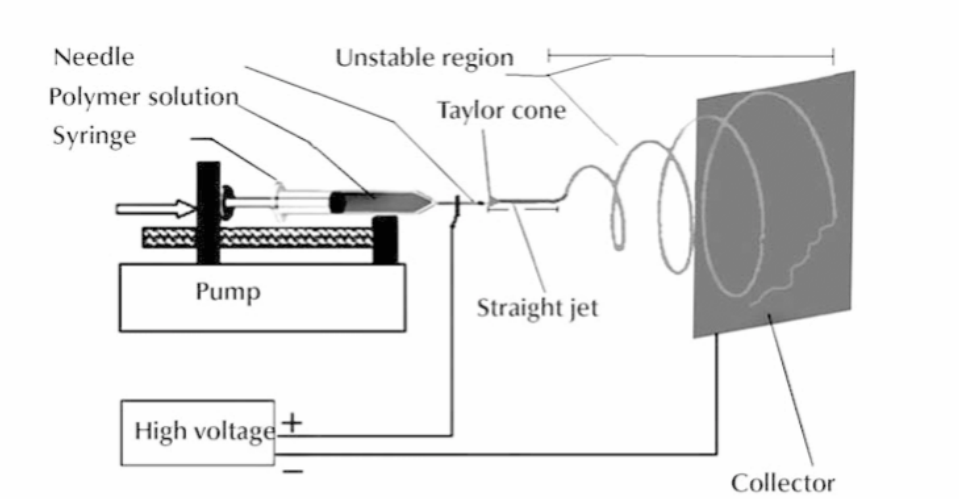

Figure 16: Electrospinning setup [122]

Sarkar et al., 2011 [123] used the electrospinning coating technique for the manufacture of a dual-layer superhydrophobic surface, including polyvinylidene fluoride (PVDF) and fluorinated silane molecules (FSM). PVDF or a combination of PVDF and FSM were dissolved in dimethyl formamide (DMF) and stirred at 50^oC until a total dissolution was obtained. The electrospinning machine, that is usually used to produce nano-fibres, was then used to spray the dissolved solutions onto a glass slide surface for $20\ h$. The electrospinning parameters were the following: voltage of $22\ kV$, a distance of $18\ cm$ between the needle and collector and traverse speed of $5\ mm/s$.

The surface wettability characterization was measured using optical contact angle tester OCA15 (DataPhysics, Germany) by the sessile drop method using $4\ \mu l$ distilled water and a rough surface was formed that presented a replicated superhydrophobic surface with a contact angle of 170.2^o and a low roll off angle $< 1^o$. Surface wettability for the diverse coated surfaces can be seen in figure 17 in which *S* donates the sample number. Solution of 5% PVDF was coated on the glass slide with different flow rates, and it was decided that a flow rate of $0.26\ ml/h$ was going to be used in all experiments.

As seen in Figure 18 and 19, the size of the particles decreased when the percentage of PVDF in the coated solution decreased and the sample also changes from close to circular to slightly oval for the different PVDF coatings.

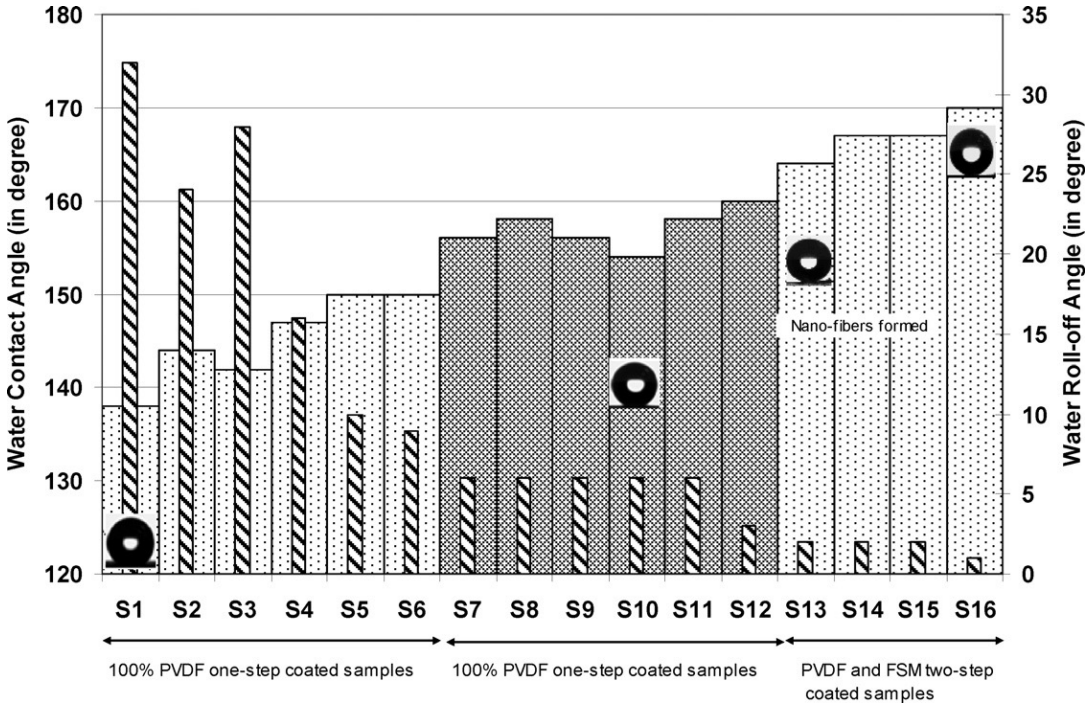

Figure 17: Contact angle and roll off angle results (broad bars represent contact angle and narrow bars roll off angle) [123]

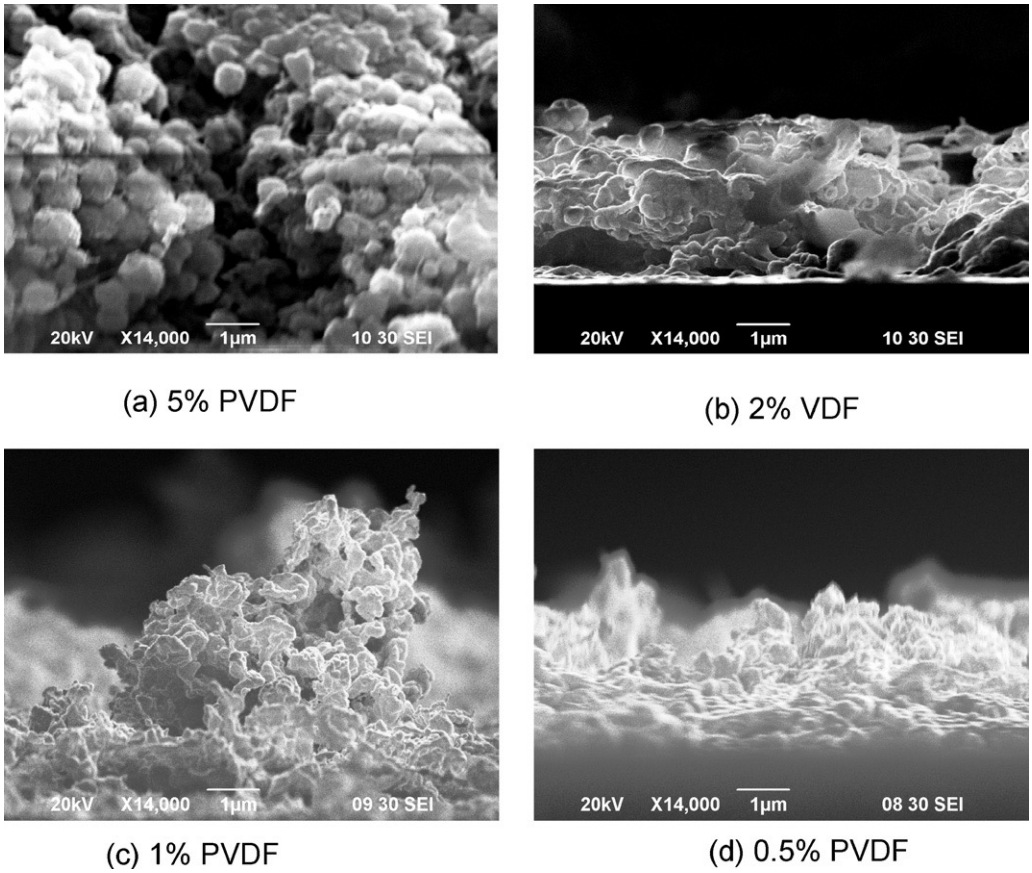

Figure 18: Cross-sectional views of the glass surfaces coated with solutions containing different concentrations of PVDF [123]

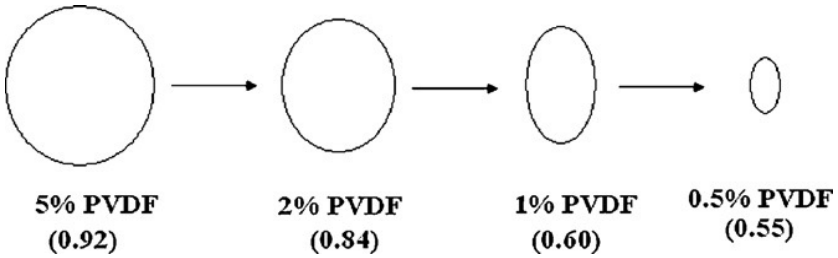

Figure 19: Schematic illustrating the change in particle shape with a reduction in % PVDF in the solution (aspect ratio is indicated in brackets) [123]

Sol-gel processing

The sol-gel is a method used for the manufacture of a porous structure composed of transition metal alkoxides [124]. Sol-gel process is divided into parts such as: *sol* was the chemical deposition behaving as a precursor adhered to the surface and formed *gel* network structure [125]. Xiu et al., 2009 [126] used a sol-gel processing to create silica superhydrophobic

surfaces, in which a eutectic liquid composed of urea and choline chloride (2:1 molar ratio) was the templating agent solution. As seen in Figure 20, the eutectic solution formulation was composed of tetraethoxysilane (TEOS), ethanol, HCl aqueous solution and ethylene oxide propylene oxide triblock copolymer P123 ($EO_{20}PO_{70}EO_{20}$). The gelation was obtained after two weeks, in which the coated glass slide was positioned in a desiccator with a container of $1\ ml$ ammonia (29%) at the bottom. The film surface was treated with a fluoroalkyl silane for 30 min, heated to 150^oC in air for 1h and at 220^oC for 5 minutes to enhance silane hydrolysis[7] and condensation; subsequently a superhydrophobic surface was obtained with a contact angle of $\sim 170^o$ and contact angle hysteresis $< 10^o$. Contact angle and contact angle hysteresis as a function of spin speed can be seen in Figure 21 and is notable that contact angle hysteresis increases as the spin speed increases, therefore is suggested that spin speed of $3000\ rpm$ is used taking in consideration that a very low hysteresis is observed.

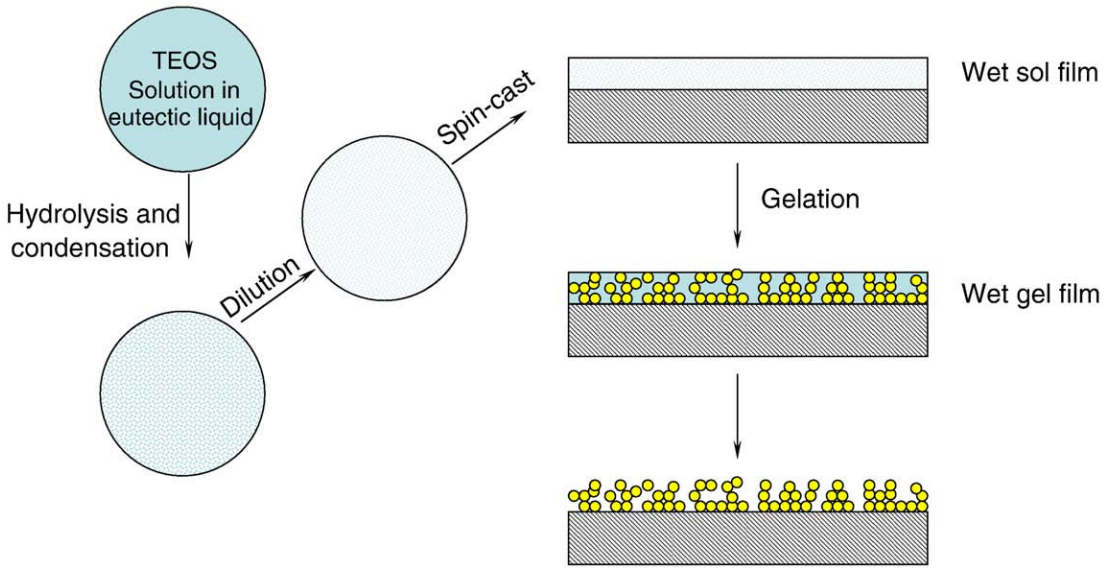

Figure 20: Schematic illustration of the procedure to prepare silica rough surfaces [126]

[7] Hydrolysis is a dual decomposition reaction in which water is one of the reactants

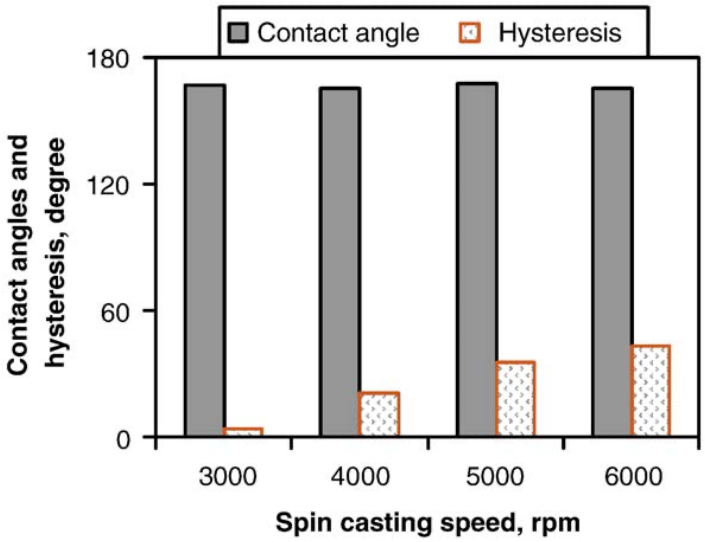

Figure 21: Effect of spin speed on contact angle and contact angle hysteresis on SiO_2 films [126]

Layer-by-layer (LBL) deposition

LBL deposition have been established as a simple and versatile technique for preparing supported multilayer thin films by alternately immersing the substrate on distinctive chemical solutions [127]. Bravo et al., 2007 [128] used LBL deposition to manufacture a superhydrophobic films based on silica nanoparticles of various sizes. They used poly (sodium 4-styrenesulfonate) (SPS) and poly (allylamine hydrochloride) (PAH) to adsorb and reverse charges of the substrate surface. The deposition process was done by dipping the glass slide substrate into different aqueous solutions and a schematic demonstration can be seen in figure 22 with their respectively main parts such as adhesion, body, and top layers and to enhance the mechanical properties some films were calcinated at $550^{o}C$ for $4\ h$. Trichloro(1H,1H,2H,2H-perfluorooctyl) silane was deposited onto the substrates coated with the multilayer films by CVD with the objective to change the surface chemistry, then placed on vacuum chamber so that the fluorosilane compound could evaporate.

As seen in Table 2, advancing contact angle up to 160^{o} and low contact angle hysteresis $< 10^{o}$ were obtained by LBL of silica nanoparticles.

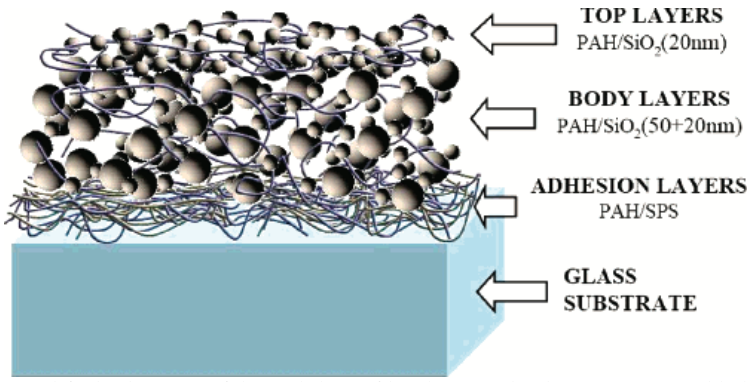

Figure 22: Simplified schematic of the multilayer film showing the three main assembly blocks [128]

Table 2: Select properties of the PAH/SiO_2 multilayer system [128]

	Without top layer		With top layer	
	As-assembled films	Calcinated films	As-assembled films	Calcinated films
Advancing CA (before silane treatment)	~7	<5	<5	<5
Advancing CA (after silane treatment)	154	152	161	157
Receding CA Advancing CA (after silane treatment)	134	134	156	150

Top-down vs bottom-up methods

The technology to coat a uniform thin layer has played an active part in evolving the manufacturing field. This is important as obtaining a smooth layer is necessary to coat plural layers simultaneously. Currently, the biggest obstacle towards applying the plural layers technique in industrial and practical uses is the durability of the superhydrophobic surface. There has been a lot of work, by researchers and engineers, which focused on improving the mechanical properties of surfaces using this technique.

Essentially, to obtain superhydrophobic surfaces it is required two main things: surface roughness and the chemical structure. To further improve superhydrophobic surfaces durability, Zhi et al. [129] suggested a manufacturing technique where the dual-scale structures were prepared through the combination of sandblasting with hydroxidion. Furthermore, the same author also extensively studies the role of low surface energy materials in manufacturing superhydrophobic surfaces. Due to the superhydrophobicity, the water droplet can easily glide off, it does not stick on the surface and bounces off when is dropped on the surface from any height.

Some methods for the fabrication on superhydrophobic surfaces are simple, inexpensive, and independent of operational expertise or specific equipment, whereas other manufacturing methods might involve multiple procedures and the use of expensive equipment is required.

In the top-down procedures, the desirable rough surface can be obtained by carving, moulding and micromachining with lasers or another instruments; the main problem is to control the quality and potential upscale. The bottom-up procedures are very simple methods, provides a more homogenous chemical composition. On the other hand, one of the disadvantages of the bottom-up methods are the establishment of long-range order.

Applications of superhydrophobic surfaces

Moreover, scientists and engineers have started to investigate the usefulness of these wetting surfaces in various fields, resulting in the commercialization of these superhydrophobic surfaces worldwide. Hence, in this section, few applications of superhydrophobic surfaces will be addressed.

Anti-icing

Superhydrophobic coating is applied on surfaces to provide icephobicity. For instance, icephobicity[8] is a field in which superhydrophobicity can effectively be implemented [130]. For instance, ice adhesion or frost formation has the capability of altering the effective form of the aircrafts which consequently changes the aerodynamic properties of air flow [131], hence, icing has an impact the reliability of aircraft. Not merely is anti-icing indispensable for aircraft

[8] Icephobicity is the capability that solid surface must repel or avoid ice formation

applications, on the other hand, it may as well be extended concerning the other applications, for example, refrigerators, air-conditioners, ships, wind turbines [132].

Normal force and/or shear force are the two main forces that acknowledge defrosting, as long as ice is formed [133]. Above all, low contact angle hysteresis and greater contact angle are in charge for the normal force and shear force. In the majority of the cases, icephobic surfaces will present shear strength with values among 150 and 500 kPa, despite the fact that normal stress is also being used [134],[135]. It is possible to delay the ice accretion of superhydrophobic surfaces in comparison to a flat hydrophobic surface, moreover it damages the surface microstructure slowly while icing and/or deicing [9], decreasing the anti-icing properties. On the other hand, at a low temperature and in a humid environment the adhesion strength[10] rises and this effect is related to the condensation (anchor effect). Consequently, the application of anti-icing on superhydrophobic surfaces is restricted [136], [137].

Boinovich et al. [132] used chemical etching and dispersion methods to fabricate icephobic surface on stainless steel with silica nanoparticles. The manufactured surface was characterized by a contact angle higher than 155^{o} and a sliding angle of 42^{o}, both results were measured after 100 icing/deicing cycles. Using a different technique, Cao et al. [138] manufactured a superhydrophobic surface with acrylic polymer and silica nanoparticles composite on glass substrate using polymerization. The resulting contact angle was higher than 150^{o} and contact angle hysteresis was less than 2^{o} on the manufactured surface, hence, the surface had excellent anti-icing properties. Farhadi et al. [139] demonstrated that the anti-icing effectiveness of the superhydrophobic surfaces deteriorates significantly in a humid atmosphere due to water condensation, furthermore, this can restrict the utilization of superhydrophobic surfaces as anti-icing materials in humid atmosphere.

Self-cleaning surfaces

A true self-cleaning surface is the combination of superhydrophilicity and photocatalytic[11] performance to break down the dirt and wash the impurities from the surfaces. The utilization of the term, self-cleaning surface, is not adequate for superhydrophobic surfaces, that are particularly dry and repel water droplets. The self-cleaning surfaces do not in fact clean by

[9] Deicing reduces the adhesion strength of ice on superhydrophobic surfaces
[10] Adhesion strength is related to the capability from one adhesive to attach into a surface and connect two surfaces together
[11] Photocatalytic is a material that uses light energy to facilitate a chemical reaction

themselves, as soon as the water droplets roll over the surface, they wash off the dirt, in addition, self-cleaning surfaces can be applied in solar applications [81]. A prevalent problem on solar panels is the dust particles formed on their surfaces which results in the reduction of the solar cell efficiency [140]. As a matter of fact, the use of transparent self-cleaning surface could avoid the aggregation of dust particles on the solar cells. Park et al. [141] manufactured a microshell array of PDMS (polydimethylsiloxane) layer, that presented a contact angle of 151^{o} and contact angle hysteresis of 19^{o}. Furthermore, the superhydrophobic surface was transparent and extremely water repellent and there was the possibility to be used in solar panels. As soon as the dust particles are deposited on the surface, a tilted angle of 45^{o} was observed and the water droplets were released at a steady rate through the surface. As a result of the superhydrophobicity, the dust particles were washed off by flowing effect. The microshell array of PDMS surface displayed an outstanding cleaning effect when compared to the hydrophilic flat surface.

Anti-corrosion resistant coatings

Corrosion is commonly highlighted as one of the most serious problems in industrial applications, moreover, this natural process results in losses of hundreds of billions of dollars every year [142]. In recent years, there has been an increased research attention of corrosion resistance. At the moment, a highly favoured approach to promote corrosion protection is the treatment of surfaces using chromium-containing compounds, that can negatively impact both health and environment [36], [143].

Liu et al. [144, p.] manufactured Magnesium (Mg) alloy[12] surfaces with stable superhydrophobic surfaces and improved corrosion resistance by using a solution immersion method and post-modification with fluoroalkylsilane. Following Lie et al. little research has focused on studying the corrosion resistance of Mg alloys, which is the lightest metal structure materials between the practical metals. For instance, Xu et al. [145] used an electrochemical machining procedure followed by fluoroalkylsilane modification to demonstrate the manufacture of superhydrophobic Mg alloy surfaces with corrosion resistance. Ishizaki et al. [146], [147, p. 3], [148] fabricated a sequence of superhydrophobic Mg alloys using the microwave plasma-enhanced chemical vapor deposition and immersion process.

[12] Magnesium alloy is the combination of Mg with different metals (called an alloy), such as, aluminium, silicon, copper.

The majority of corrosion resistant materials are chromium based, due to its anti-corrosive properties [34]. Although, chromium is toxic which makes it necessary to research an suitable non-toxic substitute materials [149]. Metal alloys, for example aluminium, titanium, and magnesium alloys, are favoured in automobile applications because of the low weight. However, those metal alloys demonstrate poor corrosion resistance which limits their use on other areas. Ou et al. [150] manufactured a superhydrophobic surface by coating perfluorooctyltriethoxysilane (PFOTES) on a magnesium alloy and a titanium alloy applying chemical etching as well as hydrothermal process. The hydrothermal processed superhydrophobic surface demonstrated stability and corrosive resistant. Ishizaki et al. [146] manufactured a superhydrophobic surface on magnesium alloys. Magnesium and its alloys have been shown to have outstanding mechanical properties, poor corrosion resistance, high damping strength, castability, and high stiffness towards weight ratio. A superhydrophobic surface can improve the anticorrosive behaviour of a surface. Superhydrophobic surface manufactured on Mg alloy with cerium oxide and fluoroalkylsilane nanoparticles through solution immersion process and the resulting static contact angle varied between 136^{o} to 152^{o}. One element or coating material that is used as an alternative to protect steel against corrosion is Zinc (Zn). Although, Zn coating has defects that could result in the formation of corrosive products, multiple efforts have been provided with the objective to enhance the performance of Zn coating. Liu et al. [151] was able to manufacture a stable superhydrophobic surfaces with static contact angle of 151^{o} by solution immersion process. The fabricated surface could operate as an obstruction to prevent water, moisture, and oxygen based on reacting among the base metal. Instead, the surfaces serve as a dielectric medium thus decreases the rate of corrosion.

Water-resistant fabrics

Superhydrophobic solutions are extremely effective when applied on rigid substrates compared to flexible substrates such as textile fabrics, since the substrates lose their superhydrophobicity when the substrate is not rigid [152]. Wang et al. [153] manufactured superhydrophobic surfaces which were fabricated by modifying cotton substrates with n-dodecanethiol and gold micro/nanostructures. The manufactured surfaces presented a static contact angle above 150^{o} and could keep the superhydrophobicity although the surfaces where folded number of times. Zimmermann et al. [154] manufactured superhydrophobic textile fabrics using

polymethylsilsesquioxane nanofilaments on eleven textile fabrics. Considering that a static contact angle is unsuitable on behalf of superhydrophobic textile properties, a technique called water shedding angle[13] [155], was used for the determination of the wettability of the fabric substrates. Once a water droplet is released towards the inclined substrate from a certain height, the lowest angle of inclination is obtained, at which the droplet of water rolls-off the surface entirely and the lowest angle is also recognized as the water shedding angle. It is established that all the important textile parameters, for example, tensile strength, colour and haptics were not influenced by the silicone nanofilament coating [156]. Wang et al. [157] manufactured fabrics substrates modified with a hydrolysis product (fluorinated-decyl polyhedral oligomeric silsesquioxane and a fluorinated alkyl silane). The manufactured fabric presented self-healable superhydrophobicity and superoleophobicity properties, as well as demonstrated enhanced durability towards acid, machine wash, ultraviolet rays, and abrasion. The superhydrophobic fabric surfaces must be durable and robust to resist things such as scratching, tensile stress, abrasion or compressive stress, as well as should endure several laundry cycles [149].

Biomedical

Platelet adhesion on synthetic material implants may result in blood coagulation and thrombosis [158], [159], [160]. This results into functional failure of synthetic organ implants, synthetic blood vessels and different medical devices that have contact with blood, for instance, blood-compatible materials are therefore necessary. However, current materials firmly depend on chemical and biological treatments and only restricted materials are accessible. If superhydrophobicity is introduced, almost all platelets are repelled from synthetic implants. Poly(carbonate urethane) is commonly used in biomedical applications as a result of its moderate blood compatibility and biostability [161], [162]. Sun et al. [163] manufactured a superhydrophobic surface on fluorinated alkyl side-grouped poly(carbonate urethane) through carbon nanotubes by applying the dip coating procedure, in this case a static contact angle above 163^{o} was obtained. The manufactured superhydrophobic surface demonstrated outstanding antiadhesion to platelets as well as an excellent blood compatibility. Such superhydrophobic materials can potentially perform a significant part for the future of biomedical applications.

[13] Water shedding angle alternative technique used to evaluate the wettability of superhydrophobic textiles the principle of repealing droplets of water once it reaches the substrate

Discussion

Over the last few decades, publications concerning the development of superhydrophobic surfaces have considerably increased although most of the methods presented above are less economically sustainable to produce large surfaces areas and are mainly used for research purposes. In this review, I initially present a brief description of fundamental principles of superhydrophobic surface followed by indicating different techniques used by researchers with the aim to fabricate these surfaces and lastly, I present different applications of superhydrophobic solutions.

For instance, the superhydrophobic manufacturing techniques presented previously have different advantages and disadvantages based on the material used during the fabrication of these artificial superhydrophobic coating. Advantages such as simple method of fabrication, controllable thickness and structural flexibility are among the most highlighted one on the fabrication technique presented used during the fabrication of the superhydrophobic surfaces. However, disadvantages such as expensive materials, brittleness, toughness, and toxicity of polymers and being unsuitable for large scale production. Nevertheless, procedures used for to manufacture superhydrophobic surface involve the use of expensive materials and complex methods such as plasma, chemical vapor deposition, electrodeposition.

Following the review of the superhydrophobic surfaces fabrication research from the last few decades, the following gaps were identified:

- Most of the methods and material used to fabricate superhydrophobic surfaces are restricted to a laboratory setting and are not adequate for industrial production.
- Numerous superhydrophobic coatings suffers from low chemical durability which indicates the resistance of the surface towards the surface-active agent (surfactant).
- The possibility of a superhydrophobic surface losing their water repellence properties and turn into hydrophilic surface if water infiltrate into the micro or nanotexture.

To meet the objectives set for this thesis, we will attempt to focus on:

- An easy and inexpensive method to manufacture superhydrophobic coatings that can be applied to diversity of surfaces.
    - Obtain superhydrophobic surface that are environmentally friendly, non-hazardous when in contact with the skin, long term durability and storability.
    - Analyse the data of the fabricated superhydrophobic surface.

We favour a method adapted from Alexander et al., 2016 [164] that easily synthesis alumina and silica nanoparticles with appropriate carboxylic acid and replacing the use of fluorocarbons for hydrocarbons. The method is reasonably simple, inexpensive and offers possibilities for large industrial scale fabrication and application. On the other hand, due to the outbreak of publications in this field, this review does not include most of the published work regarding superhydrophobic surfaces.

Chapter IV: Experimental method

This chapter focuses on the chemicals and the procedures used to fabricate a superhydrophobic surfaces. All chemicals used in this project were used as purchased without further purification. Aluminium oxide (Al_2O_3) 13 nm primary particle size 99.8%; Al_2O_3 <50 nm particle size; Silicon dioxide (SiO_2) 10-20 nm particle size trace metals basis nanoparticles were purchased from Sigma Aldrich Company, UK and Al_2O_3 5 nm were purchased from Sasol Germany GmbH. Isostearic acid ($C_{18}H_{36}O_2$) > 90.0% were purchased from Tokyo Chemical Industry UK Ltd; N-octadecyltriethoxysilane were purchased from Sigma-Aldrich, UK; which were used as the branched hydrocarbon low surface energy. Solvents such as ethanol; 2-propanol, toluene anhydrous, 99.8% and diiodomethane (CH_2I_2) were also supplied from Sigma-Aldrich, UK.

Methodology used for the development of green low surface

The development of green low surface on this project is based on two main steps: synthesis of the nanoparticles and the spray coating onto the substrates. To manufacture superhydrophobic surfaces, Al_2O_3 and SiO_2 nanoparticles were dispersed in 2-propanol (2w%) and then spray coated onto glass microscope slides.

Synthesis of carboxylate functionalized nanoparticles

The superhydrophobic surfaces were produced based on the procedure established by Alexander et al., 2016 [164]. The nanoparticles were refluxed overnight (24 h) in toluene and the appropriate amount of isostearic acid in a 1:1.4 ratio or lanolin in different ratio depending on which nanoparticles (alumina or silica) and their respectively particle size were being used. The functionalized particles were then stirred using Microstirrer Magnetic Stirrer to disperse the nanoparticles then the mixture was poured into diverse 50 mL disposable centrifuge tubes and centrifuged for 1 hour at 5000 rpm using Heraeus Megafuge 16 Centrifuge, equipment shown in Figure 25. An illustration of the refluxed nanoparticles before centrifuging can be seen in Figure 24 After centrifuge the nanoparticles, as shown in Figure 26, the supernatant was then decanted, and the nanoparticles were re-dispersed, in which Rotamixer (vortex mixer) (240 Volts, 50 Hz, 0.5 Amps) were used to mix the nanoparticles and the solvents before centrifuge it for 1 hour at 5000 rpm twice in 2-propanol and once in ethanol, this step was required to remove unreacted carboxylic acids. Finally, nanoparticles were oven-dried at 80^{o}C overnight. Table 3 illustrates different ratio of concentration for the carboxylic acids which were used during the synthesis of the nanoparticle.

Table 3: Table: Different ratio of the synthesis (functionalised agents)

Functionalised nanoparticles	Ratio
Al_2O_3 13nm with isosteric acid	1:1.4
Al_2O_3 13nm with lanolin	1:5
Al_2O_3 13nm with lanolin	1:15
Al_2O_3 50nm with lanolin	1:10
Al_2O_3 50nm with lanolin	1:15
Al_2O_3 5nm with lanolin	1:5

Al_2O_3 5nm with lanolin	1:15
SiO_2 10-20nm with lanolin	1:5
Zinc oxide 50nm with isosteric acid	1:1.4

Reflux reaction

The principal purpose of refluxing a solution is to heat the chemical reaction in a controlled manner at a constant temperature for a certain amount of time, while constantly cooling down the vapour formed on the condenser; consequently, the condensed liquid returns to the flask. An image of a reflux set up experimental rection used in this project is seen in the Figure 23, and it is important to mention that the vapours which are observed on the condenser are a result of the liquid reaction mixture which due to the heat loss a part of the mixture changed from liquid phase to gas phase and back to liquid phase. This subsequently causes the liquid in the condenser to regress into the round bottom flask.

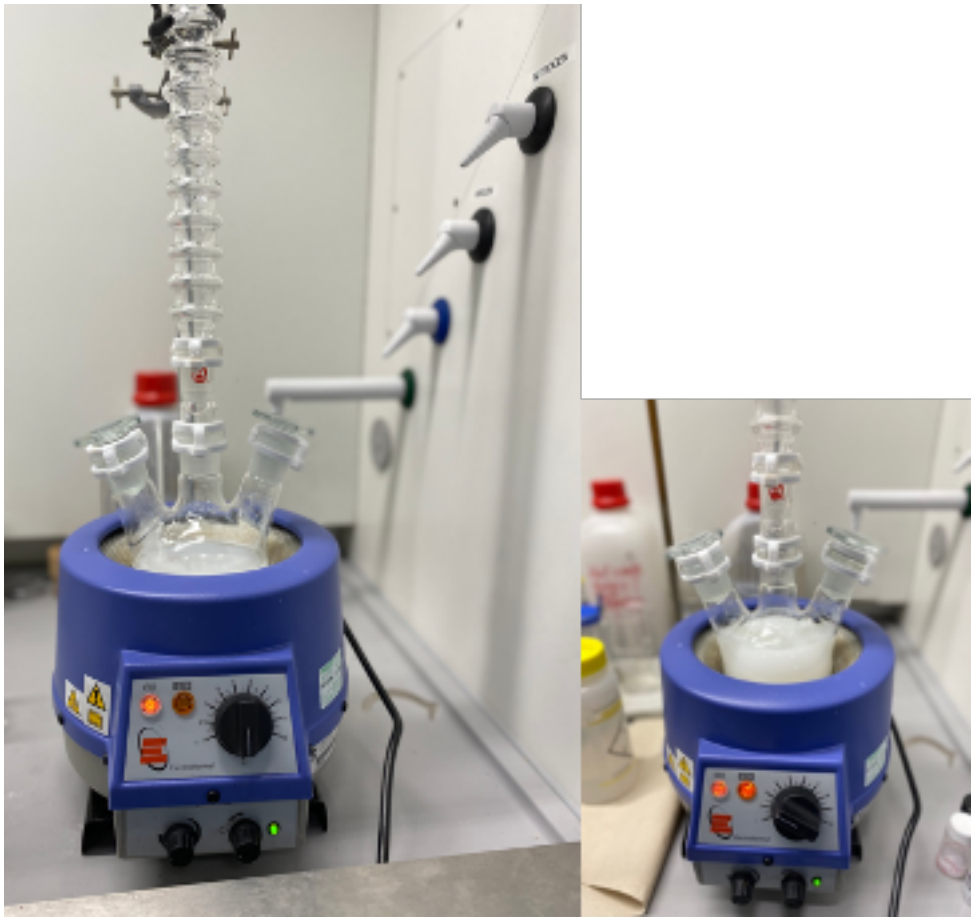

Figure 23: Image of reflux reaction of Al_2O_3 (13nm) with isostearic acid. Source: Author's picture based on the experimental setup

Centrifuge

As seen in Figure 25, the centrifuge equipment is driven by motor and used to spin liquid samples at high speed, which presents general objective such as being excellent for daily processing. As seen in the Figure 24, the refluxed nanoparticles were then placed on diverse 50 mL centrifuge tube and centrifuged using the equipment illustrated on Figure 25 and Figure 26 shows the refluxed nanoparticles after the centrifuged.

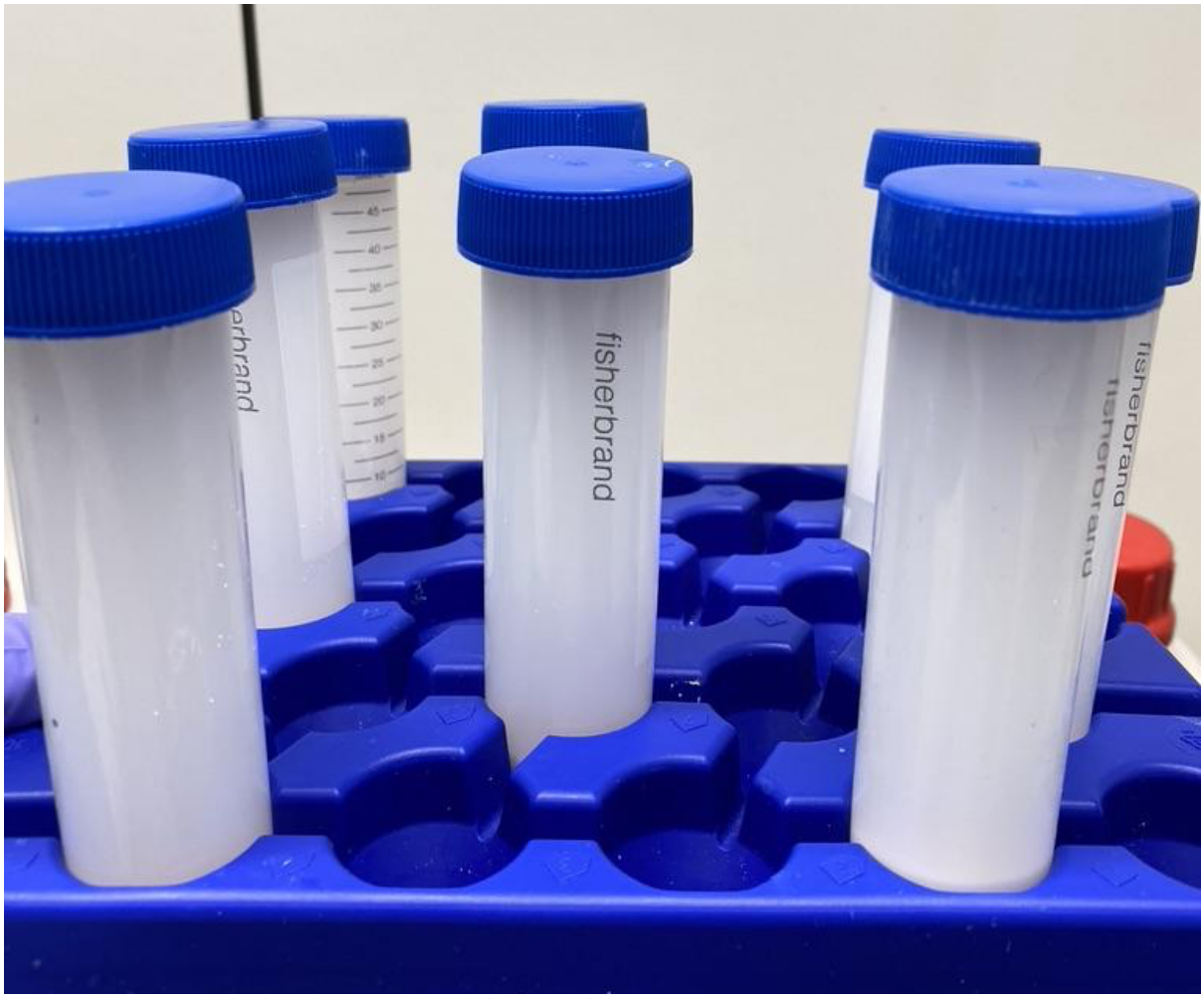

Figure 24: Image of refluxed nanoparticles before centrifugation. Source: Author's picture based on the experimental observation

Figure 25: Heraeus Megafuge 16 Centrifuge. Source: Author's picture

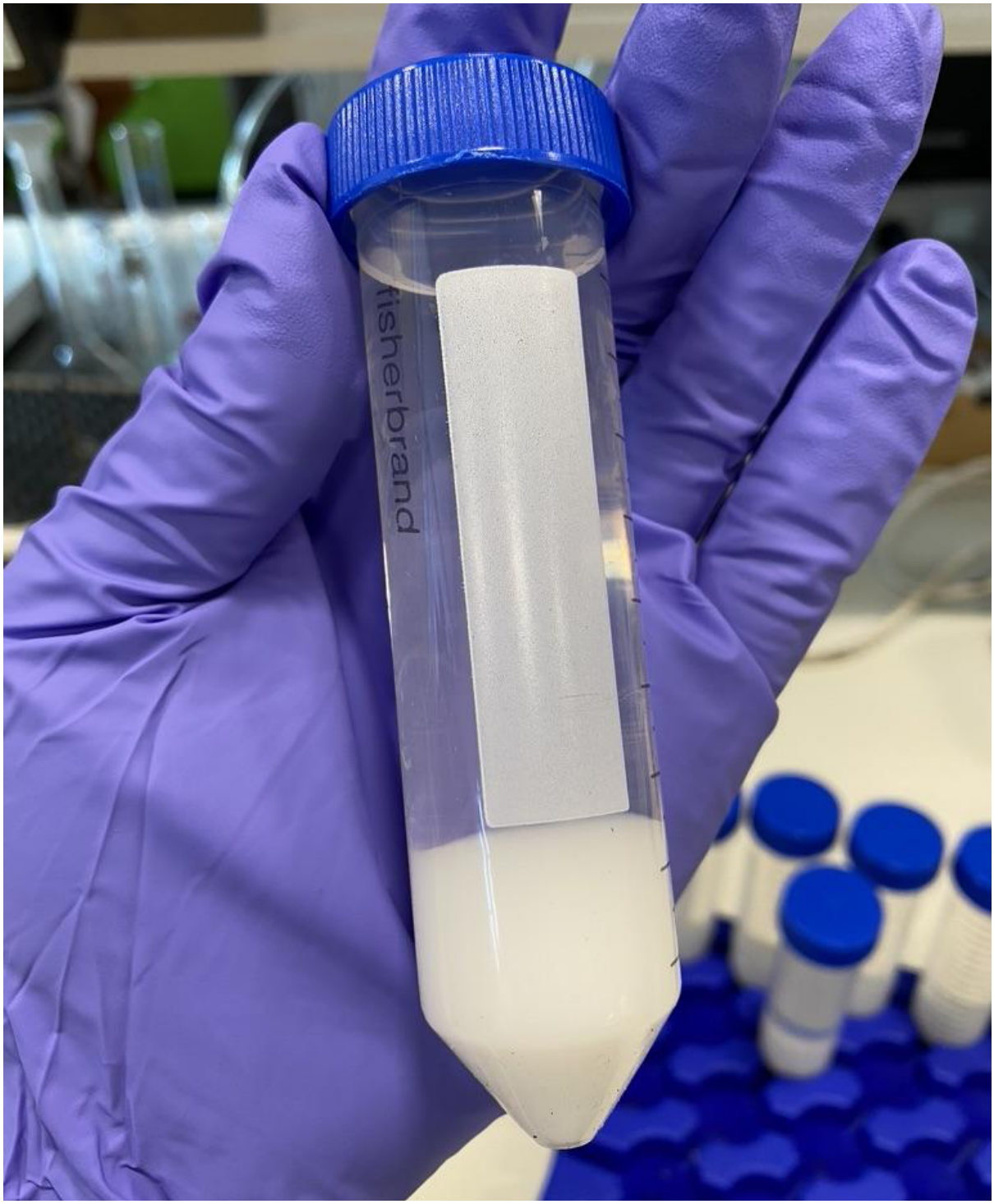

Figure 26: Image of refluxed nanoparticles after centrifugation. Source: Author's picture based on the experimental observation

Deposition technologies

The liquid phase coating can be done using one of three methods: spray coating, dip coating or spin coating. Spray coating was selected for this experimental procedure. The main purpose of the spray coating in this experience is to obtain a uniform, adherent, defect-free polymeric film over the entire substrate [111]. Spray coating is an approach used as an aerosol in form of micrometre size droplets [111] .

Preparation of the slurry

2 wt.% of functionalized alumina particles were dispersed into 2-propanol in which lyophobic system was used for the dispersion by starred the nanoparticles for 20 minutes at 740 rpm using MS-H280-Pro followed by the sonication using the device FB15053 Fisherbrand. As seen in Figure 27, the mixture of the functionalised nanoparticles was sprayed using Spray Craft onto glass substrate until the film layer was visible and left to dry under ambient temperature. Following the drying out with the help of a pipette a droplet of water is deposited on the superhydrophobic surface, such droplets remain on the substrate at any place they reach and some of the droplets bounce off and Figure 28 illustrates few droplets of water that were deposited on superhydrophobic substrate.

As seen in Figure 29, the alumina 5 nm functionalized nanoparticles with lanolin does not disperse well on 2-propanol and the slurries are seen on the bottom of the glass vials although magnetic stirrer and sonicate bath were used in this procedure.

Figure 27: Image of functionalised Al_2O_3 (13nm) nanoparticles dispersed on 2-propanol, ready to be spray coated onto substrates. Source: Author's picture based on the experimental setup

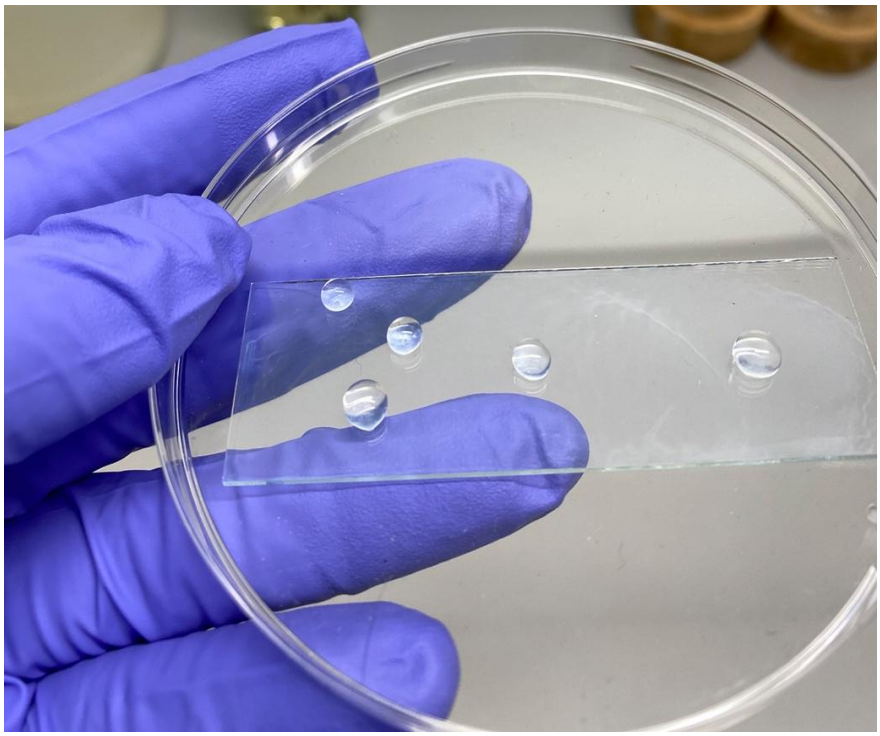

Figure 28: Image of functionalised Al_2O_3 (13 nm) nanoparticles with isostearic acid deposited on a glass substrate. Source: Author's picture based on the results obtained from the experimental setup

Figure 29: Image of functionalized Al_2O_3 (5 nm) nanoparticle after being dispersed in 2-propanol ready to be sprayed onto substrates. Source: Author's picture based on the experimental setup

Chapter V: Analytical and Measuring Instruments

In this section, we discuss the characterisation techniques used for the unfunctionalized, and functionalised material.

Attenuated total reflectance – Fourier transform infrared (ATR – FTIR) spectroscopy

ATR – FTIR spectroscopy is an analytical method used to analyse or determine organic and in certain circumstances inorganic materials, as well as polymer compounds[165], [166].

Infrared spectroscopy has been shown to be a reliable technique used for the examination of ionic interactions and complex formation. Infrared spectroscopy allows the qualitative and quantitative detection of small changes in the particles phase, therefore it became a versatile tool on the study of the structural change of aerosols [167]. Attenuated total reflectance – Fourier transform infrared (ATR – FTIR) is a more sensitive measuring modes when comparing to transmission [166], due to the infrared light. The inherent property of IR spectroscopy is the depth of the penetration of the IR beam toward the sample that is being analysed, usually on the range of 1 – 5 μm [168].

The IR spectra encompasses the wavenumber between 12500 – 10 cm^{-1} and it can be classified in three region such as, near-infrared (12500 – 4000 cm^{-1}), mid-infrared (4000 – 200 cm^{-1}) and far-infrared (200 – 10 cm^{-1}) [169]. IR spectroscopy in this thesis, have played an essential part in the structural investigation of the class of compound of the carboxylic acids and nanoparticles. One of the advantage of using IR spectroscopy for the analyse of the samples is such as the direct information provision regarding the chemical material structure [170].

Carboxylic acid can be described as an organic acid that includes a carboxyl group (C(=O) OH) connected to an R-group [171].

As seen in the Figure 30, by using OMNIC software by adopting the ATR – FTIR spectra method measured the transmittance of various infrared light wavelengths for isosteric acid, lanolin, alumina, and silica for this specific project before and after the functionalisation of the nanoparticles. The IR for all materials on the x-axis starts from 4000 cm^{-1} and anything in the region between 400 – 1000 cm^{-1} is acknowledged as the fingerprint region for each compound.

On the other hand, this region is nearly never discussed because it includes a great number of peaks and as a result, it is difficult to distinguish individual peaks.

IR spectroscopy was mainly used to look whether the carboxylic acids is chemical absorbed onto the surfaces, transmittance and wavenumber data were obtained through this equipment and in mathematical terms Equation 8 and 9, can be used to obtain the transmittance or absorbance values

Equation 8

$$Transmittance = \frac{I}{I_o}$$

Equation 9

$$Absorbance = log\frac{1}{Transmittance}$$

Where I is the intensity of light that can pass through the material and I_o is the intensity of incident light.

Figure 30: Image of IR spectroscopy. Source: The author's picture

Thermogravimetric Analyser (TGA)

Thermogravimetric analyser (TGA) is a method used in which the mass of the nanoparticles are controlled against time as the temperature changes [172] and it is performed to examine the thermal properties of the nanoparticles [173].

As seen in Figure 31, a TA instrument (SDTQ600) was used to obtain the thermal properties analysis for the functionalised nanoparticles. The instrument can provide a sample purge flow (mL/min), heat flow (mW), weight (mg), time (min) and temperature (^{o}C). Before initiating the measurements, the SDTQ600 instrument weight was tared. There are two crucibles on the TGA, one is used as a reference during the measurements, which remains empty, and the other crucible was filled with small amount of the functionalised nanoparticles that were due to be analysed. Subsequently the combustion chamber was closed and afterwards heated in the attendance of continuous air flow up to a rate of 100 mL/min to 700^{o}C at a heating rate of

10ºC/min. The TGA device results, that examined weight losses versus time when applying the heat rate, were investigated through a Universal V4.5A TA instrument analyser, which is essential for the identification of the hydrocarbon branched groups.

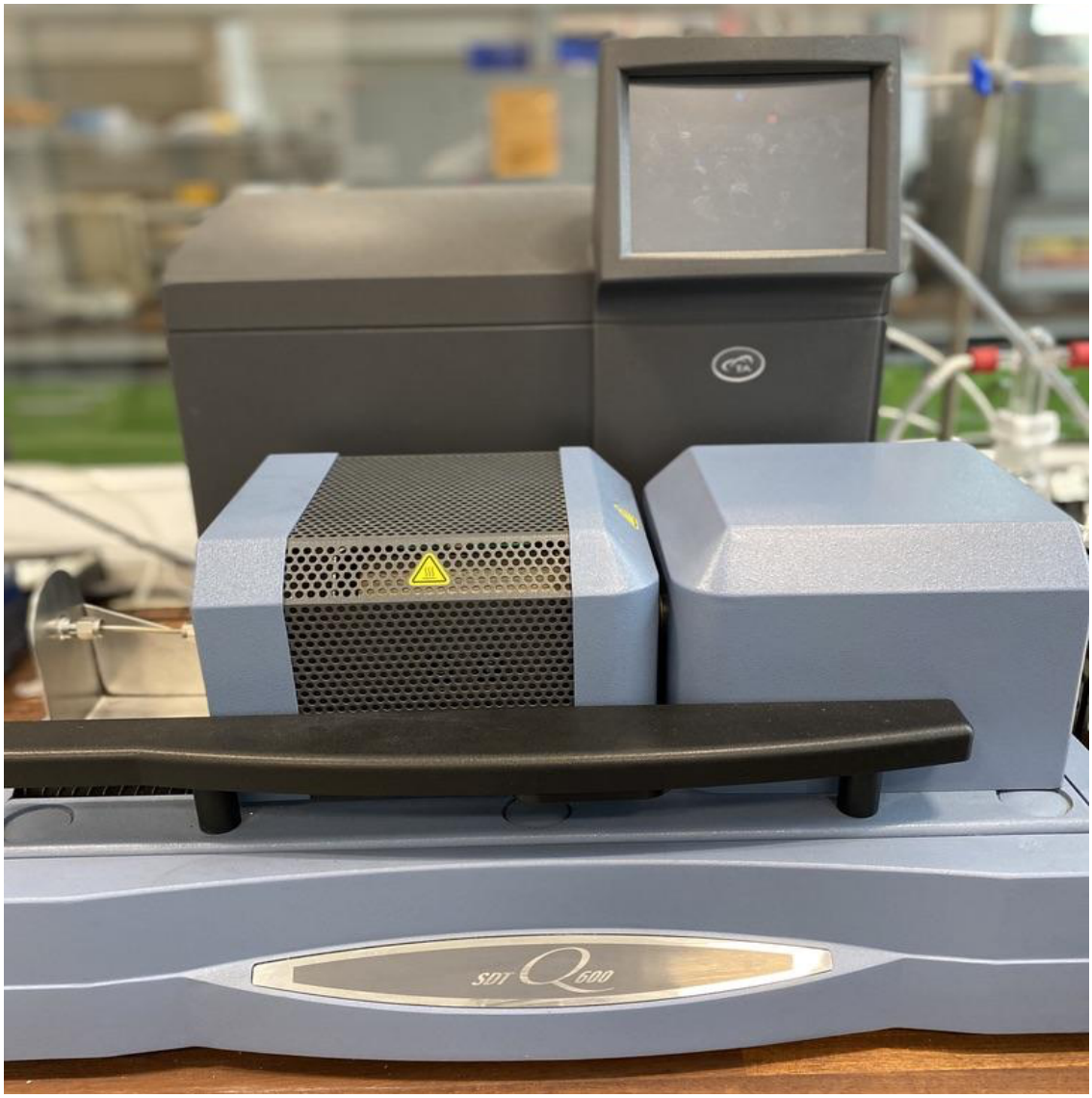

Figure 31: Thermogravimetric analyser (TGA). Source: Author's picture

Scanning Electron Microscopy (SEM)

SEM is a topographic technique used to measure the morphology of the functionalized nanoparticles spray coated onto the microscope slides. The schematic illustration of the instrument is shown in Figure 32, and the process of measurement included scanning across the sample using the beam of electrons and backscattered electrons are analysed to obtain a physical image of the substrate.

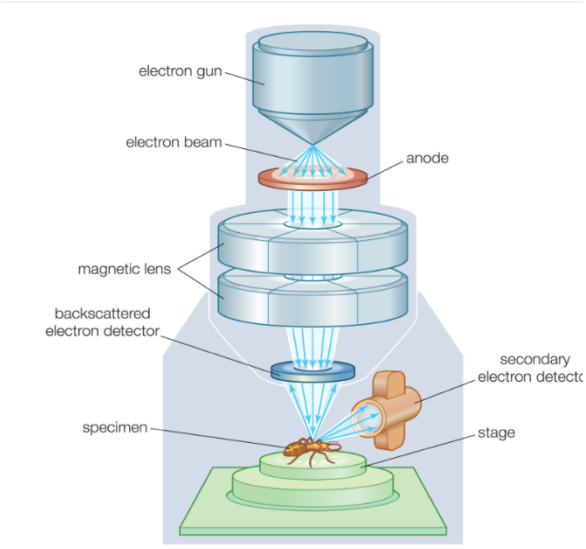

Figure 32: Scanning electron microscopy (SEM) [174]

Measurement of static contact angle

The static CA measurements is normally used to characterise the wettability on solid surfaces. Generally, volume in the range of 2 to 5 μL for each water droplets are placed on the solid surface for the characterization of the contact angles. The error in contact angles and sliding was $\pm 2^{o}$ and $\pm 1^{o}$, respectively. Standard deviation was calculated based on three measurements for each contact angle presented. When comparing the superhydrophobicity of different surfaces, the CA should be evaluated using the same volume water droplet. Taking in consideration that the CA is affected by the volume of water droplets and the gravity force [36], [85]. To decrease the effect of the shape of the droplet of water produced by the gravity

force, Zhang et al. [84] suggested a method to measure the CA by using a much smaller water droplet. First, a 5 μL water droplet is dispersed on a superhydrophobic surface and CA of 154^{o} was obtained. The volume of the droplet of water was then reduced to 0.3 μL and 173^{o} value for contact angle was obtained after been evaporated for 40 minutes under ambient conditions [36], [86].

For all analysed material, we conducted the same amount of layer of spray coating on the surface this was done to ensure consistency of the sprayed slurry onto different surfaces. This deposition was done on the fume hood at room temperature, which was then left there to dry for few minutes and finally it was used for the characterization purposes. The coating solution was prepared using different ratios of nanoparticles and their respectively carboxylic acids as seen on Table 3.

An additional step was added into the functionalisation of alumina (50 nm) to obtain the superhydrophobicity. The step included leaving the prepared slurry overnight (24 h) on the Microstirrer Magnetic Stirrer while heated to 30^{o}C before depositing it into the surface.

Drop shape analyser

The DSA25 drop shape analyser (Krüss), as seen in Figure 33, applying the sessile drop method was used to obtain the contact angle measurements. The static contact angle measurement was carried out under ambient conditions and using deionised water.

The equipment is composed of a fixed stage and microscope camera. The image displayed on the screen of the computer of the micro water droplet was measured through special software (Advance) under ambient conditions, that are originated by means of an automated syringe on the membrane surface.

Figure 33: Drop shape analyser (Krüss). Source: Author's picture

Method	Description	Advantages	Disadvantages
IR Spectroscopy	An absorption technique widely used in qualitative and quantitative analyses [175]	• Used to identify unknowns by interpretation of characteristic absorbances and comparison with spectral libraries • Does not destroy the sample and does not need any preparation	• Due to its sensitivity the equipment needs to be properly tuned • Samples having aqueous solutions and complex mixtures are complicated to analyse • Due to its sensitivity, minimum sample quantity is required to scan the sample spectrum

TGA	An analytical technique used to identify the sample thermal stability in which the mass of the sample is measured over time as the temperature changes [176].	• The furnaces allow fast heating and cooling rates • Highly accurate of balance and precise temperature control • Easy sample changing • Fast heating rate	• Very small weight of samples is used • Heterogeneous materials cannot be tested • Sensitive to heating rate and sample masses results in shift in temperature
SEM	An analysis technique that provides information regarding the microstructure of coated surface displaying an image of the sample by scanning its surface to create a high resolution image with a low energy beam of electrons [177].	• Gives quantitate on how rough the surface is • Provides digital image with resolution as low as 15 manometers • Straightforward to operate • It is a rapid process	• Limited by how much area is captured • Special training is necessary to operate the equipment • The equipment is large and expensive and needs to be kept in a place free of vibration interference •
Sessile drop (contact angle)	The amount of a droplet of water deposited on the measured surface is increased, and the value of the advancing contact angle is obtained. For the receding contact angle, the amount of the droplet of water is reduced, and the value of the	• Simple method • It is quick to perform • Small amounts of water are required • It is possible to measure samples with small surface areas • Provides information about the	• It can be a time consuming • It is sensitive therefore errors can occur if protocol is properly followed • Small number of impurities in the water can cause

	receding contact angle is obtained.	uniformity of the sample	experimental error

Chapter VI: Results and discussion

The IR spectroscopy was used to examine whether the carboxylic acid chemically absorbed on the surface, TGA to calculate the loading of the carboxylic acid on the surface of the nanoparticles, SEM to measure nanoparticles morphology and contact angle to examine the wettability.

Infrared spectroscopy

IR spectroscopy was performed to analyse if the carboxylic acids had been chemically absorbed upon the functionalised nanoparticles. For instance, the carboxylic acids used in this study are lanolin and isostearic acid and as described in the project rationale the coating of Al_2O_3 (13 nm) with lanolin is more suitable for SALTs.

The IR spectra of isosteric acid is shown in Figure 34, the peak values and their respectively assignment are presented on Table 4, the as received isosteric acid presents C = O stretching band (wavenumber = 1701 cm^{-1}) [181]. The peaks at 2952 to 2867 cm^{-1} are related to aliphatic C – H stretches. The peak of 1466 cm^{-1} is related to symmetric stretches C – H bending; 1364 cm^{-1} peak is related to the O – H bending, respectively.

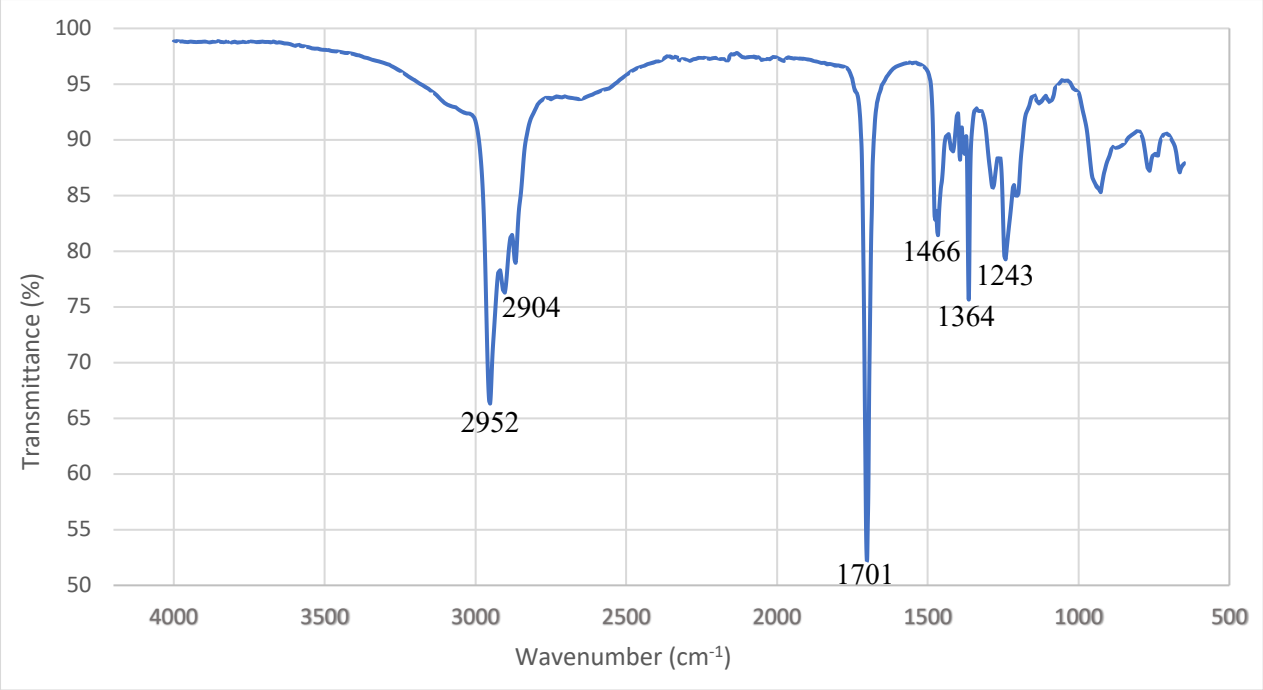

Figure 34: IR spectrum of as received isosteric acid

Table 4: IR characterisation band of as received isosteric acid [181], [182]

Wavenumber (cm^{-1})	Assignment
2952	C – H stretching
2904	C – H stretching
2867	C – H stretching
1701	C = O stretching
1466	C – H bending
1364	O – H bending
1243	C – O stretching

As seen in the Figure 35, the as received lanolin demonstrates C – H stretching bands (wavenumber = 2918 and 2850 cm^{-1}), the frequency of 1464 cm^{-1} is due to vibrations classified as CH_2 scissoring which is a bend [183], [184], and 1376 cm^{-1} peak is due to a motion of the CH_3 groups and is a bend classified as a umbrella mode [185]. The peaks are assigned in Table 5.

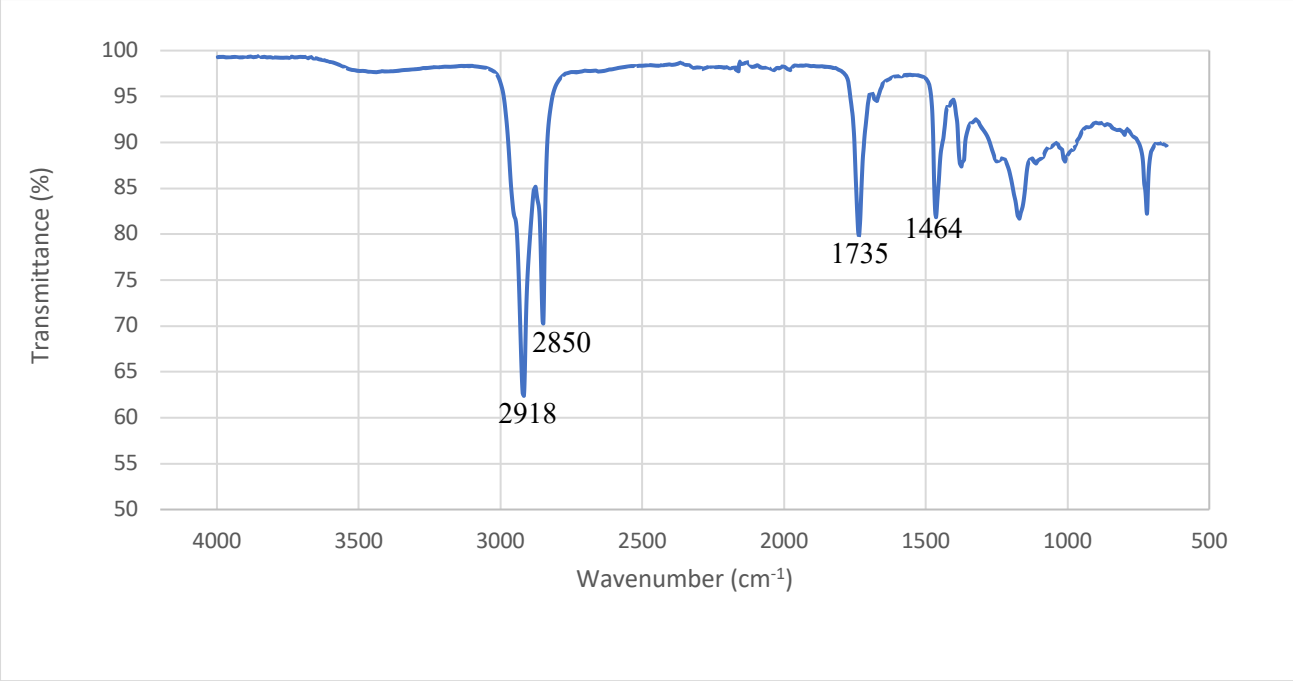

Figure 35: IR spectrum of as received lanolin

Table 5: IR characterisation band as received lanolin[182], [186], [187]

Wavenumber (cm^{-1})	Assignment
3542	O – H bending
2918	C – H stretching
2850	C – H stretching
1735	C = O stretching
1464	CH_2 / CH_3
1376	CH_2 / CH_3

The difference on IR spectra between lanolin and isosteric acid, is mainly due the fact lanolin is a mixture of alcohol, naturally formed esters originated and fatty acids, thus we measure the presence of alcohol at around 3500 cm^{-1} in lanolin[13].

As seen in the Figure 36, before the functionalization, the IR spectra of the as received Al_2O_3 (13nm) nanoparticles demonstrate no significant bands besides the – OH stretching at 3432 cm^{-1} [188]. The bands below 1000 cm^{-1} are due to the lactase vibrations of Al_2O_3 nanoparticles [189].

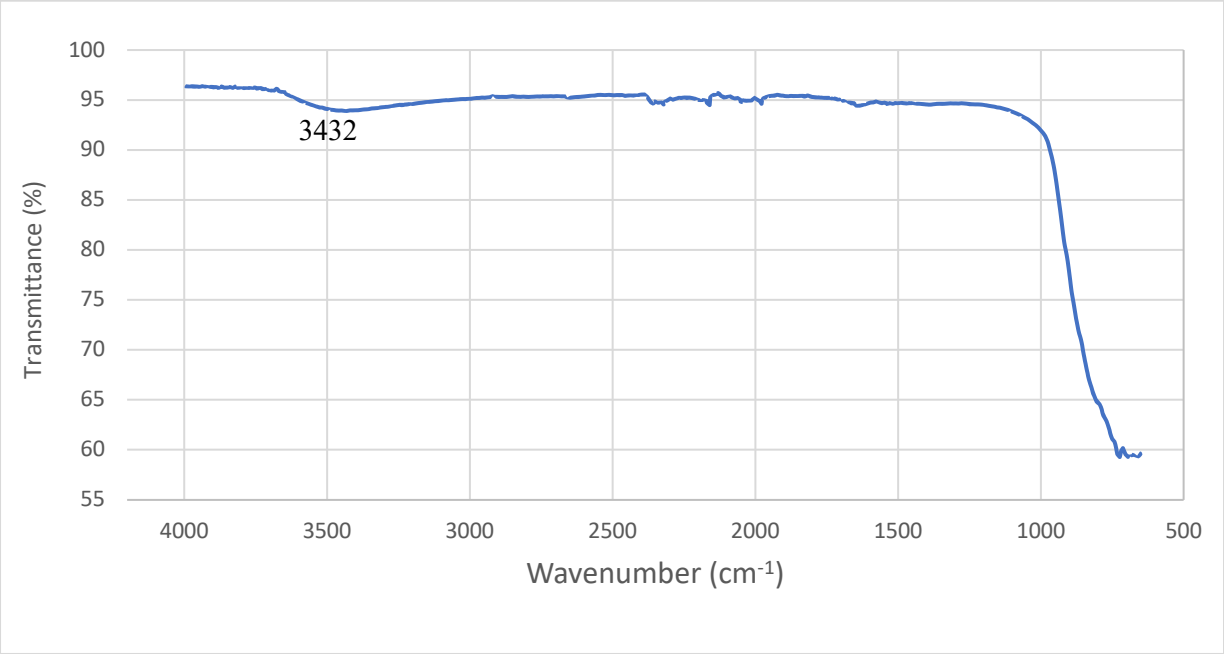

Figure 36: IR spectrum of unfunctionalized Al_2O_3 (13 nm) nanoparticles

As seen in the Figure 37, after the functionalization of the Al_2O_3 (13 nm) nanoparticles with isosteric acid and as seen in Figure 38 for the functionalized Al_2O_3 (13 nm) nanoparticles with lanolin (1:5), the nanoparticles demonstrates CH_2 / CH_3 stretching bands between 2852 – 2954 cm^{-1} due to the aliphatic C – H stretches of the acid [182], [190]. The C = O stretching band (wavenumber = 1701 cm^{-1}) as seen previously on the as received isosteric acid, when functionalised with Al_2O_3 (13 nm) nanoparticles the peak disappears and this indicates that adsorption onto the particles has occurred. Figure 37 demonstrates the remain peaks for isosteric acid such as C – H stretches, C – H bending and O – H bending.

New peaks can be seen in the product with lanolin around 1472 cm^{-1} which is due to carbonyl asymmetric stretches on the of steers, therefore this is a C = O stretching when the molecules are on the surface. Above all, C = O group is the most accessible to distinguish peak in an IR spectrum therefore, higher C = O bond order, corresponds to higher frequency. The peak values for the functionalised of the Al_2O_3 (13 nm) nanoparticles with isosteric acid and the functionalised Al_2O_3 (13 nm) nanoparticles with lanolin (1:5) are assigned in Table 6 and 7, respectively.

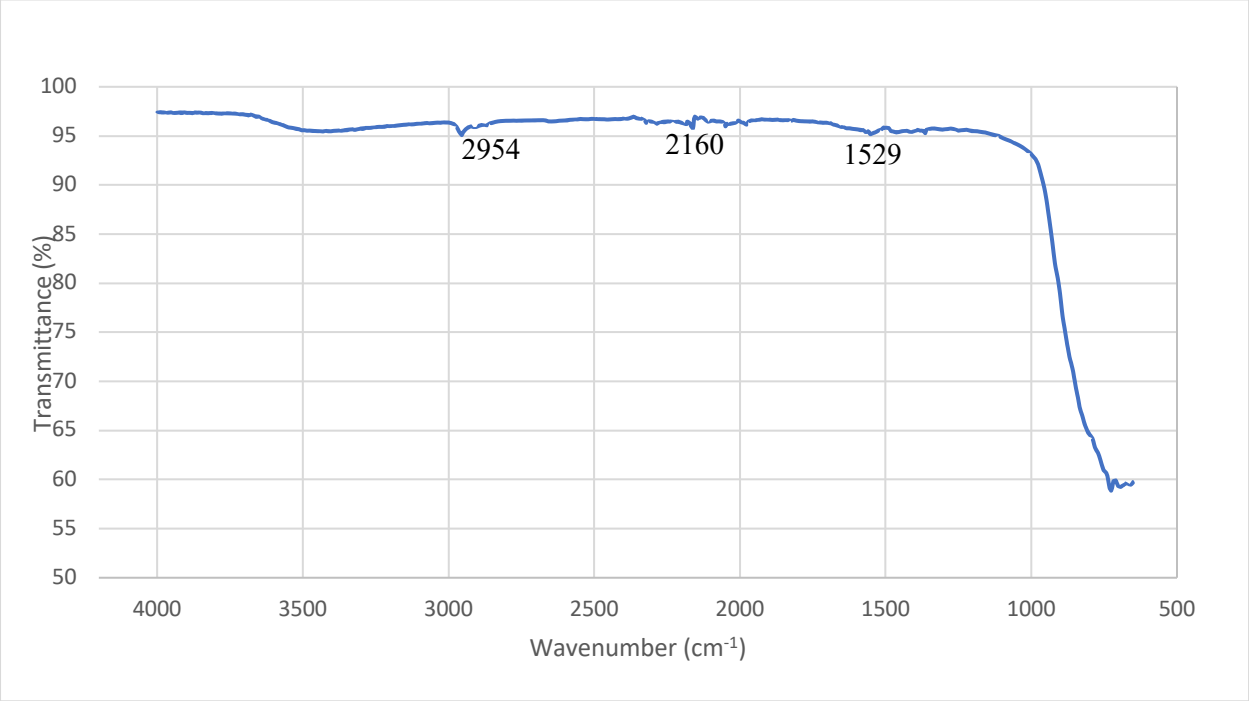

Figure 37: IR spectrum of functionalized Al_2O_3 (13 nm) nanoparticles with isosteric acid

Table 6: IR characterisation band of functionalized Al_2O_3 (13 nm) nanoparticles with isosteric acid

Wavenumber (cm^{-1})	Assignment
2954	C – H stretching
2160	C – H stretching
1978	C = O stretching
1529	C = O stretching
1464	CH_2 / CH_3 bending
1364	O – H bending

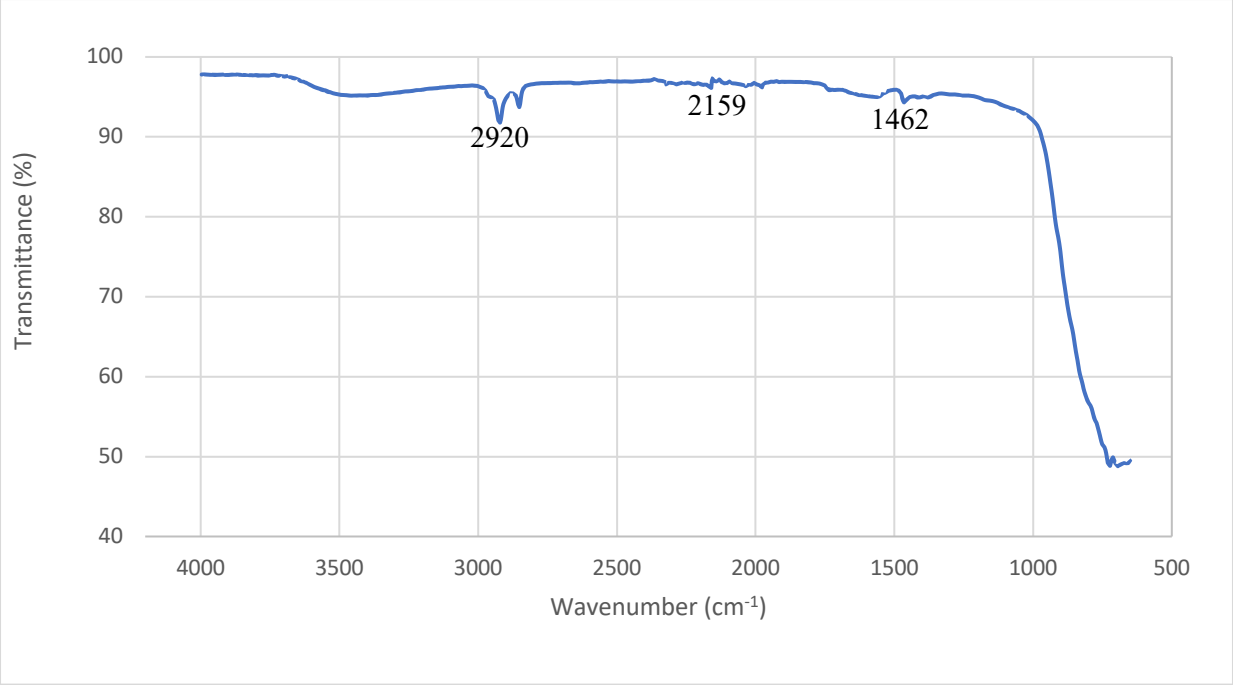

Figure 38: IR spectrum of functionalized Al_2O_3 (13 nm) nanoparticles with lanolin (1:5)

Table 7: IR characterisation band of functionalized Al_2O_3 (13 nm) nanoparticles with lanolin (1:5)

Wavenumber (cm^{-1})	Assignment
2920	C – H stretching
2849	C – H stretching
2322	C – H stretching
2273	C – H stretching
2159	C – H stretching
1978	C = O stretching
1723	C = O stretching
1462	C = O stretching
1395	CH_2 / CH_3 bending
1365	CH_2 / CH_3 bending

Figure 39 shows the IR spectra of as received Silica nanoparticles. The peak of 3383 cm^{-1} is due to the OH groups on the nanoparticles surfaces [181]. The Si – O stretching is important, resulting in a strong band located at 1057 and 794 cm^{-1} [170], [191]. For instance, this difference is essential because those bands can be used to differentiate the composition of SiO_2

(10-20nm) nanoparticles using thermal emission and remote sensing data [192], [193]. The peaks are shown in Table 8.

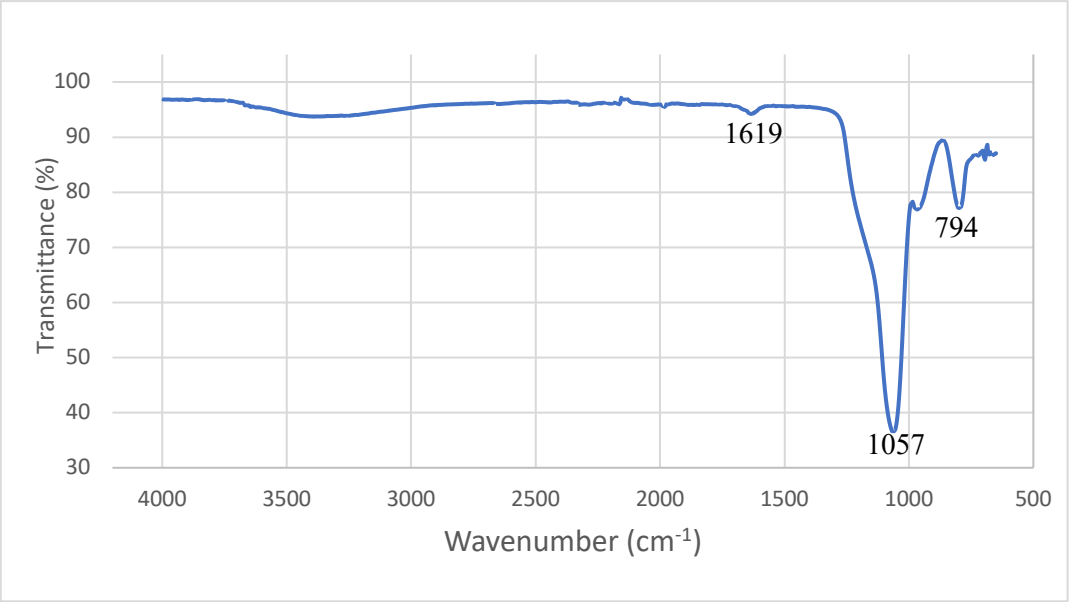

Figure 39: IR spectrum of unfunctionalized SiO_2 (10-20 nm) nanoparticles

Table 8: IR characterisation band of unfunctionalized SiO_2 (10-20 nm) nanoparticles [187]

Wavenumber (cm^{-1})	Assignment
3383	O – H stretching
1619	C = O stretching
1057	Si – O stretching
794	Si – O stretching

Upon the functionalisation of SiO_2 (10-20nm) nanoparticles with lanolin (1:5) OH stretch tends to decrease because of the existence of hydrogen bonded, as can be seen in Figure 40. New peaks also appear at around 2900 to 2800 cm^{-1} which is due to the presence of C – H stretches. The peak values are assigned in Table 10.

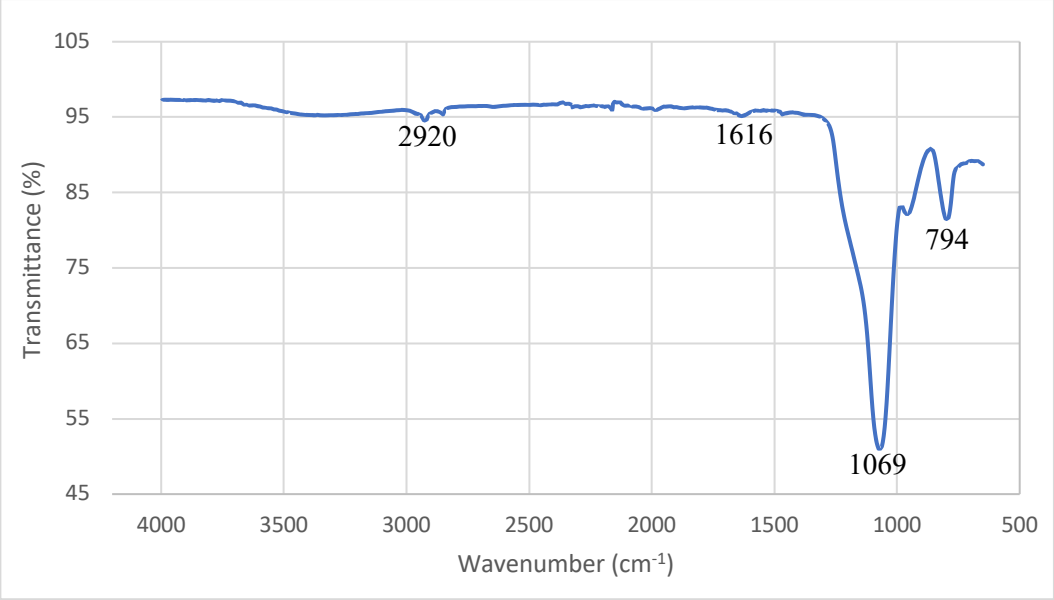

Figure 40: IR spectrum of functionalized SiO_2 (10-20 nm) nanoparticles with lanolin (1:5)

Table 9: IR characterisation band of functionalized SiO_2 (10-20 nm) nanoparticles with lanolin (1:5)

Wavenumber (cm^{-1})	Assignment
2920	C – H stretching
2848	C – H stretching
2312	C – H stretching
2280	C – H stretching
2159	C – H stretching
1977	C = O stretching
1616	C = O stretching
1462	CH_2/CH_3
1069	Si – O stretching
794	Si – O stretching

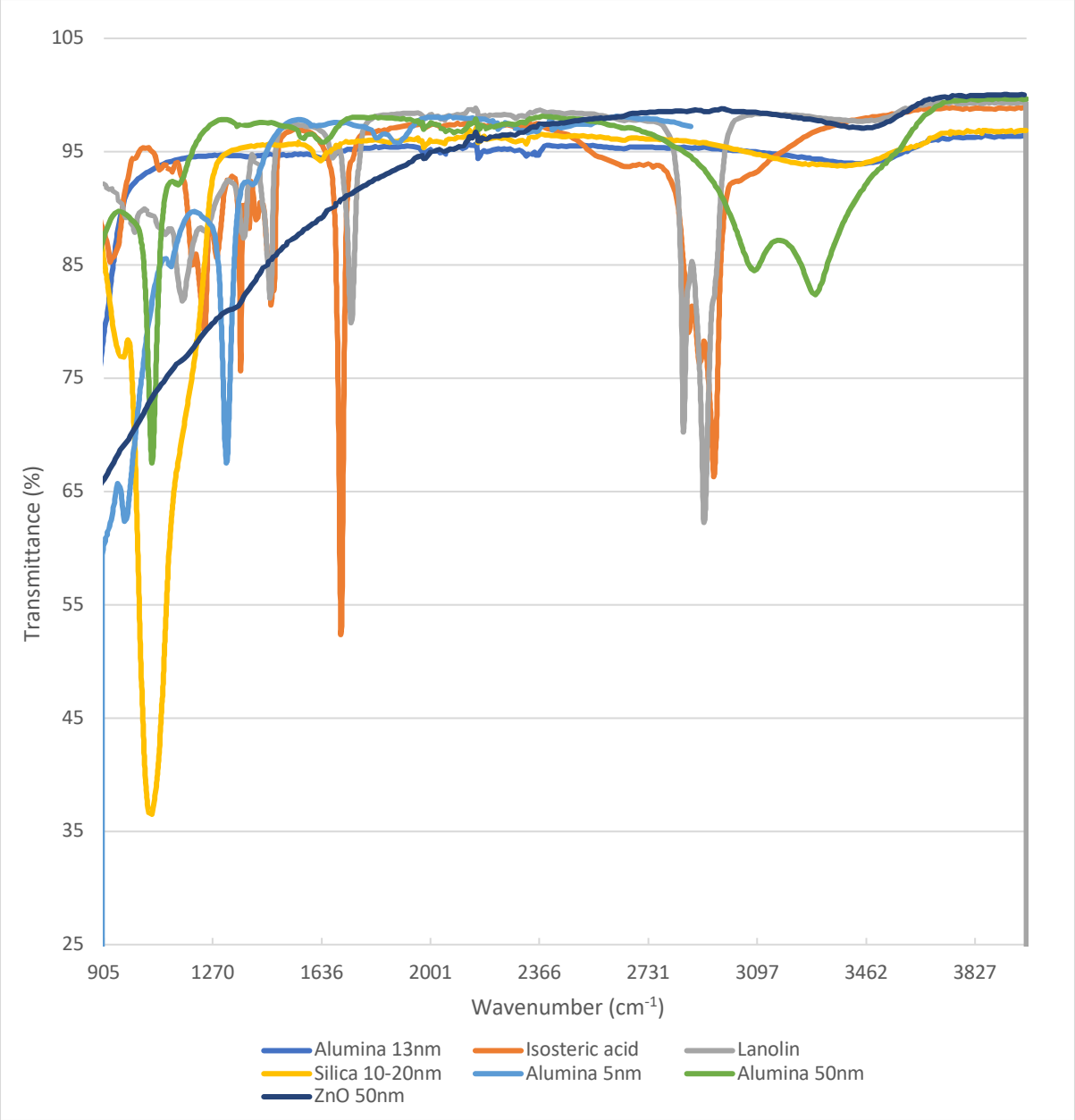

Overlaying IR graph of the unfunctionalized nanoparticles and carboxylic acids used on the manufacture of the superhydrophobic surfaces.

Thermogravimetric analysis

TGA was used to calculate the carboxylic acid grafting densities on the nanoparticles. The data obtained from the functionalised nanoparticles was performed with the aim to calculate the acid grafting densities present on surface of the nanoparticles. As seen in Figure 43.a), the Al_2O_3 (13 nm) as received nanoparticles demonstrate no significant mass loss at 760º C, despite that, after the nanoparticles were functionalised with the appropriate amount of carboxylic acid,

weight loss started at 180ºC with rapid weight loss taking place in between 270 – 580ºC and this difference is due to the loss of carboxylic acids. Weight losses of the as received nanoparticles were mainly because of the removal of surface hydroxyl groups and adsorbed H_2O [194] and at temperatures higher than 200ºC the weight losses are mostly assigned to the removal of surface hydroxyl groups from the nanoparticles [194].

It should be noted that the lanolin underwent combustion in the range between 200 – 240ºC, the substance was heated under both air and argon. The heat and the presence of oxygen cause the carboxylic acid to oxidise, as is shown in Figure 41, one possible reason for this, is the fact that it has a low flash point. As a safety concern the TGA data for lanolin is only up to 300ºC.

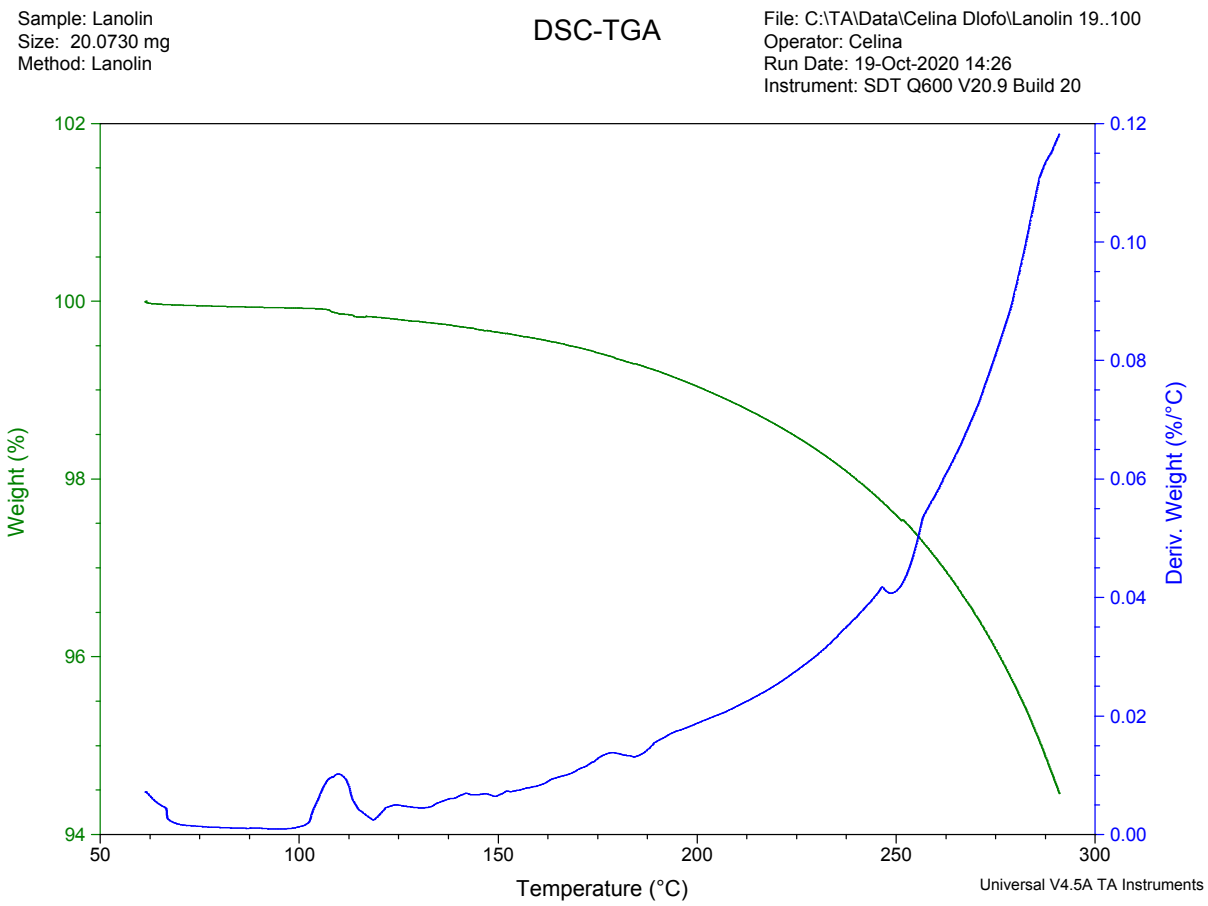

Figure 41: TGA data of the as received lanolin.

The organic weight losses presented on the Table 10 corresponds to the differences among the mass losses observed in the heating profiles of the functionalized nanoparticles. For instance,

Al_2O_3 (13 nm) nanoparticles when functionalized with isosteric acid demonstrated a weight loss of 8.38 % after heating to 760ºC. On the other hand, for functionalised Al_2O_3 (13 nm) with lanolin ratio (1:5) a weight loss of 15.65 % was observed following the heating towards the same temperature.

The weight loss values presented on the Table 10 was used to calculate the acid grafting densities for the material, and the grafting density can be described mathematically as [164]:

Equation 10

$$Grafting\ density = \left(\frac{wt\%}{100 - wt\%}\right) x \left(\frac{6.022x10^{23}}{M_w x SSA}\right)$$

wt% – percentage weight loss
M_w – molecular weight of the acids
SSA – specific surface area

- SSA for alumina $100x10^{18}$ m^2/g [164]
- SSA for silica based on sigma $175\text{-}225x10^{18}$ m^2/g [164]

As seen in the figure 42, the derivative of the TGA curve for the functionalised Al_2O_3 (13 nm) with lanolin (1:5) is largest at about 350ºC. The weight loss at this temperature is assigned to the combustion of chemisorbed isostearate from the surface of the Al_2O_3 (13 nm) nanoparticles [195]. Equation 10 were used to obtain the grafting density for the functionalized samples and their respectively values can be seen in Table 10. Presuming that the weight loosed up to 100ºC is due to the removal of water and taking the specific surface area of the as received material to be $100\pm15x10^{18}$ nm^{-2}, using the TGA data, it was noted the isosteric grafting density of the Al_2O_3 (13 nm) spherical nanoparticles were 1.9 nm^{-2}. Additionally previous group have reported isosteric grafting densities of ~1, 0.9 and 0.5 nm^{-2} for Al_2O_3 spherical nanoparticles of 5, 50 and 135 nm nanoparticles size [194]. When comparing grafting density value with the same nanoparticles but functionalized with lanolin (1:5) a grafting density of 3.35 and 5.56 nm^{-2} were obtained, and those values correspond to different molecule weight of lanolin such as 333 and 201 g/mol, respectively. Using the same molecular weight of lanolin, functionalised

Al_2O_3 (50 nm) nanoparticles with lanolin (1:15) were obtained with grafting density of ~4.67 and 7.75 nm^{-2}.

For last, it was observed a grafting density of ~1.74 and 2.88 nm^{-2} for the functionalised SiO_2 (10-20 nm) nanoparticles with lanolin (1:5), however, in this case the specific surface area of the as received SiO_2 material is assumed to be $200x10^{18}$ m^2/g, by taking the average of the values that can be considered for the silica nanoparticles.

There are two readings of grafting densities for the functionalised nanoparticles with lanolin because lanolin is such a complex mixture and it was not possible to find the exact specific surface area formula but based in literature, we found out that lanolin has carbon 13 to 24, therefore a molecular weight of one extreme for a minimum of 13 and other for a maximum of 24 carbon was calculated. The real grafting density would be somewhere between these two values also observed on Table 10.

The grafting density is an important feature to consider when designing nanoparticles for biological or environmental applications. The weight loss of organic material is presented on table 10, a percentage of mass loss results from excess of carboxylic acid. The excess of carboxylic acid was difficult to remove after repeated purification attempts, however, appropriate corrections were made for calculating the grafting density and their respective value which were also shown on the same table for the functionalised nanoparticles. The lower grafting densities suggest that they are less reactive to what we have used in the synthesis.

From the results shown on table 10, only Al_2O_3 (13 nm) with isostearic acid and Al_2O_3 (13 nm) with lanolin (1:5) had carboxylic acids high enough to create superhydrophobic surfaces.

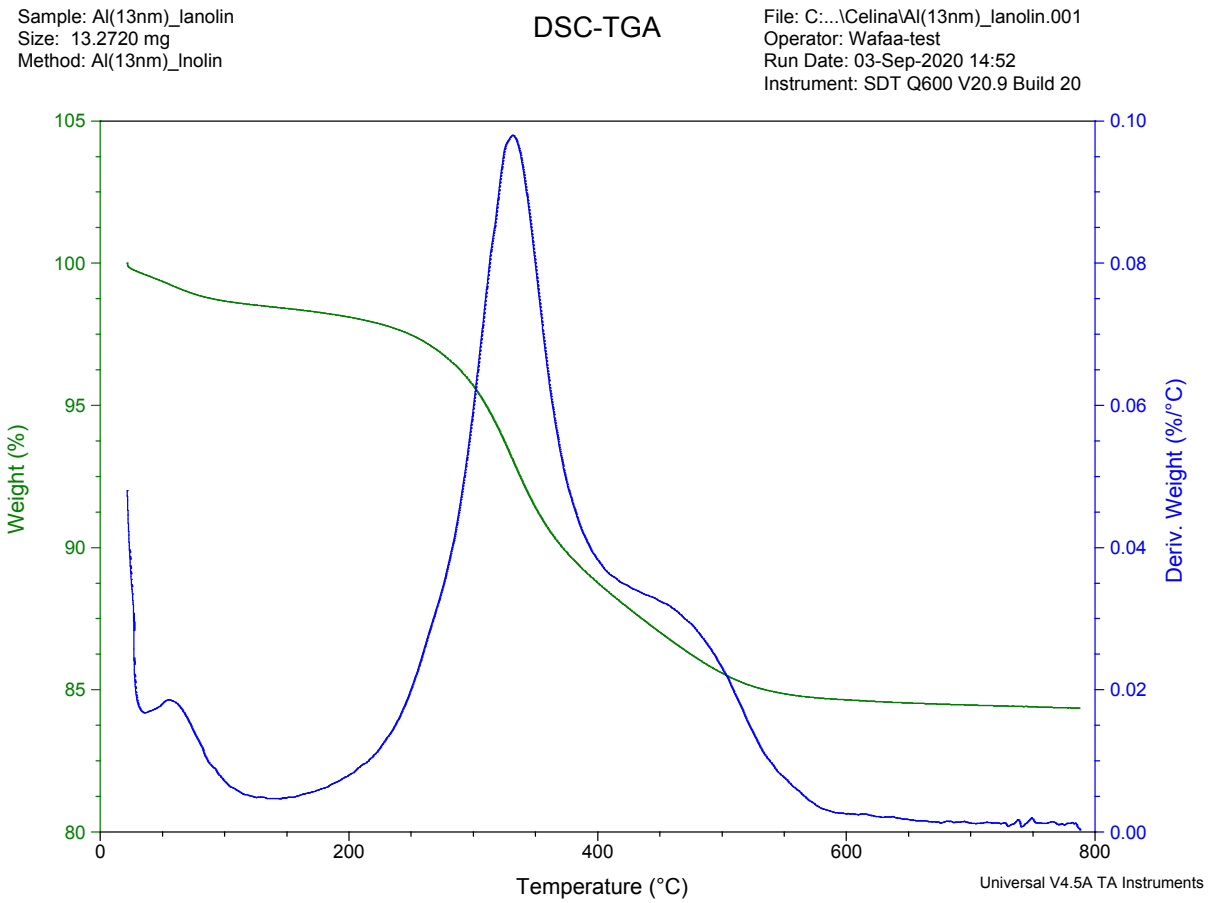

Figure 42: TGA data of the alumina (13 nm) with lanolin (1:5), dashed curves correspond to derivatives

As seen in Figure 42, the blue shoulder between 400 to 500°C are related to the presence of unreacted carboxylic acid in this case lanolin that is not well banded. The presence of the blue shoulder could have been reduced, if further purification was done on the functionalised nanoparticles and this extra step could possibly result in better contact angle measurements because the surface would likely be purer and the roughness more uniform.

Appendix A illustrates the derivative of the TGA curve for the functionalized Al_2O_3 (13 nm) with isosteric acid, functionalized Al_2O_3 (13 nm) with lanolin (1: 15), unfunctionalized Al_2O_3 (13 nm) and unfunctionalized silica (10 – 20 nm). Samples such as functionalized silica (10 – 20 nm) with isosteric acid, functionalized silica (10 – 20 nm) with lanolin (1:5), functionalized Al_2O_3 (13 nm) with lanolin (1:10) were not analysed and this was due to limitations related to COVID-19 such as not being able to access the laboratory.

Table 10: Calculated grafting density as a function of the organic mass loss data obtained using TGA for the functionalized Al_2O_3 (13 – 50 nm) and SiO_2 (10-20 nm) nanoparticles [164]

Sample	Weight loss of organic material (%)	SSA ($x10^{18}$ m^2/g)	Molecular weight (g/mol)		Grafting density (nm^{-2})	
Al_2O_3 (13 nm) with isostearic acid	8.38	100	284.48		1.9	
Al_2O_3 (13 nm) with lanolin (1:5)	15.65	100	201	333	5.56	3.35
SiO_2 (10-20 nm) with lanolin (1:5)	16.12	200	201	333	2.88	1.74
Al_2O_3 (50 nm) with lanolin (1:15)	20.56	100	201	333	7.75	4.67

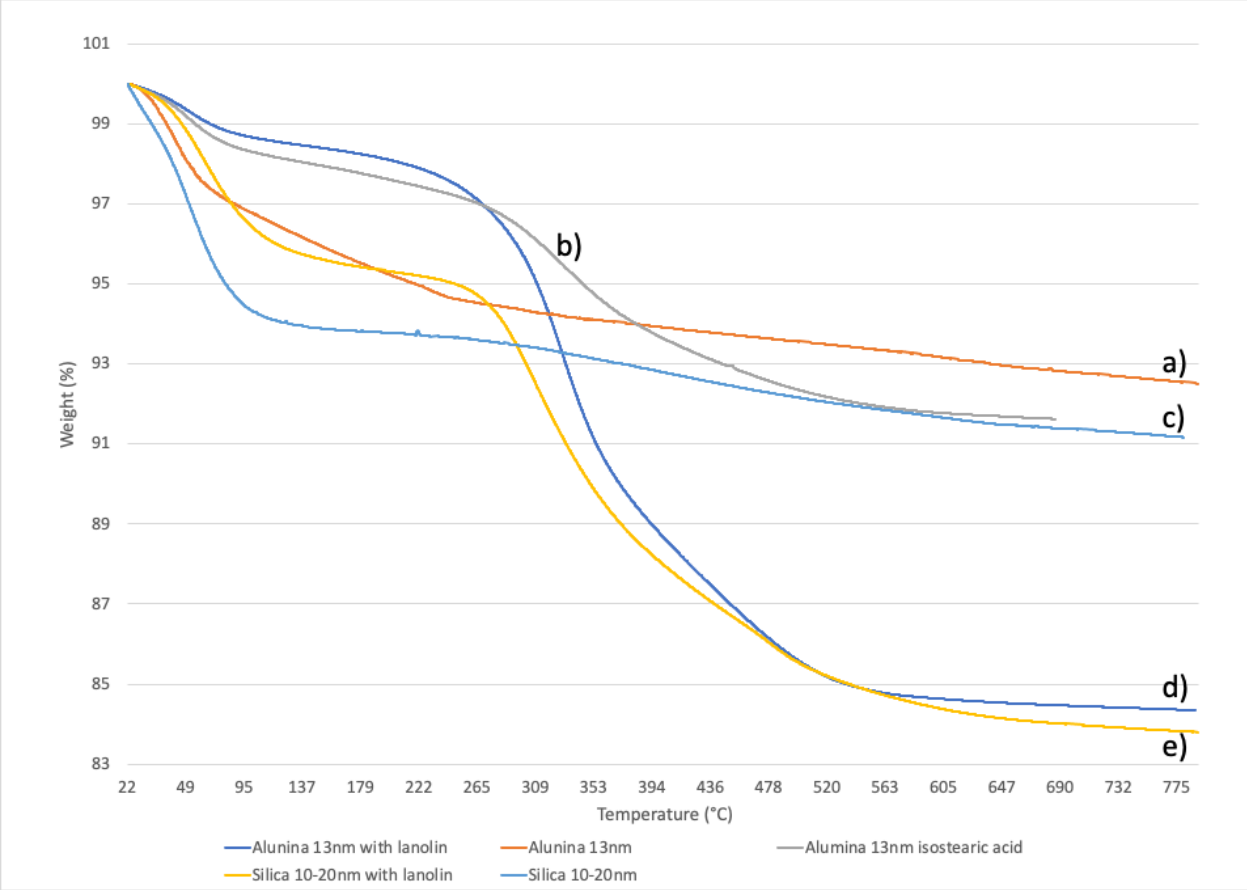

Figure 43: TGA of a) unfunctionalized Al_2O_3 (13 nm) nanoparticles, b) functionalized Al_2O_3 (13 nm) with isosteric acid, c) unfunctionalized SiO_2 (10-20 nm) nanoparticles, d) functionalized Al_2O_3 (13 nm) with lanolin (1:5) and e) functionalized SiO_2 (10-20 nm) with lanolin (1:5)

Surface morphology and surface roughness

The SEM was carried out to study the morphology of unfunctionalized and functionalized samples that were prepared through spray coating onto glass microscope slides. Different images were captured for the samples in scale bar = 1 µm and magnification between 5 – 10 KX.

Figure 44 and 45, show the SEM of the unfunctionalized Al_2O_3 (13 nm), and unfunctionalized SiO_2 (10-20 nm) nanoparticles, respectively. The pictures demonstrate almost homogeneous surface which is relatively smooth and have low surface roughness when compared to functionalised materials Figure 47 to 50. The unfunctionalized Al_2O_3 (50 nm) nanoparticles, shown in Figure 46, demonstrates quite a heterogeneous surface with visible grooves and these grooves results on surface roughness being amplified. This is because the size of the

nanoparticles play an important role on wetting behaviour and the properties of the nanoparticles may affect the experimental process.

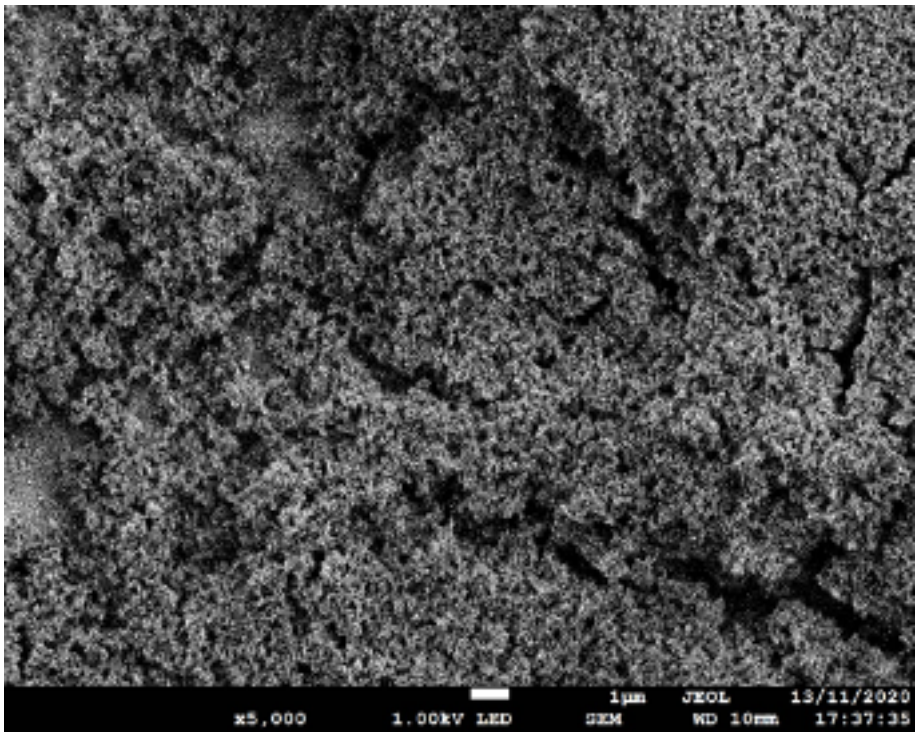

Figure 44: SEM images of film spray coated onto a microscope slide of unfunctionalized Al_2O_3 (13 nm) nanoparticles

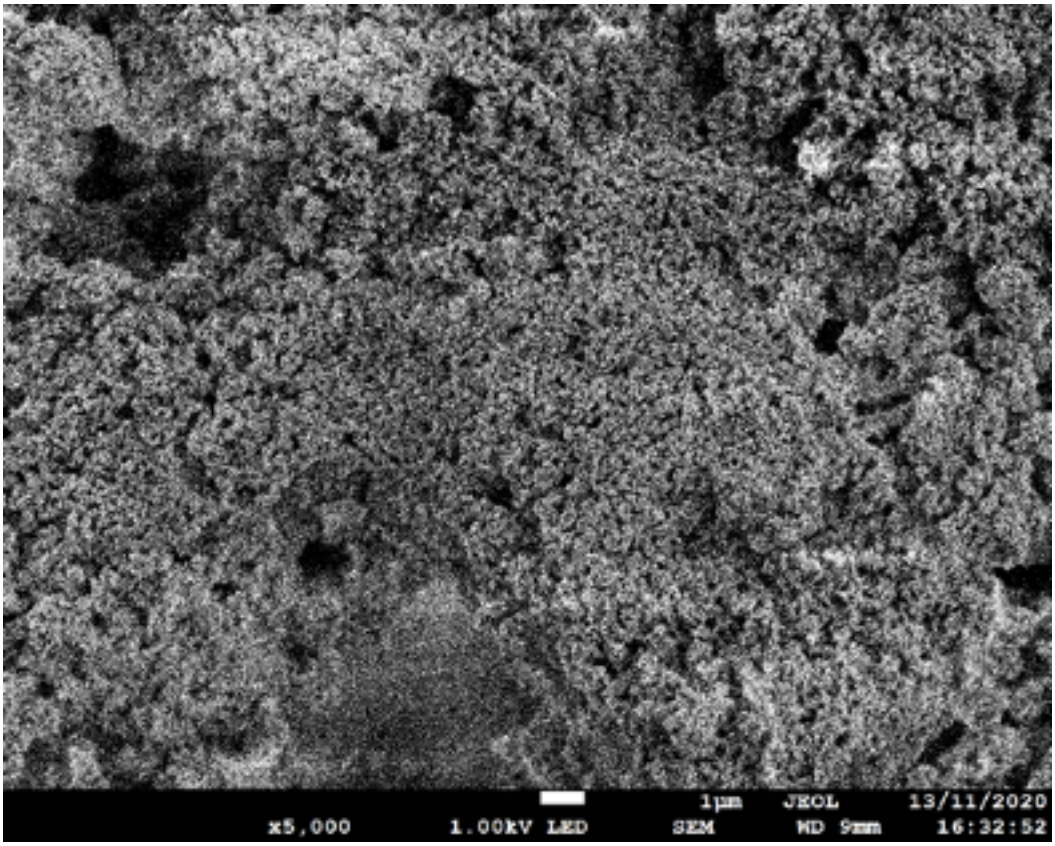

Figure 45: SEM images of films spray coated onto a microscope slide of unfunctionalized SiO_2 (10-20 nm) nanoparticles

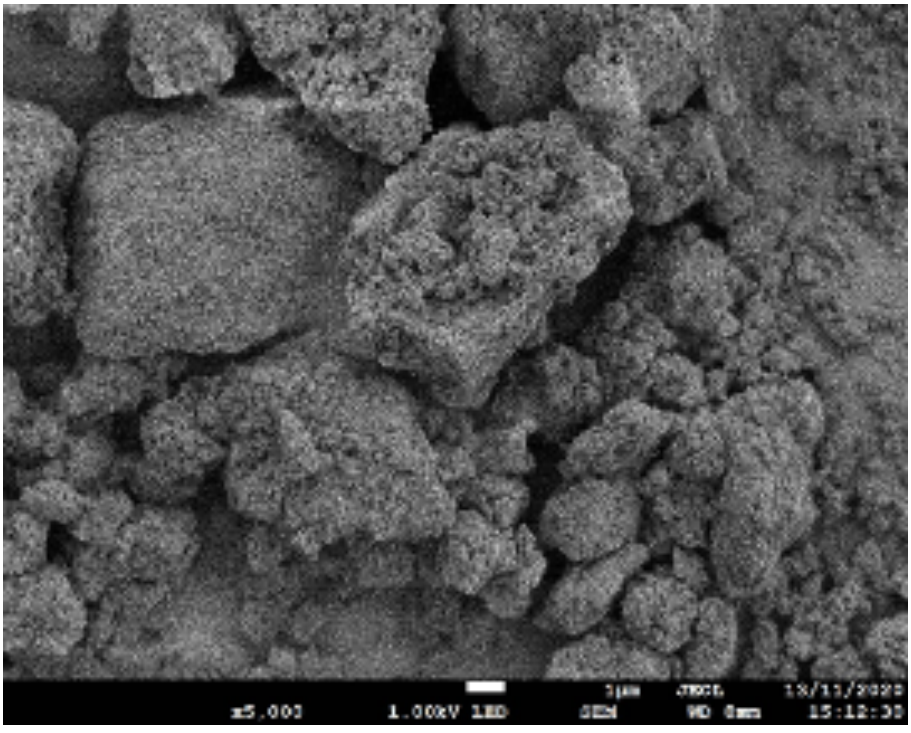

Figure 46: SEM images of film spray coated onto a microscope slide of unfunctionalized Al_2O_3 (50 nm) nanoparticles

SEM images of the functionalized nanoparticles films Figure 47.a) and 47.b) show that nanoparticles are being accumulated into a complex porous structure, but it is seen that for the functionalised Al_2O_3 (13 nm) nanoparticles with lanolin the image are brighter when compared with the sample functionalised with isosteric acid. The functionalised particles appear to be much more efficiently packed than unmodified particles, creating highly porous surfaces.

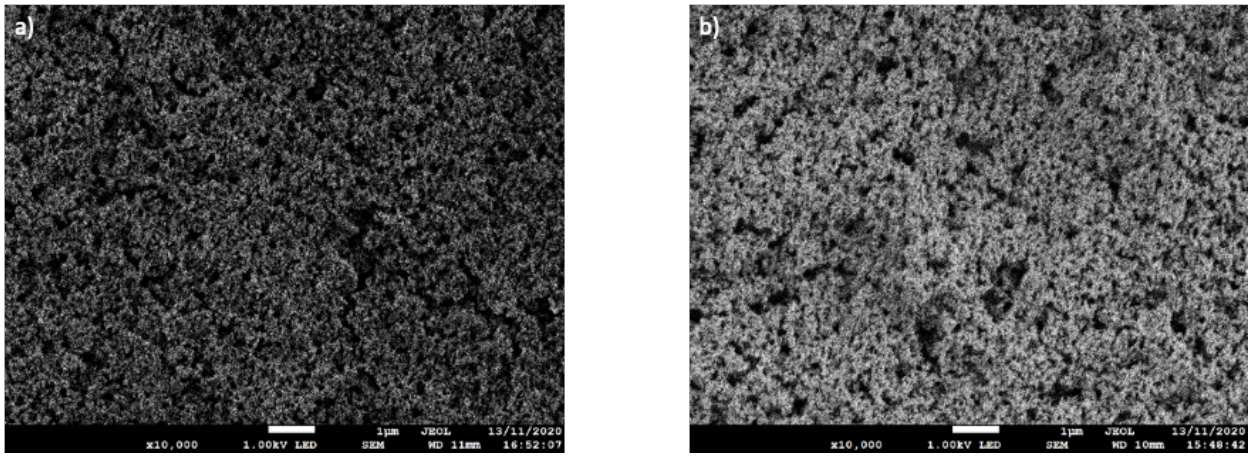

Figure 47: SEM images of film spray coated onto a microscope slide of a) functionalized Al_2O_3 (13 nm) nanoparticles with isosteric acid; b) functionalized Al_2O_3 (13 nm) nanoparticles with lanolin (1:5)

Figures 48 and 49 demonstrates the texture functionalized Al_2O_3 (13 nm) nanoparticles by lanolin with a coating prepared using different mass ratio. As can be seen in Figure 44, the morphology of the sample was relatively homogeneous, demonstrating that the particles were uniformly distributed onto the microscope slide. Despite that, the morphology manufactured from Al_2O_3 (13 nm) nanoparticles with higher concentration of lanolin demonstrated discrete areas where agglomerates of particles can be seen.

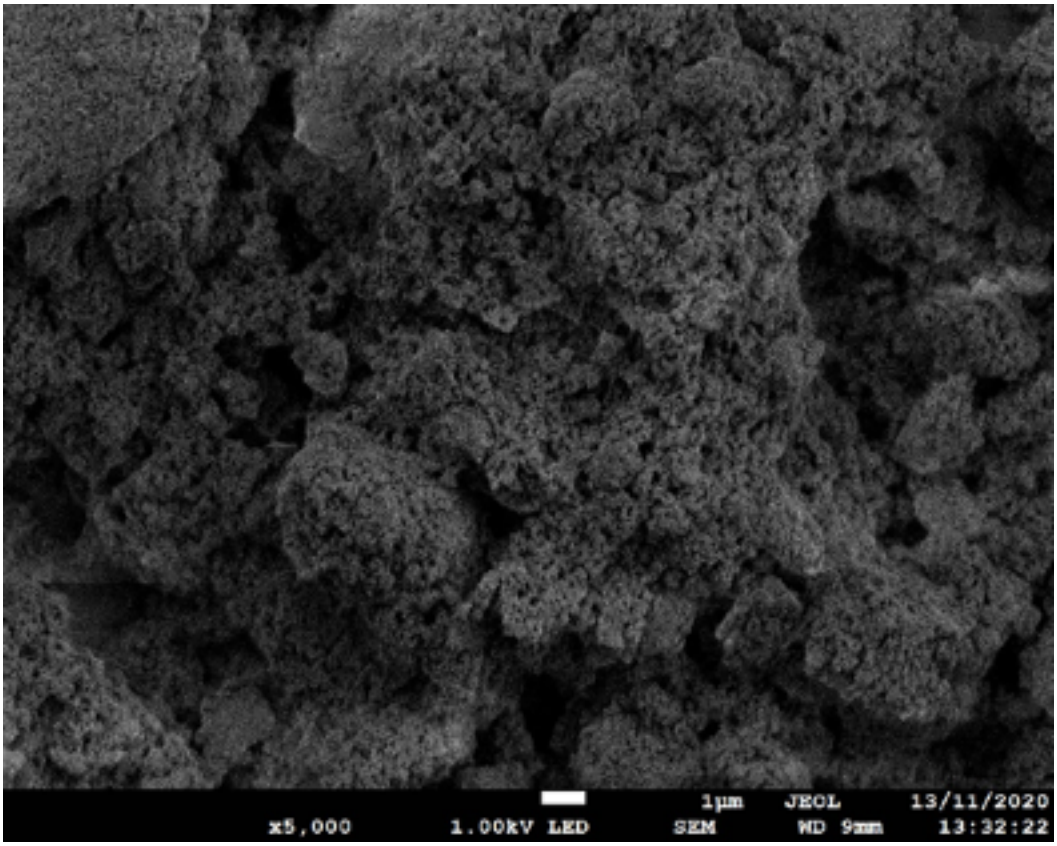

Figure 48: SEM image of film spray coated onto a microscope slide of Al_2O_3 (13 nm) nanoparticles functionalized with lanolin (1:10)

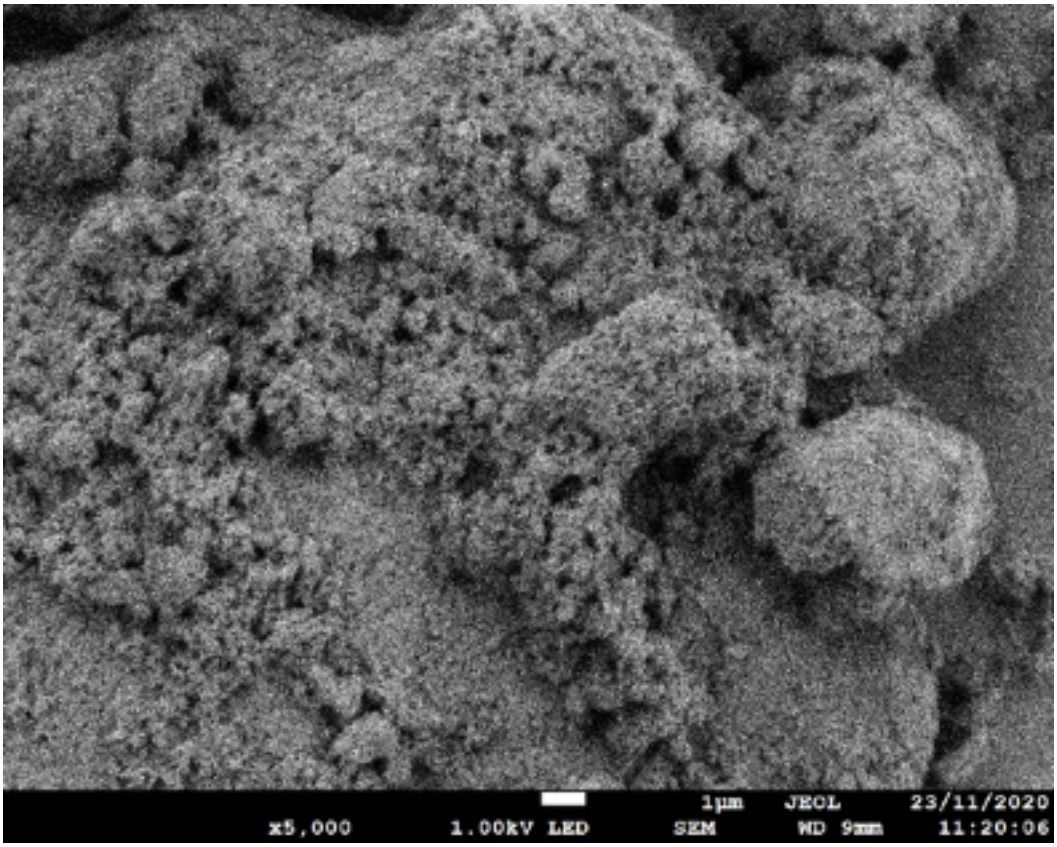

Figure 49: SEM image of film spray coated onto a microscope slide of Al_2O_3 (13 nm) nanoparticles functionalized with lanolin (1:15)

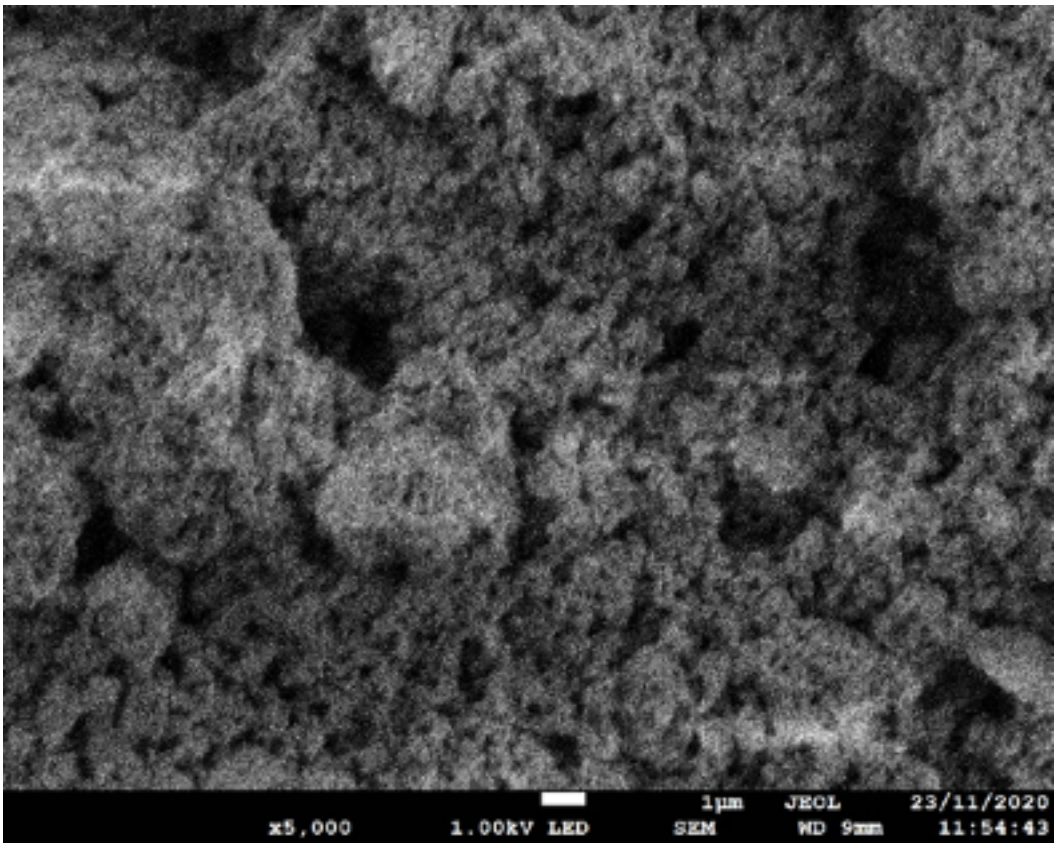

Figure 50: SEM images of film spray coated onto a microscope slide of SiO_2 (10-20 nm) nanoparticles functionalized with lanolin (1:5)

Wettability of the Nanoparticles

The contact angle is a measure of wettability. When a droplet of water is dropped on a solid, it will spread on the surface based on the intermolecular interactions between the solid and the liquid. Water contact angle will immediately give an indication of the wettability of the solid. A contact angle for a droplet of water on a microscope slide of 0^o, indicates that a surface is completely wet. In this section, we will study Wettability, which indicates the degree of wetting as soon as there is interaction between a surface and droplet of water.

Contact angle measurements require placing a droplet of liquid onto a surface and measuring the angle that a stable droplet creates on the surface. The speed and simplicity of the contact angle measurement process makes it appropriate for research and quality control applications. Despite that, these simple measurements only provide a small amount of information regarding the surface, and in some instances, more details are necessary.

Advancing contact angle can be defined as a measure of the liquid-solid cohesion while the receding contact angle is a measure of liquid-solid adhesion. For instance, the advancing contact angle is the largest contact angle in the free energy range, while the receding contact angle is the lowest contact angle.

The advancing contact angle measurements can be done by placing the needle close to the surface and at slow pace and steadily insert water onto the surface, the droplet of water will grow and advance onto the sample surface. As the droplet of water increases, the baseline which is the point where the droplet of water is in contact with the sample, the droplet of water continues to move and advances along the surface. As the droplet of water volume continue to increase, the baseline will simultaneously continue to increase, and the advancing contact angle is reached. The opposite is done for the receding contact angle measurements, in which the droplet of water on the surface is removed from the static droplet.

While obtaining the static and dynamic contact angle measurements, the receding contact angle was harder to quantify compared to the advancing contact angle, because the receding contact angle requires a larger initial droplet of water. However, it is critical to keep droplet volume constant if samples are compared. The advance contact angle has been shown to be less dependent on the droplet volume than the receding angle.

Static and dynamic contact angle measurements for the samples is outlined in the Table 11 and 12 onto a glass and fabric substrate, and photographic images of the water droplets on the surfaces are demonstrated in Figures 51, 52 and 53.

In this study, we worked with silica (10-20 nm) and different sizes of Al_2O_3 such as, 13 nm and 50 nm respectively. Al_2O_3 (13 nm) nanoparticles was the material that presented better and consistent results regarding the superhydrophobicity. Superhydrophobic properties with static contact angle of 153±2^o were obtained for the functionalized Al_2O_3 (13 nm) nanoparticles with lanolin (1:5), which was the highest reading on the thesis. It is noted based on the values presented on Table 11 that as the concentration of lanolin increases on functionalized Al_2O_3 (50nm) nanoparticles, and the surfaces changes from hydrophobic to superhydrophobic, presenting a static contact angle of 148^o and 152^o, respectively.

SiO_2 (10-20 nm) nanoparticles were functionalized with lanolin (1:5) and spray coated onto microscope slides and a contact angle of 119^o was observed, this was only obtained after sonification of the functionalized nanoparticles followed by centrifuge with ethanol. Addition step was introduced to remove unreacted lanolin, the lower contact angle observed in this case,

is related to the lower roughness and the contact angle is due to chemically adsorbed lanolin based on the observed IR spectra and TGA data.

The phenomenon of wettability is more than static contact angle, if the three-phase contact line is in motion, dynamic contact angle can be measured. The difference between advancing contact angle which represents the maximum value and receding contact angle that presents the minimum value is classified as hysteresis contact angle. The dynamic contact angle was carried out for the nanoparticles coatings with the aim to investigate the adhesion of water droplets onto the surfaces. As we can see in Table 11, it was observed that the hysteresis contact angle increased approximately the double for Al_2O_3 (13 nm) nanoparticles when functionalized with isosteric acid and lanolin, respectively. Demonstrating that the droplets of water became more adherent and less homogenous when the surface was spray coated with functionalized Al_2O_3 (13 nm) nanoparticles with lanolin.

As previously reported by Hill et al. [195] a hysteresis contact angle of 13.1º for the functionalized Al_2O_3 (13 nm) nanoparticles with isostearic acid and in this thesis a hysteresis contact angle of 14º has been obtained. The functionalized Al_2O_3 (13 nm and 50 nm) with different concentrations of lanolin were obtained the same hysteresis contact of 31º, while comparing the functionalized Al_2O_3 (50 nm) with a higher concentration of lanolin we observed a hysteresis contact angle of 6º. A large hysteresis contact angle value demonstrates a low droplet of water mobility on the surface. The hysteresis contact angle value provides details regarding the surface, how much liquid adheres to the surface [196] among others characteristics.

As described, it is noted that for the unfunctionalized or uncoated microscope slide the contact angle is low and after the reaction the contact angles are much higher, and this is due to the roughness created by the nanoparticles and chemically adsorbed carboxylic acids that we know from IR spectra and TGA data.

Tilting method was used to measure the sliding angle while the substrate was being inclined all the way to 90º before returns to normal. The functionalized Al_2O_3 (13 nm) with lanolin (1:5) showed a sliding contact angle of 20º, while a 24º sliding contact angle was observed for SiO_2 (10-20 nm) with lanolin (1:5). The temperature difference between the droplet of water and the coating surface can hold greater influence on the sliding angle compared with their individual temperatures. Above all, the sliding angle measurements were mainly obtained to characterize the mobility on the functionalized superhydrophobic surfaces sample supported on a dynamic evaluation approach.

Pieces of fabric were also spray coated with unfunctionalized and functionalized Al_2O_3 and the wetting behaviour are shown in Table 12. Unfunctionalized Al_2O_3 (13 nm) nanoparticles were dispersed in 2-propanol and spray coated onto fabric and a static contact angle of 145^o was obtained. A polyester fabric was used in this part of the experiment and the unfunctionalized Al_2O_3 (13 nm) nanoparticles were observed to be hydrophobicity, this is due to the roughness created by the fibre. As it can be seen in Figure 53, the static contact angle for the functionalized nanoparticles increased compared to the unfunctionalized, meaning the spray coat on the surface has worked.

The functionalized Al_2O_3 (13 nm) nanoparticles with lanolin (1:5) and isosteric acid, respectively, show the same static contact angle of 151^o but the results suggest a higher receding contact angle for the functionalized Al_2O_3 (13 nm) nanoparticles with lanolin (1:5).
To obtain the static contact angle for the functionalized Al_2O_3 (50 nm) nanoparticles with lanolin (1:10) and (1:15) ratios, the dispersed nanoparticles on 2-propanol had to be heated at a temperature of 30^{o}C overnight before they were spray coated onto the fabric surface and a static contact angle of 147^o and 137^o, was respectively obtained. On the other hand, for the Al_2O_3 (50 nm) nanoparticles with lanolin, the static contact angle decreased as the concentration of lanolin increased, which is the opposite of what was observed for the same synthesis, but spray coated on microscope slides.
The size and shape (small and spherical) of the nanoparticles played a role in improving the understanding and determination of the wetting behaviour of the ability to react and observe superhydrophobic surfaces. The results from Al_2O_3 (13 nm) nanoparticles suggests that when these particles are functionalized with isosteric acid or lanolin, we obtained superhydrophobic surface.

When comparing the static contact angle results obtained with the use of carboxylic acids during the synthesis, lanolin presented the best results regarding the superhydrophobicity. These results could be suggesting an advantage when using this particle because lanolin is cheaper compared to isosteric acid which is the commonly used by researchers. Above all, lanolin and isosteric acid offer the superhydrophobic function groups. Most of the functionalised alumina nanoparticles displayed advancing contact angle greater than 144^o except for Al_2O_3 (50 nm) that was synthesised with lanolin (1:15).

Table 11: Contact angle measurements with deionised water obtained on a glass substrate for different functionalised nanoparticles

Sample	Static CA (±1 or 2°)	Dynamic CA (±1 or 2°)			Sliding angle (°)
		Advancing	Receding	Hysteresis	
Al_2O_3 (13 nm) with isostearic acid	151	148	134	14	-
Al_2O_3 (13 nm) with lanolin (1:5)	153	152	121.28	31	20
Al_2O_3 (50 nm) with lanolin (1:10)	148	145	114.49	31	-
Al_2O_3 (50 nm) with lanolin (1:15)	152	147	141	6	-
SiO_2 (10-20 nm) with lanolin (1:5)	119 Sonicate then centrifuge to get rid of lanolin	111	52	59	24

Table 12: contact angle measurements with deionised water obtained on a fabric substrate for different functionalised nanoparticles

Sample	Static CA (±1 or 2°)	Dynamic CA (±1 or 2°)			Sliding angle (°)
		Advancing	Receding	Hysteresis	
Pure	145	144	105	39	-
Al_2O_3 (13 nm) with isostearic acid	151	150	137	13	8
Al_2O_3 (13 nm) with lanolin (1:5)	151	150	139	11	18
Al_2O_3 (50 nm) with lanolin (1:10)	147	146	123	23	-
Al_2O_3 (50 nm) with lanolin (1:15)	137	133	115	18	31
SiO_2 (10-20 nm) with lanolin (1:5)	139	137	114	23	-

SiO_2 (10-20 nm) with lanolin (1:5) dip coating	138	136	115	21	-

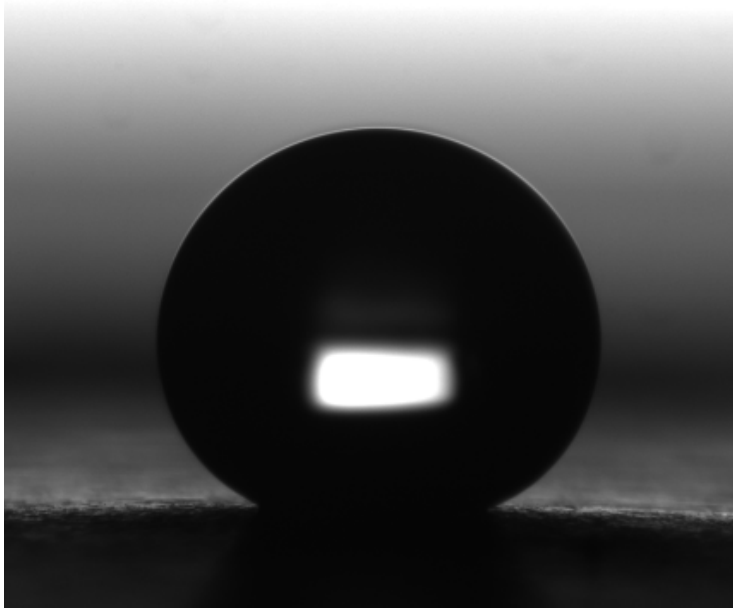

Figure 51: Functionalised Al_2O_3 (13 nm) nanoparticles with isostearic acid deposited onto microscope slide

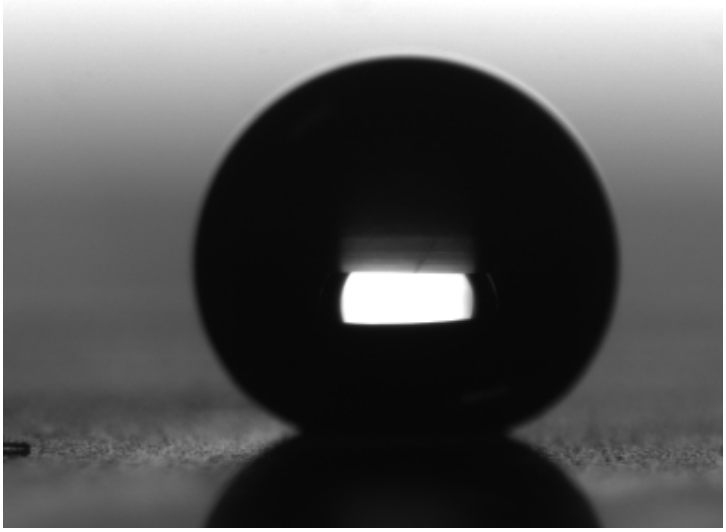

Figure 52: Functionalised Al_2O_3 (13 nm) nanoparticles with lanolin (1:5) deposited onto microscope slide

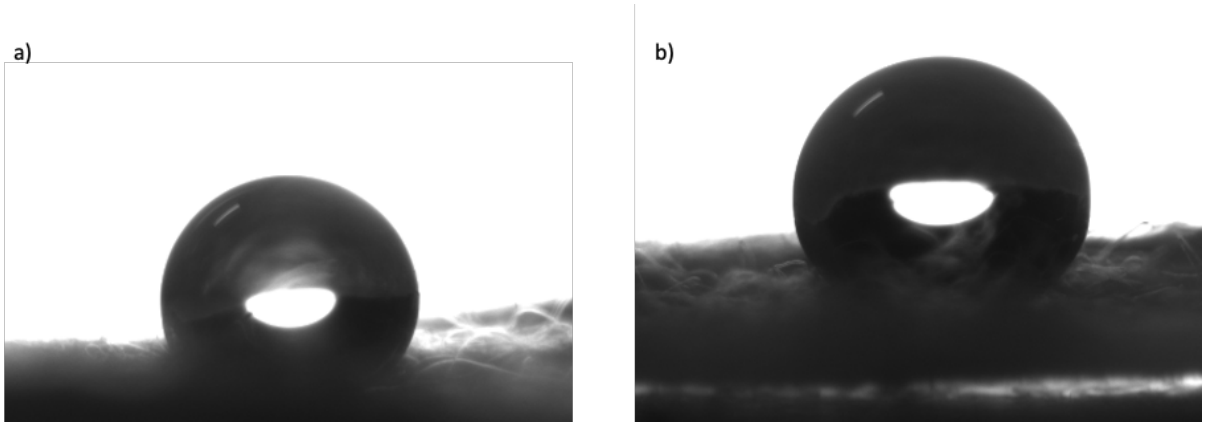

Figure 53: Droplet of water onto fabric substrate a) uncoated b) functionalized Al_2O_3 (50 nm) with lanolin (1:10)

Wettability behaviour of a cardboard coated with the nanoparticles

Cardboard is one of the substrates that SALTs is interested in, mainly for delivery packages, therefore we decided to coat cardboard substrates and expose it into the rain to check its behaviour and durability. As seen in Figure 55.a), a square piece of cardboard with dimensions 10x10 cm were cut, for Figures 55.b), c) and d) the functionalized nanoparticles were spray coated to see the effect of coating on wettability.

The samples in Figure 55 were exposed to the rain in three different days, the weight of the samples was recorded and can be seen in Table 13. The weight seen on the first attempt on Table 13 reflects the data on Figure 56 when the substrates dried. When comparing the images seen in Figure 55 to Figure 56, only the functionalized Al_2O_3 (50 nm) with lanolin ratio (1:15) water was not absorbed onto the surface on the spray coated area. Therefore, the difference of 1.3 g between the same sample for the first and second attempt is due to the water absorbed on the uncoated area.

For the second- and third-day Figures 57, 58, 59 and 60, respectively, when comparing to the first day Figure 56, it is was observed that as the sample exposure to water increased, the wetter the surface became, and the amount of spray coated solution on the surfaces was reduced.

On the third attempt, the unfunctionalized and all functionalized surfaces, one of the cardboard layers started to open, and this was due to the amount of water absorbed by the substrate.

As seen in table 13, based on mass increasement isosteric acid is the best formulation, which presents the least/low mass increase on the cardboard after it was exposed to water.

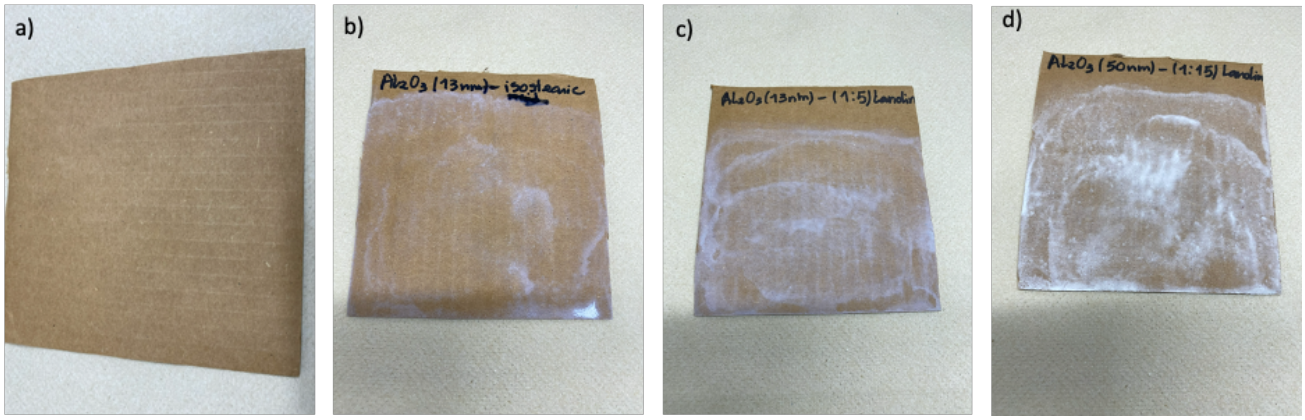

Figure 55: Images of cardboard before water were deposited a) uncoated; b) functionalized Al_2O_3 nanoparticles with isosteric acid; c) functionalized Al_2O_3 (13 nm) nanoparticles with lanolin (1:5); d) functionalized Al_2O_3 (50 nm) nanoparticles with lanolin (1:15)

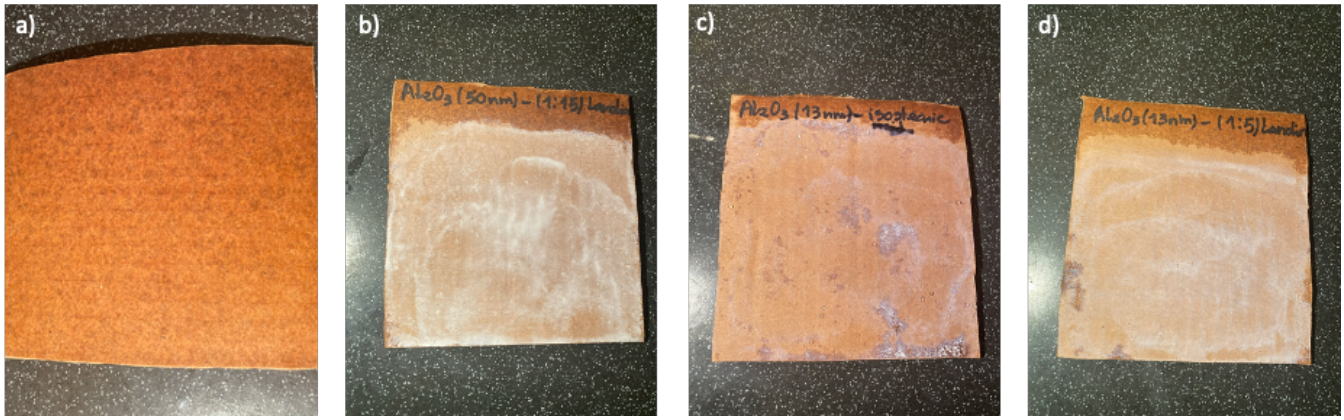

Figure 56: Images of cardboards after water were deposited on the surface, first attempt (wet) a) uncoated; b) functionalized Al_2O_3 (50 nm) nanoparticles with lanolin (1;15); c) functionalized Al_2O_3 (13 nm) nanoparticles with isosteric acid; d) functionalized Al_2O_3 (13 nm) with lanolin (1:5)

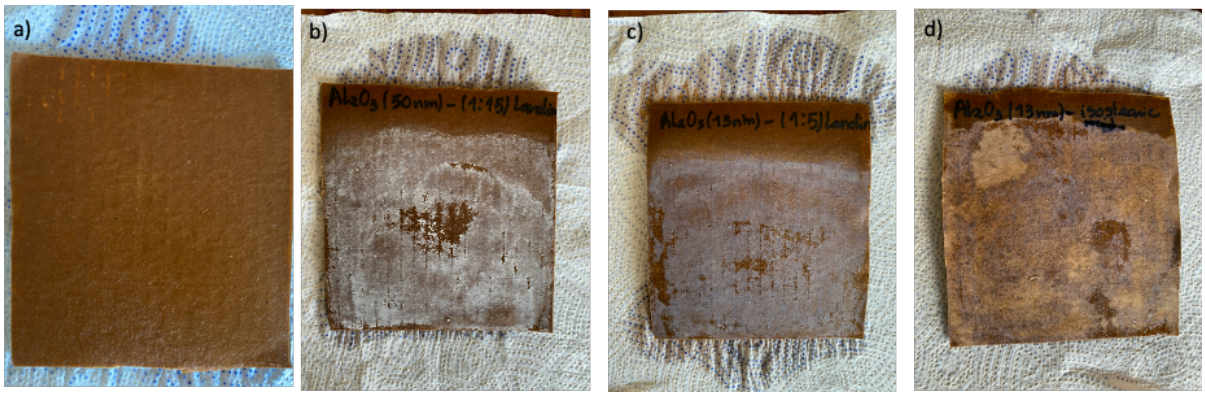

Figure 57: Images of cardboards after water were deposited on the surface, second attempt (wet) a) uncoated; b functionalized Al_2O_3 (50 nm) nanoparticles with lanolin (1;15); c) functionalized Al_2O_3 (13 nm) nanoparticles with lanolin (1:5); d) functionalized Al_2O_3 (13 nm) nanoparticles with isosteric acid

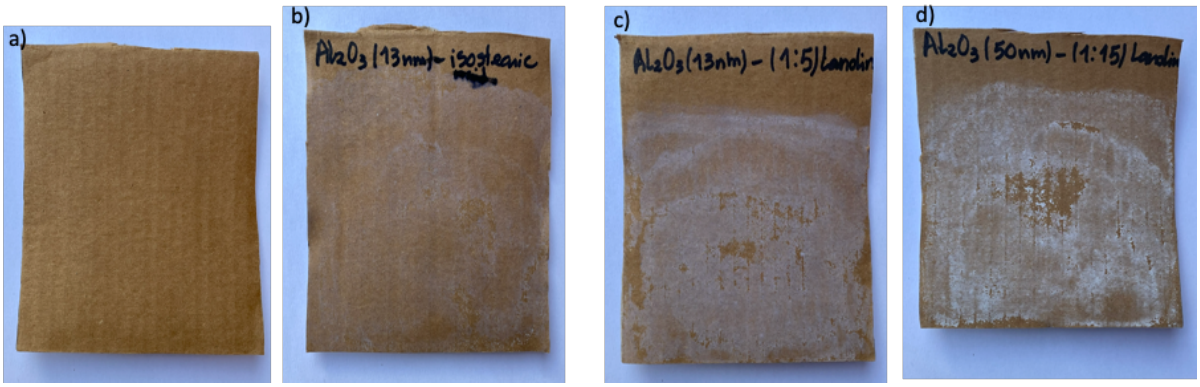

Figure 58: Images of cardboards after water were deposited on the surface, second attempt (dry) a) uncoated; b) functionalized Al_2O_3 (13 nm) nanoparticles with isosteric acid; c) functionalized Al_2O_3 (13 nm) nanoparticles with lanolin (1:5); d) functionalized Al_2O_3 (50 nm) with lanolin (1:15)

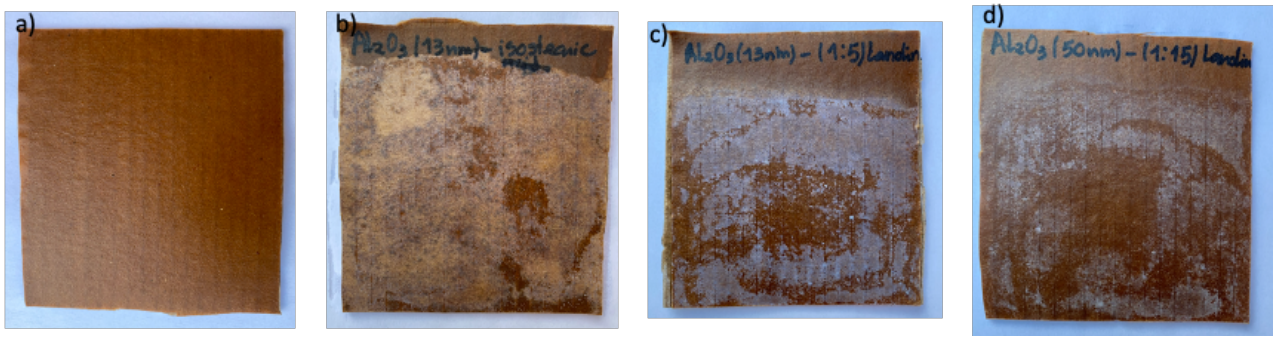

Figure 59: Images of cardboard after water were deposited onto the surface ,third attempt (wet) a) uncoated; b) functionalized Al_2O_3 (13 nm) nanoparticles with isosteric acid; c) functionalized Al_2O_3 (13 nm) nanoparticles with lanolin (1:5); d) functionalized Al_2O_3 (50 nm) with lanolin (1:15)

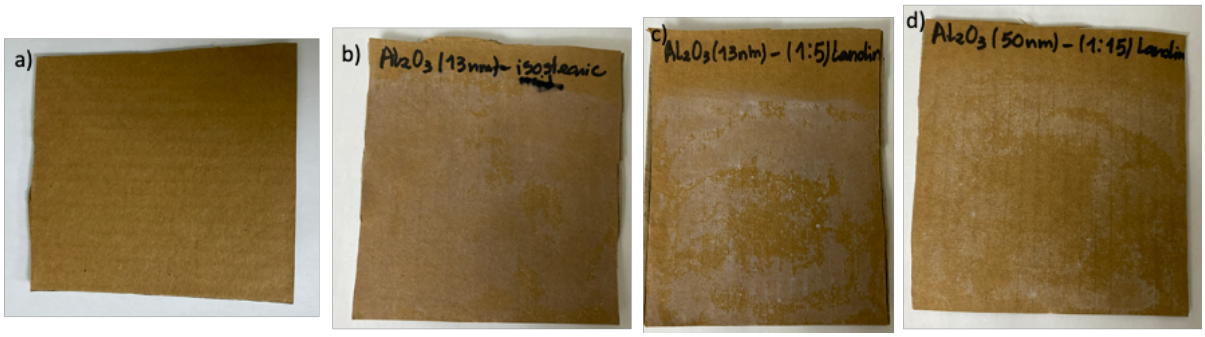

Figure 60: Images of cardboards after water were deposited onto surface, third attempt (dry) a) uncoated; b) functionalized Al_2O_3 (13 nm) nanoparticles with isosteric acid; c) functionalized Al_2O_3 (13 nm) nanoparticles with lanolin (1:5); d) spray coated Al_2O_3 (50 nm) with lanolin (1:15)

Table 13: Weight of the uncoated and coated cardboard with the functionalised nanoparticles

Sample	Weight (g)				
	1st attempt	2nd attempt		3rd attempt	
	Dry	Wet	Dry	Wet	Dry
Cardboard without coating	8.8	18.1	9.9	21.9	11.2
Al_2O_3 (13nm) with isosteric acid	9	15.4	9.3	19	11
Al_2O_3 (13nm) with lanolin (1:5)	8.9	21.8	9.2	22.5	12
Al_2O_3 (50nm) with lanolin (1:15)	8.7	20.1	10	21.2	12.2

Chapter VII: Conclusions

In this chapter we outline the main findings from this project, recommendations, and challenges. We first discuss the conclusion of the study, validate our hypotheses and answer our main research question. We then discuss the main recommendations and challenges.

Conclusions

The concept of superhydrophobic surface is generally described as state of nearly non-wetting surface, characterized by low water contact angle hysteresis $<10^{o}$ and a contact angle of at least 150^{o}, that upon contact results in the water droplets easily rolling off.

This project discussed the use of green low surface energy materials (LSEMs) to obtain alternatives to the current costly and environmentally hazardous waterproof analogues. While most widely used waterproof coatings are non-scalable, manufactured in laboratories using fluorocarbons which are toxic compounds and produce greenhouse gases. Furthermore, they are based in methods such as: photolithography, plasma, chemical, electrospinning, sol-gel processing, layer-by layer deposition and chemical vapour deposition are complex and requires expensive equipment.

For this project, we proposed using a novel method to produce non-hazardous superhydrophobic surfaces that is cost effective and environmentally friendly. Our proposed method of manufacturing a superhydrophobic surface was based on two steps: synthesis of Al_2O_3 or SiO_2 nanoparticles with the appropriate carboxylic acid, followed by the dispersion of functionalized nanoparticles on 2-propanol. Following this process, the produced solution can be spray coated onto different surfaces, such as: microscope slide and fabric and the resulting surface should become superhydrophobic.

Using both alumina and silica nanoparticles, we fabricated five different solutions. Four solutions were based on alumina; namely: Al_2O_3 (13 nm) with isostearic acid (ratio 1:1.4); Al_2O_3 (13 nm) with lanolin (ratio 1:5); Al_2O_3 (50 nm) with lanolin (ratio 1:10); Al_2O_3 (50 nm) with lanolin (ratio 1:15); and one based on silica, SiO_2 (10-20 nm) with lanolin (ratio 1:5). The functionalized solutions were spray coated onto a microscope slide and a fabric surface, except for Al_2O_3 with isostearic acid (ratio 1:1.4) and Al_2O_3 (13 nm) with lanolin (ratio 1:5) and Al_2O_3 (50 nm) with lanolin (ratio 1:15) which were spray coated onto all three surfaces.

To assess whether the resulting surface can be characterized as superhydrophobic, we analysed the surface wettability by using the DSA25 drop shape analyser to measure the contact angles, we analysed the loading of carboxylic acids absorbed onto the surface using TGA, we analysed whether the carboxylic acids is chemical absorbed onto the particles using IR spectroscopy and used SEM to measure the nanoparticles morphology. Based on all four tests, we observed superhydrophobic surfaces for the functionalized nanoparticles Al_2O_3 (13 nm) with isostearic acid and Al_2O_3 (13 nm) with lanolin on both a microscope slide and a fabric surface. Additionally, we observed superhydrophobic surface values for the functionalized Al_2O_3 (50 nm) with lanolin (1:15) only on a microscope slide, as for the fabric surface the contact angle values were below the superhydrophobic surface threshold. We also observed a superhydrophobic surface for the functionalized Al_2O_3 (13 nm) with lanolin (1:5) on the microscope slide. The functionalized Al_2O_3 (50 nm) with lanolin (1:10) and SiO_2 (10-20nm) with lanolin (1:5) spray coated onto the microscope slide and fabric did not present a superhydrophobic surface; analogously, Al_2O_3 (50 nm) with lanolin (1:15); did not observed superhydrophobic surface on the fabric substrate.

The superhydrophobicity process using both silica and alumina nanoparticles was successfully accomplished through the combination of the surface roughness of the nanoparticles and low surface energy properties. These cheap hydrocarbon-based green low surface energy have a lot of potential regarding the new coating applications on the microscope slides and fabric substrates and can be used as a substitution for the widely used fluorocarbons which are hazardous and expensive. The functionalised Al_2O_3 (13 nm) nanoparticles with lanolin or isosteric acid could be used for the manufacture of superhydrophobic surfaces. Furthermore, functionalised Al_2O_3 (13 nm) with lanolin or isosteric acid can be applicable for SALT's, above all, lanolin is the cheaper carboxylic acid when compared with isosteric acid, and both are environmentally friendly. This research also shows that nanoparticles size play an important role on surface superhydrophobicity, since only when using Al_2O_3 (13 nm) nanoparticles was it possible to obtain superhydrophobicity on both microscope slide and fabric substrate, when the nanoparticle was functionalised with both carboxylic acids.

This research concentrated on fabricating superhydrophobic surface using alumina and silica nanoparticles when functionalised with non-fluorinated chains such as highly branched hydrocarbon chains.

In standard laboratory conditions lanolin will be the better formulation based on superhydrophobicity. However, in practice isosteric acid has better potential, since it absorbs less mass on a cardboard layer.

Recommendations

Even though we successfully fabricated several superhydrophobic surfaces using our proposed fabrication process, there are several recommendations for future research that could be worth exploring, for example:

1. For this research, we used alumina 13nm and silica 10-20nm nanoparticles were used as the main source for the functionalisation of the non-fluorinated superhydrophobic surfaces. It is important to explore the use of different nanoparticles diameters because it was through the fabrication process that alumina 50nm when functionalised with a higher concentration of lanolin (1:15) demonstrated superhydrophobicity but only on the microscope slide. Further research to analyse the effect of nanoparticle size on fibre roughness can be used to verify the effect of size of the nanoparticles on fibre roughness, as well as the grafting density as a function of the mass loss of the material.
2. The majority of the methods discussed on this paper used to manufacture superhydrophobic surfaces requires special equipment, complex method to obtain the water repellent surfaces and many of the fabricated coating solution when deposited onto the surface are easily damaged. To increase the number of practical applications, there is a significant research interest in the development of durable surfaces that can be accomplished by using simpler and cheaper methods.

Challenges

As technology advances, manufacturing a superhydrophobic surface at a micro/nano scale, becomes less of a problem, but outside of a laboratory setting and time it can be challenging to guarantee surface robustness and fragility. Moreover, the superhydrophobic surfaces are motivated by Lotus leaves in nature leading to numerous applications on our everyday life.
Another fundamental challenge on the fabrication of superhydrophobic surface is their durability. Even though it is possible to manufacture durable superhydrophobic surfaces, long-term stability of such surfaces continuous to be a big challenge. This is related to the fact that

microscale or nanoscale structures are highly sensitive to mechanical stresses. Resulting on the surface being damaged by rain, dust, etc. Wettability behaviour of the cardboard coated with the alumina nanoparticles were previously described and it was observed that after the substrate were exposed for too long and on the third attempt under rain the cardboard were damaged and as seen in Figure 60 the coated layers deposited on the cardboard are less when compared to the initial sample that is seen in Figure 55.
To solve these problems, passive regeneration and active repairing methods should be considered. Nevertheless, research is required to fabricate such durable superhydrophobic surfaces for daily use.

Most research discussed in this thesis was carried out on flat and rigid substrate materials, such as microscope slides, and most manufacturing methods discussed in the literature review are very expensive and are applicable for small surface. Which are not suitable for large-scale production although large-scale are required for industry applications on a flexible substrate.
Research on validating large scale manufacturing methods, that are less expensive and environmentally friendly.

Reference:

[1] J. Hulla, S. Sahu, and A. Hayes, 'Nanotechnology: History and future', *Hum Exp Toxicol*, vol. 34, no. 12, pp. 1318–1321, Dec. 2015, doi: 10.1177/0960327115603588.

[2] Richard P. Feynman, 'There's Plenty of Room at the Bottom: an invitation to enter a new field of physics', *Engineering and Science magazine*, vol. XXIII, Feb. 1960.

[3] R. Blossey, 'Self-cleaning surfaces — virtual realities', *Nature Mater*, vol. 2, no. 5, pp. 301–306, May 2003, doi: 10.1038/nmat856.

[4] W. Barthlott and C. Neinhuis, 'Purity of the sacred lotus, or escape from contamination in biological surfaces', *Planta*, vol. 202, no. 1, pp. 1–8, Apr. 1997, doi: 10.1007/s004250050096.

[5] Y.-T. Cheng and D. E. Rodak, 'Is the lotus leaf superhydrophobic?', *Appl. Phys. Lett.*, vol. 86, no. 14, p. 144101, Apr. 2005, doi: 10.1063/1.1895487.

[6] Y. Yoon, D. Kim, and J.-B. Lee, 'Hierarchical micro/nano structures for super-hydrophobic surfaces and super-lyophobic surface against liquid metal', *Micro and Nano Syst Lett*, vol. 2, no. 1, p. 3, Dec. 2014, doi: 10.1186/s40486-014-0003-x.

[7] X. J. Feng and L. Jiang, 'Design and Creation of Superwetting/Antiwetting Surfaces', *Adv. Mater.*, vol. 18, no. 23, pp. 3063–3078, Dec. 2006, doi: 10.1002/adma.200501961.

[8] L. Feng *et al.*, 'Super-Hydrophobic Surfaces: From Natural to Artificial', *Adv. Mater.*, vol. 14, no. 24, pp. 1857–1860, Dec. 2002, doi: 10.1002/adma.200290020.

[9] F. Zhang *et al.*, 'Superhydrophobic carbon nanotubes/epoxy nanocomposite coating by facile one-step spraying', *Surface and Coatings Technology*, vol. 341, pp. 15–23, May 2018, doi: 10.1016/j.surfcoat.2018.01.045.

[10] Moore, James Alexander, 'Lanolin'. McGraw-Hill Education. doi: 10.1036/1097-8542.370500.

[11] W. F. Tinto, T. O. Elufioye, and J. Roach, 'Waxes', in *Pharmacognosy*, Elsevier, 2017, pp. 443–455. doi: 10.1016/B978-0-12-802104-0.00022-6.

[12] 'Esters', *Introduction to Chemistry*. [Online]. Available: https://courses.lumenlearning.com/introchem/chapter/esters/

[13] M. L. Schlossman and J. P. McCarthy, 'Lanolin and its derivatives', *J Amer Oil Chem Soc*, vol. 55, no. 4, pp. 447–450, Apr. 1978, doi: 10.1007/BF02911911.

[14] S. Badal McCreath and R. Delgoda, *Pharmacognosy: Fundamentals, Applications and Strategies*. 2017. Accessed: Jun. 01, 2021. [Online]. Available: http://ezproxy.uniandes.edu.co:8080/login?url=http://www.sciencedirect.com/science/book/9780128021040

[15] L. Chen, R. A. Yokel, B. Hennig, and M. Toborek, 'Manufactured Aluminum Oxide Nanoparticles Decrease Expression of Tight Junction Proteins in Brain Vasculature', *J Neuroimmune Pharmacol*, vol. 3, no. 4, pp. 286–295, Dec. 2008, doi: 10.1007/s11481-008-9131-5.

[16] I. Khan, K. Saeed, and I. Khan, 'Nanoparticles: Properties, applications and toxicities', *Arabian Journal of Chemistry*, vol. 12, no. 7, pp. 908–931, Nov. 2019, doi: 10.1016/j.arabjc.2017.05.011.

[17] A. S. Karakoti, L. L. Hench, and S. Seal, 'The potential toxicity of nanomaterials—The role of surfaces', *JOM*, vol. 58, no. 7, pp. 77–82, Jul. 2006, doi: 10.1007/s11837-006-0147-0.

[18] S. Chatterjee, R. Mankamna Kumari, and S. Nimesh, 'Nanotoxicology', in *Advances in Nanomedicine for the Delivery of Therapeutic Nucleic Acids*, Elsevier, 2017, pp. 187–201. doi: 10.1016/B978-0-08-100557-6.00010-9.
[19] G. Wypych, 'PHYSICAL PROPERTIES OF FILLERS AND FILLED MATERIALS', in *Handbook of Fillers*, Elsevier, 2016, pp. 303–371. doi: 10.1016/B978-1-895198-91-1.50007-5.
[20] K. Guo, K. Wu, X. Li, B. Jiang, Y. Wu, and C. Mi, 'The research on Surface charge of super-bihydrophobic nano-coating materials', *IOP Conf. Ser.: Mater. Sci. Eng.*, vol. 493, p. 012099, Mar. 2019, doi: 10.1088/1757-899X/493/1/012099.
[21] A. Casadevall and F. C. Fang, 'Mechanistic Science', *Infect Immun*, vol. 77, no. 9, pp. 3517–3519, Sep. 2009, doi: 10.1128/IAI.00623-09.
[22] A. Pross, 'The Reactivity—Selectivity Principle and its Mechanistic Applications', in *Advances in Physical Organic Chemistry*, vol. 14, Elsevier, 1977, pp. 69–132. doi: 10.1016/S0065-3160(08)60108-2.
[23] W. Birmili and T. Hoffmann, 'ENVIRONMENTAL POLLUTANTS | Particulate and Dust Pollution, Inorganic and Organic Compounds', in *Encyclopedia of Respiratory Medicine*, Elsevier, 2006, pp. 110–120. doi: 10.1016/B0-12-370879-6/00133-2.
[24] R. Mishra and J. Militky, 'Nanoparticles and textile technology', in *Nanotechnology in Textiles*, Elsevier, 2019, pp. 181–217. doi: 10.1016/B978-0-08-102609-0.00004-3.
[25] J. Karavitis and E. J. Kovacs, 'Macrophage phagocytosis: effects of environmental pollutants, alcohol, cigarette smoke, and other external factors', *Journal of Leukocyte Biology*, vol. 90, no. 6, pp. 1065–1078, Dec. 2011, doi: 10.1189/jlb.0311114.
[26] C. Liao, Y. Chiang, and C. Chio, 'Model-based assessment for human inhalation exposure risk to airborne nano/fine titanium dioxide particles', *Science of The Total Environment*, vol. 407, no. 1, pp. 165–177, Dec. 2008, doi: 10.1016/j.scitotenv.2008.09.028.
[27] G. Bystrzejewska-Piotrowska, J. Golimowski, and P. L. Urban, 'Nanoparticles: Their potential toxicity, waste and environmental management', *Waste Management*, vol. 29, no. 9, pp. 2587–2595, Sep. 2009, doi: 10.1016/j.wasman.2009.04.001.
[28] Albert Ernest Alexander and Paley Johnson, *Colloid Science*. Oxford: Clarendon Press, 1950.
[29] K. Maroof and F. Zafar, 'Scope of Nanotechnology in Drug Delivery', *J Bioequiv Availab*, vol. 08, no. 01, 2015, doi: 10.4172/jbb.1000257.
[30] S. L. Lombardi, Ed., *Nanoparticles: new research*. New York: Nova Science Publishers, 2008.
[31] Popa, Adriana and Samia, Anna, 'Functional inorganic nanomaterials'. McGraw-Hill Education, 2014. doi: 10.1036/1097-8542.YB150548.
[32] H. H. Gatzen, V. Saile, and J. Leuthold, *Micro and Nano Fabrication*. Berlin, Heidelberg: Springer Berlin Heidelberg, 2015. doi: 10.1007/978-3-662-44395-8.
[33] H. Gundersen, H. P. Leinaas, and C. Thaulow, 'Surface Structure and Wetting Characteristics of Collembola Cuticles', *PLoS ONE*, vol. 9, no. 2, p. e86783, Feb. 2014, doi: 10.1371/journal.pone.0086783.
[34] J. Jeevahan, M. Chandrasekaran, G. Britto Joseph, R. B. Durairaj, and G. Mageshwaran, 'Superhydrophobic surfaces: a review on fundamentals, applications, and challenges', *J Coat Technol Res*, vol. 15, no. 2, pp. 231–250, Mar. 2018, doi: 10.1007/s11998-017-0011-x.
[35] S. Wang and G. Zhao, *Superhydrophobic coatings for corrosion and tribology*. 2019. Accessed: Apr. 07, 2020. [Online]. Available: https://doi.org/10.3390/books978-3-03921-785-4

[36] S. Wang, K. Liu, X. Yao, and L. Jiang, 'Bioinspired Surfaces with Superwettability: New Insight on Theory, Design, and Applications', *Chem. Rev.*, vol. 115, no. 16, pp. 8230–8293, Aug. 2015, doi: 10.1021/cr400083y.

[37] B. Chen, J. Qiu, E. Sakai, N. Kanazawa, R. Liang, and H. Feng, 'Robust and Superhydrophobic Surface Modification by a "Paint + Adhesive" Method: Applications in Self-Cleaning after Oil Contamination and Oil–Water Separation', *ACS Appl. Mater. Interfaces*, vol. 8, no. 27, pp. 17659–17667, Jul. 2016, doi: 10.1021/acsami.6b04108.

[38] D. Zhang, L. Wang, H. Qian, and X. Li, 'Superhydrophobic surfaces for corrosion protection: a review of recent progresses and future directions', *J Coat Technol Res*, vol. 13, no. 1, pp. 11–29, Jan. 2016, doi: 10.1007/s11998-015-9744-6.

[39] A. Tuteja, W. Choi, J. M. Mabry, G. H. McKinley, and R. E. Cohen, 'Robust omniphobic surfaces', *Proceedings of the National Academy of Sciences*, vol. 105, no. 47, pp. 18200–18205, Nov. 2008, doi: 10.1073/pnas.0804872105.

[40] C. Neinhuis, 'Characterization and Distribution of Water-repellent, Self-cleaning Plant Surfaces', *Annals of Botany*, vol. 79, no. 6, pp. 667–677, Jun. 1997, doi: 10.1006/anbo.1997.0400.

[41] P. Roach, N. J. Shirtcliffe, and M. I. Newton, 'Progess in superhydrophobic surface development', *Soft Matter*, vol. 4, no. 2, pp. 224–240, 2008, doi: 10.1039/B712575P.

[42] K. L. Mittal, Ed., *Advances in contact angle, wettability and adhesion*. Salem, Massachusetts: Scrivener Publishing, Wiley, 2013.

[43] R. Fürstner, W. Barthlott, C. Neinhuis, and P. Walzel, 'Wetting and Self-Cleaning Properties of Artificial Superhydrophobic Surfaces', *Langmuir*, vol. 21, no. 3, pp. 956–961, Feb. 2005, doi: 10.1021/la0401011.

[44] W. Xu, R. Leeladhar, Y.-T. Tsai, E.-H. Yang, and C.-H. Choi, 'Evaporative self-assembly of nanowires on superhydrophobic surfaces of nanotip latching structures', *Appl. Phys. Lett.*, vol. 98, no. 7, p. 073101, Feb. 2011, doi: 10.1063/1.3554360.

[45] M. A. Sarshar, C. Swarctz, S. Hunter, J. Simpson, and C.-H. Choi, 'Effects of contact angle hysteresis on ice adhesion and growth on superhydrophobic surfaces under dynamic flow conditions', *Colloid Polym Sci*, vol. 291, no. 2, pp. 427–435, Feb. 2013, doi: 10.1007/s00396-012-2753-4.

[46] R. J. Daniello, N. E. Waterhouse, and J. P. Rothstein, 'Drag reduction in turbulent flows over superhydrophobic surfaces', *Physics of Fluids*, vol. 21, no. 8, p. 085103, Aug. 2009, doi: 10.1063/1.3207885.

[47] C.-H. Choi and C.-J. "CJ" Kim, 'Droplet Evaporation of Pure Water and Protein Solution on Nanostructured Superhydrophobic Surfaces of Varying Heights', *Langmuir*, vol. 25, no. 13, pp. 7561–7567, Jul. 2009, doi: 10.1021/la803614h.

[48] S. H. Kim, 'Fabrication of Superhydrophobic Surfaces', *Journal of Adhesion Science and Technology*, vol. 22, no. 3–4, pp. 235–250, Jan. 2008, doi: 10.1163/156856108X305156.

[49] N. J. Shirtcliffe, G. McHale, S. Atherton, and M. I. Newton, 'An introduction to superhydrophobicity', *Advances in Colloid and Interface Science*, vol. 161, no. 1–2, pp. 124–138, Dec. 2010, doi: 10.1016/j.cis.2009.11.001.

[50] A. H. P. Skelland, 'Bubbler, drops, and particles, by R. Clift, J. R. Grace, and M. E. Weber, Academic Press, Inc., 1978, 380 pages,$32.00', *AIChE J.*, vol. 25, no. 4, pp. 733–733, Jul. 1979, doi: 10.1002/aic.690250425.

[51] J. Berthier and K. A. Brakke, *The physics of microdroplets*. Hoboken, New Jersey : Salem, Massachusetts: John Wiley & Sons, Inc ; Scrivener Publishing LLC, 2012.

[52] M. Ma and R. M. Hill, 'Superhydrophobic surfaces', *Current Opinion in Colloid & Interface Science*, vol. 11, no. 4, pp. 193–202, Oct. 2006, doi: 10.1016/j.cocis.2006.06.002.

[53] B. Bhushan and Y. C. Jung, 'Natural and biomimetic artificial surfaces for superhydrophobicity, self-cleaning, low adhesion, and drag reduction', *Progress in Materials Science*, vol. 56, no. 1, pp. 1–108, Jan. 2011, doi: 10.1016/j.pmatsci.2010.04.003.

[54] A. Marmur, 'The Lotus Effect: Superhydrophobicity and Metastability', *Langmuir*, vol. 20, no. 9, pp. 3517–3519, Apr. 2004, doi: 10.1021/la036369u.

[55] H. J. Ensikat, P. Ditsche-Kuru, C. Neinhuis, and W. Barthlott, 'Superhydrophobicity in perfection: the outstanding properties of the lotus leaf', *Beilstein J. Nanotechnol.*, vol. 2, pp. 152–161, Mar. 2011, doi: 10.3762/bjnano.2.19.

[56] Bi *et al.*, 'Robust Super-Hydrophobic Coating Prepared by Electrochemical Surface Engineering for Corrosion Protection', *Coatings*, vol. 9, no. 7, p. 452, Jul. 2019, doi: 10.3390/coatings9070452.

[57] Shirin Alexander and Daniel Johnson, 'Colloidal and interface science - Class notes', Swansea University, 2020.

[58] C. Antonini, F. Villa, and M. Marengo, 'Oblique impacts of water drops onto hydrophobic and superhydrophobic surfaces: outcomes, timing, and rebound maps', *Exp Fluids*, vol. 55, no. 4, p. 1713, Apr. 2014, doi: 10.1007/s00348-014-1713-9.

[59] V. Senez, *Nanotechnologies for synthetic super non-wetting surfaces*. London, UK: ISTE/ Wiley, 2014.

[60] J. Tam, G. Palumbo, and U. Erb, 'Recent Advances in Superhydrophobic Electrodeposits', *Materials*, vol. 9, no. 3, p. 151, Mar. 2016, doi: 10.3390/ma9030151.

[61] A. B. D. Cassie and S. Baxter, 'Wettability of porous surfaces', *Trans. Faraday Soc.*, vol. 40, p. 546, 1944, doi: 10.1039/tf9444000546.

[62] G. Zhao *et al.*, 'One-step electrodeposition of a self-cleaning and corrosion resistant Ni/WS_2 superhydrophobic surface', *RSC Adv.*, vol. 6, no. 64, pp. 59104–59112, 2016, doi: 10.1039/C6RA07899K.

[63] M. Liu, S. Wang, Z. Wei, Y. Song, and L. Jiang, 'Bioinspired Design of a Superoleophobic and Low Adhesive Water/Solid Interface', *Adv. Mater.*, vol. 21, no. 6, pp. 665–669, Feb. 2009, doi: 10.1002/adma.200801782.

[64] P. M. Martin, *Introduction to Surface Engineering and Functionally Engineered Materials: Martin/Introduction*. Hoboken, NJ, USA: John Wiley & Sons, Inc., 2011. doi: 10.1002/9781118171899.

[65] M. AlMaadeed, D. Ponnamma, and M. Carignano, Eds., *Polymer science and innovative applications: materials, techniques, and future developments*, 1st ed. Cambridge: Elsevier, 2020.

[66] M. Y. Ali and W. N. P. Hung, '1.11 Micromachining', in *Comprehensive Materials Finishing*, Elsevier, 2017, pp. 322–343. doi: 10.1016/B978-0-12-803581-8.09156-6.

[67] I. S. Putra *et al.*, 'The influence of fiber surface profile and roughness to fiber–matrix interfacial properties', *Journal of Composite Materials*, vol. 54, no. 11, pp. 1441–1452, May 2020, doi: 10.1177/0021998319883418.

[68] C.-O. Lee, K. Park, B. C. Park, and Y. W. Lee, 'An algorithm for stylus instruments to measure aspheric surfaces', *Meas. Sci. Technol.*, vol. 16, no. 5, pp. 1215–1222, May 2005, doi: 10.1088/0957-0233/16/5/023.

[69] M. Aliofkhazraei and N. Ali, 'AFM Applications in Micro/Nanostructured Coatings', in *Comprehensive Materials Processing*, Elsevier, 2014, pp. 191–241. doi: 10.1016/B978-0-08-096532-1.00712-3.

[70] G. Morris, S. J. Neethling, and J. J. Cilliers, 'An investigation of the stable orientations of orthorhombic particles in a thin film and their effect on its critical failure pressure', *Journal of Colloid and Interface Science*, vol. 361, no. 1, pp. 370–380, Sep. 2011, doi: 10.1016/j.jcis.2011.05.061.

[71] E. C. Donaldson and W. Alam, *Wettability*. Houston, Tex: Gulf Pub. Co, 2008.
[72] N. Eustathopoulos, M. G. Nicholas, and B. Drevet, *Wettability at high temperatures*, 1st ed. Amsterdam ; New York: Pergamon, 1999.
[73] T. Cosgrove, Ed., *Colloid science: principles, methods and applications*, 2nd ed. Chichester, West Sussex: Wiley, 2010.
[74] T. Young, 'III. An essay on the cohesion of fluids', *Phil. Trans. R. Soc.*, vol. 95, pp. 65–87, Dec. 1805, doi: 10.1098/rstl.1805.0005.
[75] X.-J. Huang, D.-H. Kim, M. Im, J.-H. Lee, J.-B. Yoon, and Y.-K. Choi, '"Lock-and-Key" Geometry Effect of Patterned Surfaces: Wettability and Switching of Adhesive Force', *Small*, vol. 5, no. 1, pp. 90–94, Jan. 2009, doi: 10.1002/smll.200800649.
[76] H. J. Lee and S. Michielsen, 'Lotus effect: Superhydrophobicity', *Journal of the Textile Institute*, vol. 97, no. 5, pp. 455–462, Aug. 2006, doi: 10.1533/joti.2006.0271.
[77] Ramé-Hart, 'Information on contact angle'. Mar. 04, 2020. [Online]. Available: http://www.ramehart.com/contactangle.htm
[78] G. A. Parks, 'Surface and interfacial free energies of quartz', *J. Geophys. Res.*, vol. 89, no. B6, pp. 3997–4008, Jun. 1984, doi: 10.1029/JB089iB06p03997.
[79] L. Makkonen, 'Young's equation revisited', *J. Phys.: Condens. Matter*, vol. 28, no. 13, p. 135001, Apr. 2016, doi: 10.1088/0953-8984/28/13/135001.
[80] A. Mucherino, Ed., *Distance geometry: theory, methods, and applications*. New York ; London: Springer, 2013.
[81] W. A. Daoud, Ed., *Self-cleaning materials and surfaces: a nanotechnology approach*. Chichester, West Sussex, United Kingdom: Wiley, 2013.
[82] A. Marmur, 'Thermodynamic aspects of contact angle hysteresis', *Advances in Colloid and Interface Science*, vol. 50, pp. 121–141, May 1994, doi: 10.1016/0001-8686(94)80028-6.
[83] H. Li, A. Li, Z. Zhao, M. Li, and Y. Song, 'Heterogeneous Wettability Surfaces: Principle, Construction, and Applications', *Small Structures*, vol. 1, no. 2, p. 2000028, Nov. 2020, doi: 10.1002/sstr.202000028.
[84] X. Zhang *et al.*, 'Polyelectrolyte Multilayer as Matrix for Electrochemical Deposition of Gold Clusters: Toward Super-Hydrophobic Surface', *J. Am. Chem. Soc.*, vol. 126, no. 10, pp. 3064–3065, Mar. 2004, doi: 10.1021/ja0398722.
[85] M. Ferrari, F. Ravera, S. Rao, and L. Liggieri, 'Surfactant adsorption at superhydrophobic surfaces', *Appl. Phys. Lett.*, vol. 89, no. 5, p. 053104, Jul. 2006, doi: 10.1063/1.2226771.
[86] K. Liu, J. Du, J. Wu, and L. Jiang, 'Superhydrophobic gecko feet with high adhesive forces towards water and their bio-inspired materials', *Nanoscale*, vol. 4, no. 3, pp. 768–772, 2012, doi: 10.1039/C1NR11369K.
[87] J. Drelich, 'The Effect of Drop (Bubble) Size on Contact Angle at Solid Surfaces', *The Journal of Adhesion*, vol. 63, no. 1–3, pp. 31–51, Jun. 1997, doi: 10.1080/00218469708015212.
[88] A. Marmur, 'Soft contact: measurement and interpretation of contact angles', *Soft Matter*, vol. 2, no. 1, pp. 12–17, 2006, doi: 10.1039/B514811C.
[89] L. Gao and T. J. McCarthy, 'Contact Angle Hysteresis Explained', *Langmuir*, vol. 22, no. 14, pp. 6234–6237, Jul. 2006, doi: 10.1021/la060254j.
[90] S. J. Kwoun, R. M. Lee, R. A. Cairncross, P. Shah, and C. Jeffrey Brinker, 'Characterization of superhydrophobic materials using multiresonance acoustic shear wave sensors', *IEEE Trans. Ultrason., Ferroelect., Freq. Contr.*, vol. 53, no. 8, pp. 1400–1403, Aug. 2006, doi: 10.1109/TUFFC.2006.1665096.
[91] F. Shi, Z. Wang, and X. Zhang, 'Combining a Layer-by-Layer Assembling Technique with Electrochemical Deposition of Gold Aggregates to Mimic the Legs of Water

Striders', *Adv. Mater.*, vol. 17, no. 8, pp. 1005–1009, Apr. 2005, doi: 10.1002/adma.200402090.
[92] L. Gao and T. J. McCarthy, 'A Perfectly Hydrophobic Surface ($\theta_A/\theta_R = 180°/180°$)', *J. Am. Chem. Soc.*, vol. 128, no. 28, pp. 9052–9053, Jul. 2006, doi: 10.1021/ja062943n.
[93] P. Aussillous and D. Quéré, 'Liquid marbles', *Nature*, vol. 411, no. 6840, pp. 924–927, Jun. 2001, doi: 10.1038/35082026.
[94] P. R. Bhattacharjee, 'Refinement of the definitions of angles of incidence, reflection, refraction, and critical angle in ray optics', *Optik*, vol. 172, pp. 1187–1192, Nov. 2018, doi: 10.1016/j.ijleo.2018.06.144.
[95] T. A. Otitoju, A. L. Ahmad, and B. S. Ooi, 'Superhydrophilic (superwetting) surfaces: A review on fabrication and application', *Journal of Industrial and Engineering Chemistry*, vol. 47, pp. 19–40, Mar. 2017, doi: 10.1016/j.jiec.2016.12.016.
[96] R. J. Good, 'Contact angle, wetting, and adhesion: a critical review', *Journal of Adhesion Science and Technology*, vol. 6, no. 12, pp. 1269–1302, Jan. 1992, doi: 10.1163/156856192X00629.
[97] B. Krasovitski and A. Marmur, 'Drops Down the Hill: Theoretical Study of Limiting Contact Angles and the Hysteresis Range on a Tilted Plate', *Langmuir*, vol. 21, no. 9, pp. 3881–3885, Apr. 2005, doi: 10.1021/la0474565.
[98] H. B. Eral, D. J. C. M. 't Mannetje, and J. M. Oh, 'Contact angle hysteresis: a review of fundamentals and applications', *Colloid Polym Sci*, vol. 291, no. 2, pp. 247–260, Feb. 2013, doi: 10.1007/s00396-012-2796-6.
[99] R. Evans, M. C. Stewart, and N. B. Wilding, 'A unified description of hydrophilic and superhydrophobic surfaces in terms of the wetting and drying transitions of liquids', *Proc Natl Acad Sci USA*, vol. 116, no. 48, pp. 23901–23908, Nov. 2019, doi: 10.1073/pnas.1913587116.
[100] S. Hussain, T. T. Y. Le, and S.-Y. Lin, 'An interpretation for the breakpoint of the relaxation profiles of the advancing and receding contact angles', *Journal of Molecular Liquids*, vol. 298, p. 112162, Jan. 2020, doi: 10.1016/j.molliq.2019.112162.
[101] R. N. Wenzel, 'RESISTANCE OF SOLID SURFACES TO WETTING BY WATER', *Ind. Eng. Chem.*, vol. 28, no. 8, pp. 988–994, Aug. 1936, doi: 10.1021/ie50320a024.
[102] P.-G. de Gennes, F. Brochard-Wyart, and D. Quéré, *Capillarity and wetting phenomena: drops, bubbles, pearls, waves*. New York, NY: Springer, 2010.
[103] Th. Uelzen and J. Müller, 'Wettability enhancement by rough surfaces generated by thin film technology', *Thin Solid Films*, vol. 434, no. 1–2, pp. 311–315, Jun. 2003, doi: 10.1016/S0040-6090(03)00484-X.
[104] S. H. Kim, J.-H. Kim, B.-K. Kang, and H. S. Uhm, 'Superhydrophobic CF_x Coating via In-Line Atmospheric RF Plasma of $He{-}CF_4{-}H_2$', *Langmuir*, vol. 21, no. 26, pp. 12213–12217, Dec. 2005, doi: 10.1021/la0521948.
[105] J. Bico, C. Marzolin, and D. Quéré, 'Pearl drops', *Europhys. Lett.*, vol. 47, no. 6, pp. 743–744, Sep. 1999, doi: 10.1209/epl/i1999-00453-y.
[106] J. Ou, B. Perot, and J. P. Rothstein, 'Laminar drag reduction in microchannels using ultrahydrophobic surfaces', *Physics of Fluids*, vol. 16, no. 12, pp. 4635–4643, Dec. 2004, doi: 10.1063/1.1812011.
[107] Y. Xiu, Y. Liu, B. Balu, D. W. Hess, and C. Wong, 'Robust Superhydrophobic Surfaces Prepared With Epoxy Resin and Silica Nanoparticles', *IEEE Trans. Compon., Packag. Manufact. Technol.*, vol. 2, no. 3, pp. 395–401, Mar. 2012, doi: 10.1109/TCPMT.2011.2177088.

[108] N. J. Shirtcliffe, G. McHale, M. I. Newton, and C. C. Perry, 'Wetting and Wetting Transitions on Copper-Based Super-Hydrophobic Surfaces', *Langmuir*, vol. 21, no. 3, pp. 937–943, Feb. 2005, doi: 10.1021/la048630s.
[109] Walter H. Gitzen, *Alumina as a ceramic material*, Walter H. Gitzen., vol. Special Publication No.4. Columbus, Ohio: The American Ceramic Society, Inc, 1970.
[110] E. Dörre and H. Hübner, *Alumina: processing, properties, and applications*. Berlin ; New York: Springer-Verlag, 1984.
[111] H.-H. Gatzen, V. Saile, J. Leuthold, and R. S. Muller, *Micro and nano fabrication: tools and processes*. Berlin: Springer, 2015.
[112] N. Miyamoto *et al.*, 'Mesoporous Silica Particles as Topologically Crosslinking Fillers for Poly(*N* -isopropylacrylamide) Hydrogels', *Chem. Eur. J.*, vol. 20, no. 46, pp. 14955–14958, Nov. 2014, doi: 10.1002/chem.201403762.
[113] Y. Lian, W. Zhang, L. Ding, X. Zhang, Y. Zhang, and X. Wang, 'Nanomaterials for Intracellular pH Sensing and Imaging', in *Novel Nanomaterials for Biomedical, Environmental and Energy Applications*, Elsevier, 2019, pp. 241–273. doi: 10.1016/B978-0-12-814497-8.00008-4.
[114] S. A. Rice, *Advances in chemical physics. Volume 136 Volume 136*. Hoboken, N.J.: Wiley, 2007. Accessed: Mar. 07, 2020. [Online]. Available: http://site.ebrary.com/id/10232648
[115] J. Vivero-Escoto, *Silica nanoparticles preparation, properties and uses*. New York: Nova Science Publishers, 2012. Accessed: Jan. 28, 2020. [Online]. Available: http://site.ebrary.com/id/10683027
[116] S. Wang *et al.*, 'Preparation of a durable superhydrophobic membrane by electrospinning poly (vinylidene fluoride) (PVDF) mixed with epoxy–siloxane modified SiO2 nanoparticles: A possible route to superhydrophobic surfaces with low water sliding angle and high water contact angle', *Journal of Colloid and Interface Science*, vol. 359, no. 2, pp. 380–388, Jul. 2011, doi: 10.1016/j.jcis.2011.04.004.
[117] L.-Y. Meng and S.-J. Park, 'Effect of growth of graphite nanofibers on superhydrophobic and electrochemical properties of carbon fibers', *Materials Chemistry and Physics*, vol. 132, no. 2–3, pp. 324–329, Feb. 2012, doi: 10.1016/j.matchemphys.2011.11.024.
[118] A. Hozumi, D. F. Cheng, and M. Yagihashi, 'Hydrophobic/superhydrophobic oxidized metal surfaces showing negligible contact angle hysteresis', *Journal of Colloid and Interface Science*, vol. 353, no. 2, pp. 582–587, Jan. 2011, doi: 10.1016/j.jcis.2010.09.075.
[119] Z. Shen, C. Hou, S. Liu, and Z. Guan, 'Micro-nanostructured silicone-carbon composite coatings with superhydrophobicity and photoluminescence prepared by oxidative chemical vapor deposition', *J. Appl. Polym. Sci.*, vol. 131, no. 12, p. n/a-n/a, Jun. 2014, doi: 10.1002/app.40400.
[120] K. Acatay, E. Simsek, C. Ow-Yang, and Y. Z. Menceloglu, 'Tunable, Superhydrophobically Stable Polymeric Surfaces by Electrospinning', *Angew. Chem. Int. Ed.*, vol. 43, no. 39, pp. 5210–5213, Oct. 2004, doi: 10.1002/anie.200461092.
[121] E. Celia, T. Darmanin, E. Taffin de Givenchy, S. Amigoni, and F. Guittard, 'Recent advances in designing superhydrophobic surfaces', *Journal of Colloid and Interface Science*, vol. 402, pp. 1–18, Jul. 2013, doi: 10.1016/j.jcis.2013.03.041.
[122] A. K. Haghi, *Electrospinning of nanofibers in textiles*. Toronto: Apple Academic Press, 2012. Accessed: Jun. 20, 2020. [Online]. Available: http://www.crcnetbase.com/isbn/9781926895048

[123] M. K. Sarkar, K. Bal, F. He, and J. Fan, 'Design of an outstanding super-hydrophobic surface by electro-spinning', *Applied Surface Science*, vol. 257, no. 15, pp. 7003–7009, May 2011, doi: 10.1016/j.apsusc.2011.03.057.
[124] D. S. Peterson, 'Sol–Gel Technique', in *Encyclopedia of Microfluidics and Nanofluidics*, D. Li, Ed. Boston, MA: Springer US, 2014, pp. 1–7. doi: 10.1007/978-3-642-27758-0_1432-2.
[125] W. Ma, H. Wu, Y. Higaki, H. Otsuka, and A. Takahara, 'A "non-sticky" superhydrophobic surface prepared by self-assembly of fluoroalkyl phosphonic acid on a hierarchically micro/nanostructured alumina gel film', *Chem. Commun.*, vol. 48, no. 54, p. 6824, 2012, doi: 10.1039/c2cc32513f.
[126] Y. Xiu, F. Xiao, D. W. Hess, and C. P. Wong, 'Superhydrophobic optically transparent silica films formed with a eutectic liquid', *Thin Solid Films*, vol. 517, no. 5, pp. 1610–1615, Jan. 2009, doi: 10.1016/j.tsf.2008.09.081.
[127] W. Chen and T. J. McCarthy, 'Layer-by-Layer Deposition: A Tool for Polymer Surface Modification', *Macromolecules*, vol. 30, no. 1, pp. 78–86, Jan. 1997, doi: 10.1021/ma961096d.
[128] J. Bravo, L. Zhai, Z. Wu, R. E. Cohen, and M. F. Rubner, 'Transparent Superhydrophobic Films Based on Silica Nanoparticles', *Langmuir*, vol. 23, no. 13, pp. 7293–7298, Jun. 2007, doi: 10.1021/la070159q.
[129] J.-H. Zhi, L.-Z. Zhang, Y. Yan, and J. Zhu, 'Mechanical durability of superhydrophobic surfaces: The role of surface modification technologies', *Applied Surface Science*, vol. 392, pp. 286–296, Jan. 2017, doi: 10.1016/j.apsusc.2016.09.049.
[130] S. Jung, M. Dorrestijn, D. Raps, A. Das, C. M. Megaridis, and D. Poulikakos, 'Are Superhydrophobic Surfaces Best for Icephobicity?', *Langmuir*, vol. 27, no. 6, pp. 3059–3066, Mar. 2011, doi: 10.1021/la104762g.
[131] Y. Shen, X. Wu, J. Tao, C. Zhu, Y. Lai, and Z. Chen, 'Icephobic materials: Fundamentals, performance evaluation, and applications', *Progress in Materials Science*, vol. 103, pp. 509–557, Jun. 2019, doi: 10.1016/j.pmatsci.2019.03.004.
[132] L. B. Boinovich, A. M. Emelyanenko, V. K. Ivanov, and A. S. Pashinin, 'Durable Icephobic Coating for Stainless Steel', *ACS Appl. Mater. Interfaces*, vol. 5, no. 7, pp. 2549–2554, Apr. 2013, doi: 10.1021/am3031272.
[133] M. A. Sarshar, D. Song, C. Swarctz, J. Lee, and C.-H. Choi, 'Anti-Icing or Deicing: Icephobicities of Superhydrophobic Surfaces with Hierarchical Structures', *Langmuir*, vol. 34, no. 46, pp. 13821–13827, Nov. 2018, doi: 10.1021/acs.langmuir.8b02231.
[134] V. Hejazi, K. Sobolev, and M. Nosonovsky, 'From superhydrophobicity to icephobicity: forces and interaction analysis', *Sci Rep*, vol. 3, no. 1, p. 2194, Dec. 2013, doi: 10.1038/srep02194.
[135] D. K. Sarkar and M. Farzaneh, 'Superhydrophobic Coatings with Reduced Ice Adhesion', *Journal of Adhesion Science and Technology*, vol. 23, no. 9, pp. 1215–1237, Jan. 2009, doi: 10.1163/156856109X433964.
[136] M. He, H. Li, J. Wang, and Y. Song, 'Superhydrophobic surface at low surface temperature', *Appl. Phys. Lett.*, vol. 98, no. 9, p. 093118, Feb. 2011, doi: 10.1063/1.3558911.
[137] S. A. Kulinich, S. Farhadi, K. Nose, and X. W. Du, 'Superhydrophobic Surfaces: Are They Really Ice-Repellent?', *Langmuir*, vol. 27, no. 1, pp. 25–29, Jan. 2011, doi: 10.1021/la104277q.
[138] L. Cao, A. K. Jones, V. K. Sikka, J. Wu, and D. Gao, 'Anti-Icing Superhydrophobic Coatings', *Langmuir*, vol. 25, no. 21, pp. 12444–12448, Nov. 2009, doi: 10.1021/la902882b.

[139] S. Farhadi, M. Farzaneh, and S. A. Kulinich, 'Anti-icing performance of superhydrophobic surfaces', *Applied Surface Science*, vol. 257, no. 14, pp. 6264–6269, May 2011, doi: 10.1016/j.apsusc.2011.02.057.
[140] A. Hussain, A. Batra, and R. Pachauri, 'An experimental study on effect of dust on power loss in solar photovoltaic module', *Renewables*, vol. 4, no. 1, p. 9, Dec. 2017, doi: 10.1186/s40807-017-0043-y.
[141] Y.-B. Park, H. Im, M. Im, and Y.-K. Choi, 'Self-cleaning effect of highly water-repellent microshell structures for solar cell applications', *J. Mater. Chem.*, vol. 21, no. 3, pp. 633–636, 2011, doi: 10.1039/C0JM02463E.
[142] K. P. Balan, 'Corrosion', in *Metallurgical Failure Analysis*, Elsevier, 2018, pp. 155–178. doi: 10.1016/B978-0-12-814336-0.00009-3.
[143] X. Li *et al.*, 'Improvement of corrosion resistance of H59 brass through fabricating superhydrophobic surface using laser ablation and heating treatment', *Corrosion Science*, vol. 180, p. 109186, Mar. 2021, doi: 10.1016/j.corsci.2020.109186.
[144] K. Liu, M. Zhang, J. Zhai, J. Wang, and L. Jiang, 'Bioinspired construction of Mg–Li alloys surfaces with stable superhydrophobicity and improved corrosion resistance', *Appl. Phys. Lett.*, vol. 92, no. 18, p. 183103, May 2008, doi: 10.1063/1.2917463.
[145] W. Xu, J. Song, J. Sun, Y. Lu, and Z. Yu, 'Rapid Fabrication of Large-Area, Corrosion-Resistant Superhydrophobic Mg Alloy Surfaces', *ACS Appl. Mater. Interfaces*, vol. 3, no. 11, pp. 4404–4414, Nov. 2011, doi: 10.1021/am2010527.
[146] T. Ishizaki, Y. Masuda, and M. Sakamoto, 'Corrosion Resistance and Durability of Superhydrophobic Surface Formed on Magnesium Alloy Coated with Nanostructured Cerium Oxide Film and Fluoroalkylsilane Molecules in Corrosive NaCl Aqueous Solution', *Langmuir*, vol. 27, no. 8, pp. 4780–4788, Apr. 2011, doi: 10.1021/la2002783.
[147] T. Ishizaki, J. Hieda, N. Saito, N. Saito, and O. Takai, 'Corrosion resistance and chemical stability of super-hydrophobic film deposited on magnesium alloy AZ31 by microwave plasma-enhanced chemical vapor deposition', *Electrochimica Acta*, vol. 55, no. 23, pp. 7094–7101, Sep. 2010, doi: 10.1016/j.electacta.2010.06.064.
[148] T. Ishizaki and N. Saito, 'Rapid Formation of a Superhydrophobic Surface on a Magnesium Alloy Coated with a Cerium Oxide Film by a Simple Immersion Process at Room Temperature and Its Chemical Stability', *Langmuir*, vol. 26, no. 12, pp. 9749–9755, Jun. 2010, doi: 10.1021/la100474x.
[149] T. Darmanin and F. Guittard, 'Recent advances in the potential applications of bioinspired superhydrophobic materials', *J. Mater. Chem. A*, vol. 2, no. 39, pp. 16319–16359, 2014, doi: 10.1039/C4TA02071E.
[150] J. Ou, W. Hu, M. Xue, F. Wang, and W. Li, 'Superhydrophobic Surfaces on Light Alloy Substrates Fabricated by a Versatile Process and Their Corrosion Protection', *ACS Appl. Mater. Interfaces*, vol. 5, no. 8, pp. 3101–3107, Apr. 2013, doi: 10.1021/am4000134.
[151] H. Liu, S. Szunerits, W. Xu, and R. Boukherroub, 'Preparation of Superhydrophobic Coatings on Zinc as Effective Corrosion Barriers', *ACS Appl. Mater. Interfaces*, vol. 1, no. 6, pp. 1150–1153, Jun. 2009, doi: 10.1021/am900100q.
[152] P. B. Weisensee, J. Tian, N. Miljkovic, and W. P. King, 'Water droplet impact on elastic superhydrophobic surfaces', *Sci Rep*, vol. 6, no. 1, p. 30328, Jul. 2016, doi: 10.1038/srep30328.
[153] T. Wang, X. Hu, and S. Dong, 'A general route to transform normal hydrophilic cloths into superhydrophobic surfaces', *Chem. Commun.*, no. 18, p. 1849, 2007, doi: 10.1039/b616778k.

[154] J. Zimmermann, F. A. Reifler, G. Fortunato, L.-C. Gerhardt, and S. Seeger, 'A Simple, One-Step Approach to Durable and Robust Superhydrophobic Textiles', *Adv. Funct. Mater.*, vol. 18, no. 22, pp. 3662–3669, Nov. 2008, doi: 10.1002/adfm.200800755.

[155] J. Zimmermann, S. Seeger, and F. A. Reifler, 'Water Shedding Angle: A New Technique to Evaluate the Water-Repellent Properties of Superhydrophobic Surfaces', *Textile Research Journal*, vol. 79, no. 17, pp. 1565–1570, Nov. 2009, doi: 10.1177/0040517509105074.

[156] J. Zimmermann, G. R. J. Artus, and S. Seeger, 'Superhydrophobic Silicone Nanofilament Coatings', *Journal of Adhesion Science and Technology*, vol. 22, no. 3–4, pp. 251–263, Jan. 2008, doi: 10.1163/156856108X305165.

[157] H. Wang, Y. Xue, J. Ding, L. Feng, X. Wang, and T. Lin, 'Durable, Self-Healing Superhydrophobic and Superoleophobic Surfaces from Fluorinated-Decyl Polyhedral Oligomeric Silsesquioxane and Hydrolyzed Fluorinated Alkyl Silane', *Angew. Chem. Int. Ed.*, vol. 50, no. 48, pp. 11433–11436, Nov. 2011, doi: 10.1002/anie.201105069.

[158] M. Koupenova, B. E. Kehrel, H. A. Corkrey, and J. E. Freedman, 'Thrombosis and platelets: an update', *Eur Heart J*, p. ehw550, Dec. 2016, doi: 10.1093/eurheartj/ehw550.

[159] R. C. Becker and F. Andreotti, 'Genetics and Genomics in the Management of Hemostasis and Thrombosis', in *Essentials of Genomic and Personalized Medicine*, Elsevier, 2010, pp. 374–389. doi: 10.1016/B978-0-12-374934-5.00030-1.

[160] X. R. Xu *et al.*, 'Platelets and platelet adhesion molecules: novel mechanisms of thrombosis and anti-thrombotic therapies', *Thrombosis J*, vol. 14, no. S1, p. 29, Oct. 2016, doi: 10.1186/s12959-016-0100-6.

[161] P. Jankowski, D. Ogonczyk, A. Kosinski, W. Lisowski, and P. Garstecki, 'Hydrophobic modification of polycarbonate for reproducible and stable formation of biocompatible microparticles', *Lab Chip*, vol. 11, no. 4, pp. 748–752, 2011, doi: 10.1039/C0LC00360C.

[162] H. Yahyaei, H. Makki, and M. Mohseni, 'Superhydrophobic coatings for medical applications', in *Superhydrophobic Polymer Coatings*, Elsevier, 2019, pp. 321–338. doi: 10.1016/B978-0-12-816671-0.00015-1.

[163] T. Sun, H. Tan, D. Han, Q. Fu, and L. Jiang, 'No Platelet Can Adhere—Largely Improved Blood Compatibility on Nanostructured Superhydrophobic Surfaces', *Small*, vol. 1, no. 10, pp. 959–963, Oct. 2005, doi: 10.1002/smll.200500095.

[164] S. Alexander, J. Eastoe, A. M. Lord, F. Guittard, and A. R. Barron, 'Branched Hydrocarbon Low Surface Energy Materials for Superhydrophobic Nanoparticle Derived Surfaces', *ACS Appl. Mater. Interfaces*, vol. 8, no. 1, pp. 660–666, Jan. 2016, doi: 10.1021/acsami.5b09784.

[165] R. Paul and E. Genescà, 'The use of enzymatic techniques in the finishing of technical textiles', in *Advances in the Dyeing and Finishing of Technical Textiles*, Elsevier, 2013, pp. 177–198. doi: 10.1533/9780857097613.2.177.

[166] J. D. Schuttlefield and V. H. Grassian, 'ATR–FTIR Spectroscopy in the Undergraduate Chemistry Laboratory. Part I: Fundamentals and Examples', *J. Chem. Educ.*, vol. 85, no. 2, p. 279, Feb. 2008, doi: 10.1021/ed085p279.

[167] H.-J. Tong, J. P. Reid, J.-L. Dong, and Y.-H. Zhang, 'Observation of the Crystallization and Supersaturation of Mixed Component $NaNO_3$ −Na_2SO_4 Droplets by FTIR-ATR and Raman Spectroscopy', *J. Phys. Chem. A*, vol. 114, no. 46, pp. 12237–12243, Nov. 2010, doi: 10.1021/jp1080548.

[168] T. Norman, 'Alarm Detection and Emerging Video Technologies', in *Integrated Security Systems Design*, Elsevier, 2014, pp. 311–325. doi: 10.1016/B978-0-12-800022-9.00016-4.

[169] A. Ramírez-Hernández, C. Aguilar-Flores, and A. Aparicio-Saguilán, 'Fingerprint analysis of FTIR spectra of polymers containing vinyl acetate', *DYNA*, vol. 86, no. 209, pp. 198–205, Apr. 2019, doi: 10.15446/dyna.v86n209.77513.
[170] A. A. Stolov and D. A. Simoff, 'Micro Attenuated Total Reflection Spectra of Bulk Silica Glass: Effects of Experimental Conditions and Glass Thermal History on Appearance of a Surface Polariton in the Si—O Stretching Region', *Appl Spectrosc*, vol. 62, no. 6, pp. 624–633, Jun. 2008, doi: 10.1366/000370208784658020.
[171] M. Tasumi and A. Sakamoto, Eds., *Introduction to experimental infrared spectroscopy*. Hoboken, N.J: Wiley, 2015.
[172] W. M. Groenewoud, 'THERMOGRAVIMETRY', in *Characterisation of Polymers by Thermal Analysis*, Elsevier, 2001, pp. 61–76. doi: 10.1016/B978-044450604-7/50003-0.
[173] S. Bandyopadhyay-Ghosh, S. B. Ghosh, and M. Sain, 'The use of biobased nanofibres in composites', in *Biofiber Reinforcements in Composite Materials*, Elsevier, 2015, pp. 571–647. doi: 10.1533/9781782421276.5.571.
[174] David C. Joy, 'Scanning Electron Microscope'. [Online]. Available: https://www.britannica.com/technology/scanning-electron-microscope
[175] 'Infrared Spectroscopy', in *ACS Reagent Chemicals*, Washington, DC: American Chemical Society, 2017. doi: 10.1021/acsreagents.2008.
[176] D. Fraenkel, P. C. Andersen, G. Cooper, and H. H. Funke, 'A Modified Thermogravimetric Analysis Apparatus of Improved Performance', *Ind. Eng. Chem. Res.*, vol. 41, no. 7, pp. 1885–1891, Apr. 2002, doi: 10.1021/ie010565j.
[177] M. Farré and D. Barceló, 'Introduction to the Analysis and Risk of Nanomaterials in Environmental and Food Samples', in *Comprehensive Analytical Chemistry*, vol. 59, Elsevier, 2012, pp. 1–32. doi: 10.1016/B978-0-444-56328-6.00001-3.
[178] P. Callahan *et al.*, 'Defect Characterization using Transmission Scanning Electron Microscopy', *Microsc Microanal*, vol. 24, no. S1, pp. 1836–1837, Aug. 2018, doi: 10.1017/S1431927618009662.
[179] S. McKernan, 'Environmental Scanning Electron Microscopy: - Advantages and Disadvantages', *Microsc Microanal*, vol. 3, no. S2, pp. 381–382, Aug. 1997, doi: 10.1017/S1431927600008795.
[180] T. Huhtamäki, X. Tian, J. T. Korhonen, and R. H. A. Ras, 'Surface-wetting characterization using contact-angle measurements', *Nat Protoc*, vol. 13, no. 7, pp. 1521–1538, Jul. 2018, doi: 10.1038/s41596-018-0003-z.
[181] D. H. Williams and I. Fleming, *Spectroscopic methods in organic chemistry*. London: McGraw-Hill, 2008.
[182] R. R. Sahoo and S. K. Biswas, 'Frictional response of fatty acids on steel', *Journal of Colloid and Interface Science*, vol. 333, no. 2, pp. 707–718, May 2009, doi: 10.1016/j.jcis.2009.01.046.
[183] H. Zhang, X. Zeng, Y. Gao, F. Shi, P. Zhang, and J.-F. Chen, 'A Facile Method To Prepare Superhydrophobic Coatings by Calcium Carbonate', *Ind. Eng. Chem. Res.*, vol. 50, no. 6, pp. 3089–3094, Mar. 2011, doi: 10.1021/ie102149y.
[184] Y. Koide and A. R. Barron, '[Al5(tBu)5(.mu.3-O)2(.mu.3-OH)2(.mu.-OH)2(.mu.-O2CPh)2]: A Model for the Interaction of Carboxylic Acids with Boehmite', *Organometallics*, vol. 14, no. 8, pp. 4026–4029, Aug. 1995, doi: 10.1021/om00008a060.
[185] L. Portilla and M. Halik, 'Smoothly Tunable Surface Properties of Aluminum Oxide Core–Shell Nanoparticles By A Mixed-Ligand Approach', *ACS Appl. Mater. Interfaces*, vol. 6, no. 8, pp. 5977–5982, Apr. 2014, doi: 10.1021/am501155r.
[186] L. Senak, M. A. Davies, and R. Mendelsohn, 'A quantitative IR study of hydrocarbon chain conformation in alkanes and phospholipids: CH2 wagging modes in disordered

bilayer and HII phases', *J. Phys. Chem.*, vol. 95, no. 6, pp. 2565–2571, Mar. 1991, doi: 10.1021/j100159a084.
[187] A. Putnis, *Introduction to mineral sciences*. Cambridge: Cambridge University Press, 1992. doi: 10.1017/CBO9781139170383.
[188] A. Boumaza *et al.*, 'Transition alumina phases induced by heat treatment of boehmite: An X-ray diffraction and infrared spectroscopy study', *Journal of Solid State Chemistry*, vol. 182, no. 5, pp. 1171–1176, May 2009, doi: 10.1016/j.jssc.2009.02.006.
[189] F. Fan, P. Xiang, and L. Zhao, 'Vibrational spectra analysis of amorphous lactose in structural transformation: Water/temperature plasticization, crystal formation, and molecular mobility', *Food Chemistry*, vol. 341, p. 128215, Mar. 2021, doi: 10.1016/j.foodchem.2020.128215.
[190] Q. Zhang, Y. Wan, Y. Li, S. Yang, and W. Yao, 'Friction reducing behavior of stearic acid film on a textured aluminum substrate', *Applied Surface Science*, vol. 280, pp. 545–549, Sep. 2013, doi: 10.1016/j.apsusc.2013.05.024.
[191] S. P. Thompson, 'Si-O stretch modes in amorphous silicates', *Astrophys Space Sci*, vol. 224, no. 1–2, pp. 575–576, Feb. 1995, doi: 10.1007/BF00667962.
[192] R. M. Goody and X. Huang, 'RADIATION TRANSFER IN THE ATMOSPHERE | Absorption and Thermal Emission', in *Encyclopedia of Atmospheric Sciences*, Elsevier, 2015, pp. 5–12. doi: 10.1016/B978-0-12-382225-3.00337-6.
[193] A. Morlok, S. Klemme, I. Weber, A. Stojic, M. Sohn, and H. Hiesinger, 'IR spectroscopy of synthetic glasses with Mercury surface composition: Analogs for remote sensing', *Icarus*, vol. 296, pp. 123–138, Nov. 2017, doi: 10.1016/j.icarus.2017.05.024.
[194] D. Hill, H. Attia, A. R. Barron, and S. Alexander, 'Size and morphology dependent surface wetting based on hydrocarbon functionalized nanoparticles', *Journal of Colloid and Interface Science*, vol. 543, pp. 328–334, May 2019, doi: 10.1016/j.jcis.2019.02.058.
[195] D. Hill, A. R. Barron, and S. Alexander, 'Comparison of hydrophobicity and durability of functionalized aluminium oxide nanoparticle coatings with magnetite nanoparticles–links between morphology and wettability', *Journal of Colloid and Interface Science*, vol. 555, pp. 323–330, Nov. 2019, doi: 10.1016/j.jcis.2019.07.080.
[196] K. Liu, M. Vuckovac, M. Latikka, T. Huhtamäki, and R. H. A. Ras, 'Improving surface-wetting characterization', *Science*, vol. 363, no. 6432, pp. 1147–1148, Mar. 2019, doi: 10.1126/science.aav5388.

Appendix

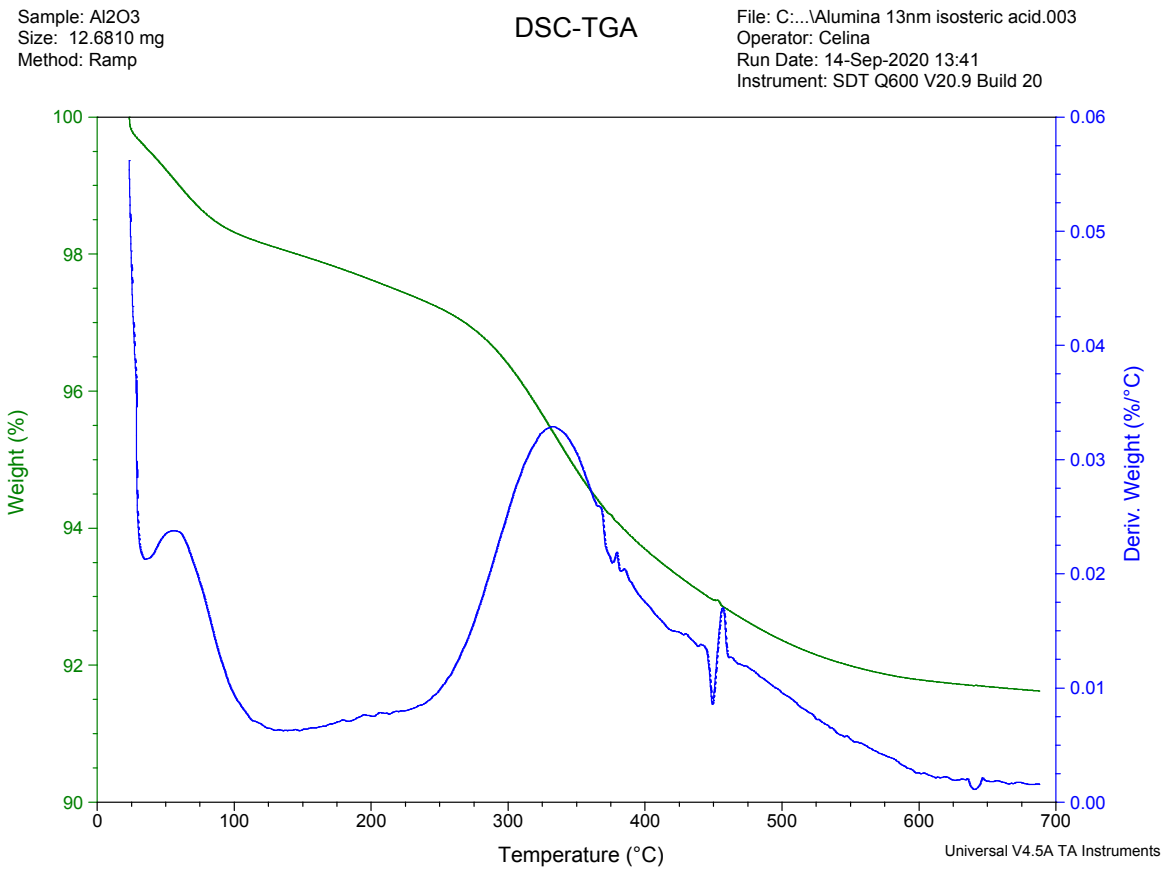

TGA data of the alumina (13 nm) with isosteric acid, dashed curves correspond to derivatives

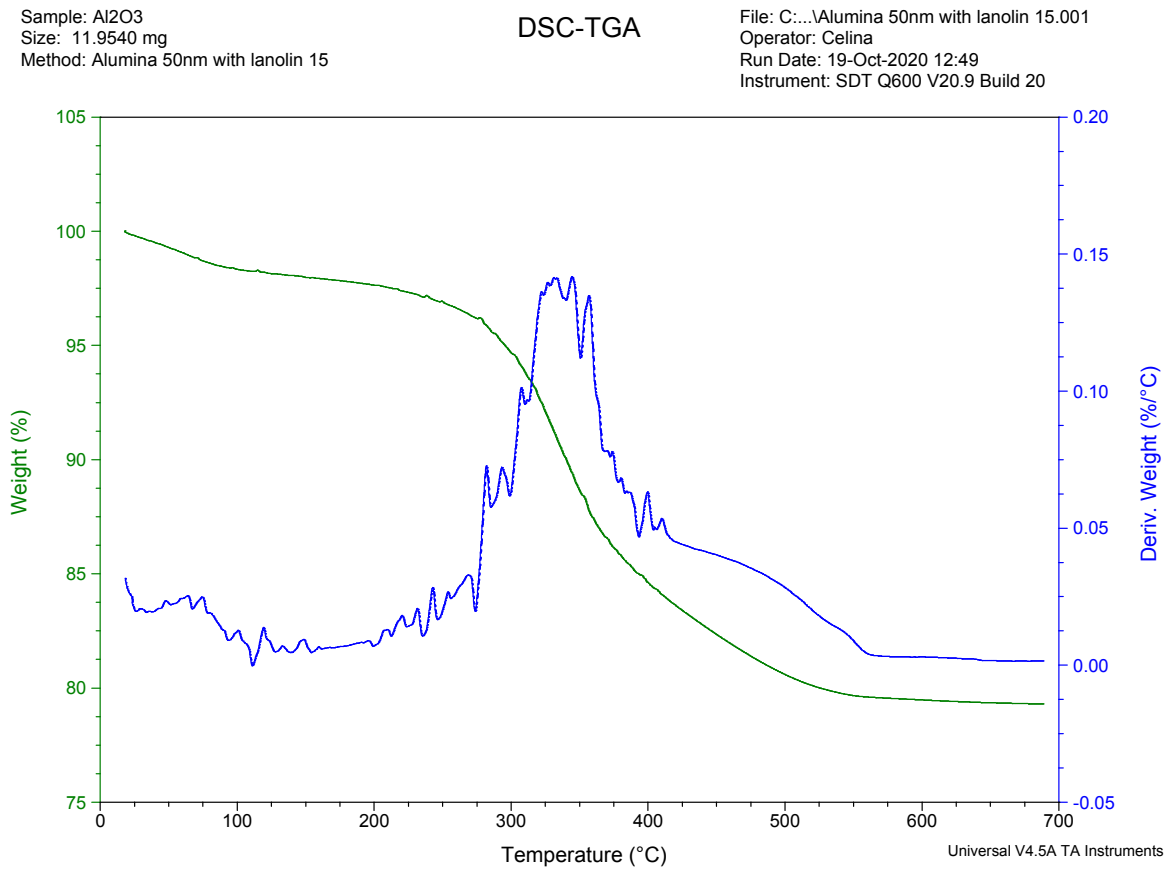

TGA data of the alumina (50 nm) with lanolin (1:15), dashed curves correspond to derivatives

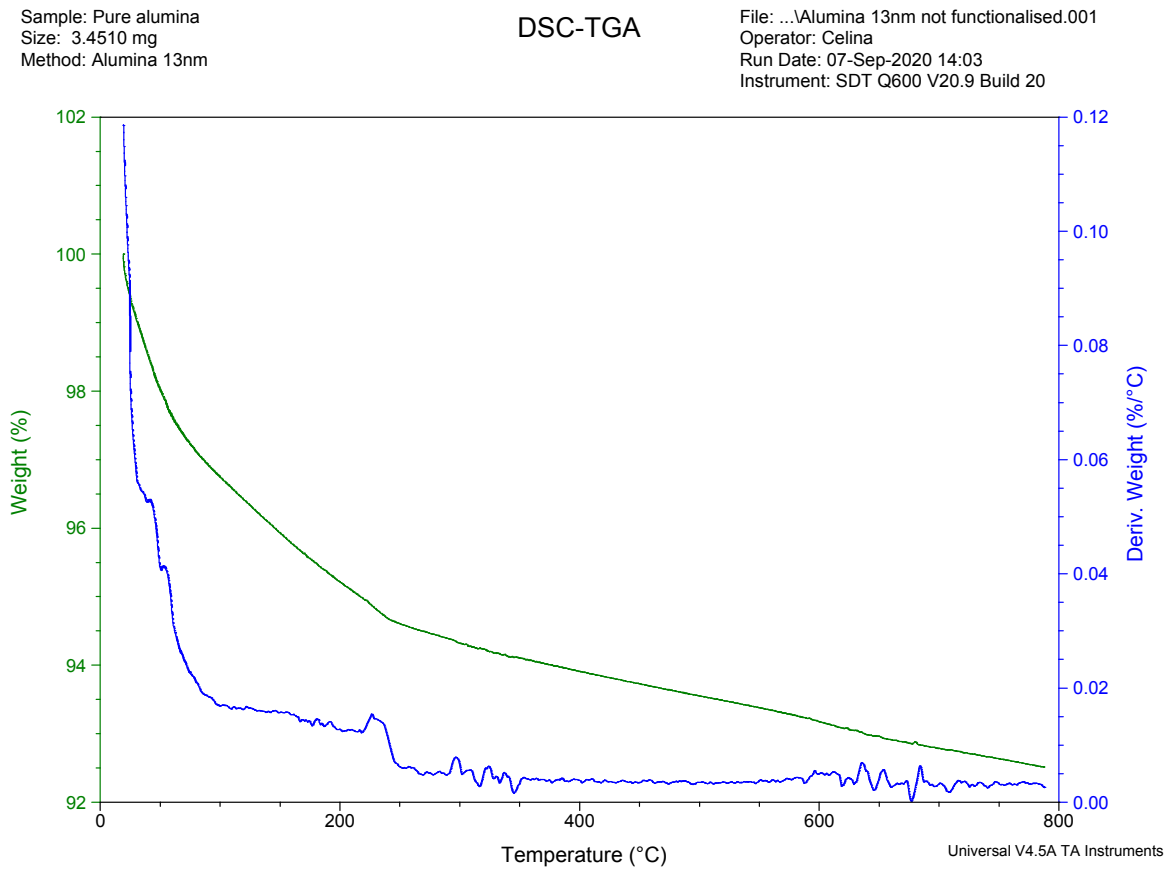

TGA data of the unfunctionalized alumina (13 nm), dashed curves correspond to derivatives

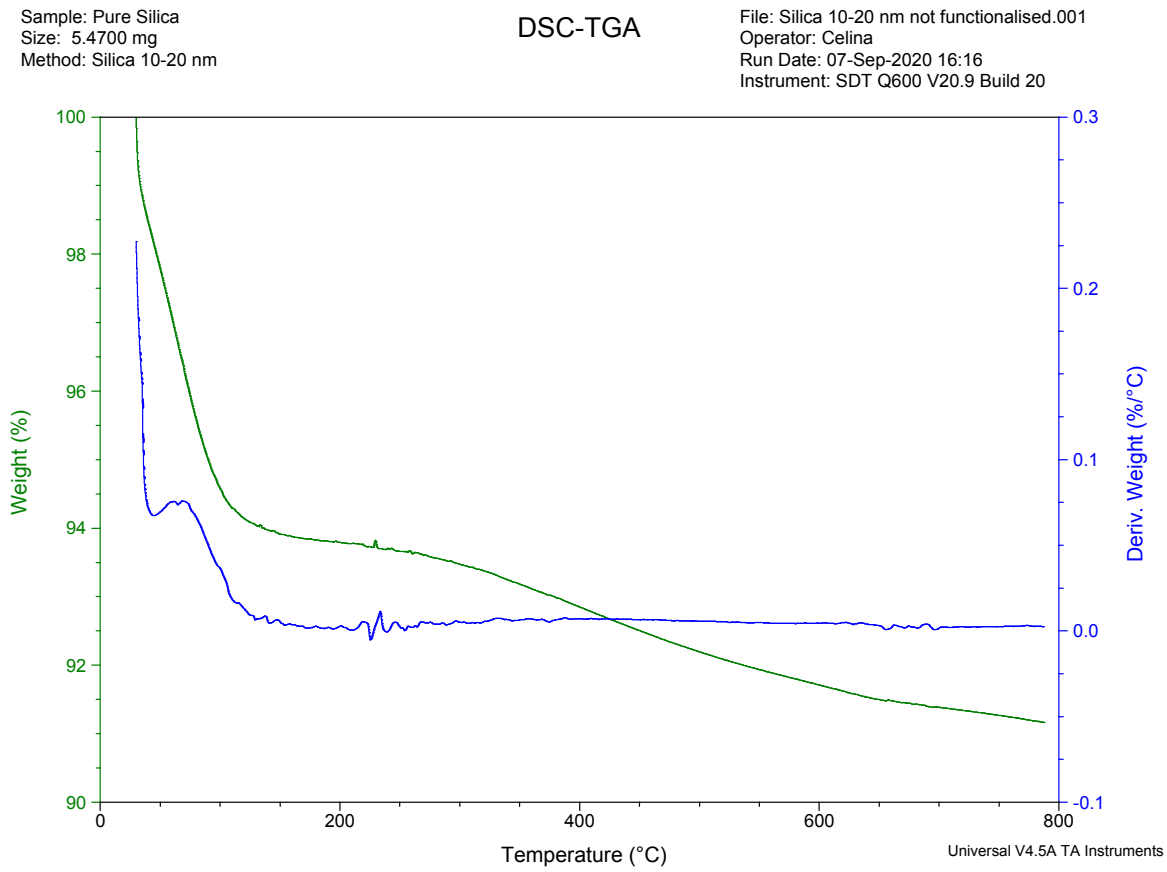

TGA data of the unfunctionalized silica (10 – 20 nm), dashed curves correspond to derivatives